

**STRUCTURAL PERFORMANCE OF NON-ICE CLASS
SHIPS IN SLIDING COLLISION WITH ICE**

by

© Mahdi Omidali

A thesis submitted to the School of Graduate Studies

in partial fulfillment of the requirements for the degree of

Master of Engineering

Faculty of Engineering and Applied Science

Memorial University of Newfoundland

October 2021

St. John's

Newfoundland and Labrador

Canada

Abstract

Stiffened structures have a high load-bearing capacity beyond the elastic region that can be used in structural design. Collision and grounding scenarios are among the accidental limit states that threaten the structural integrity of marine structures. Collision with ice is one of the scenarios that can occur in Canadian Arctic waters. It is a high priority to understand the structural performance of ships in probable collision cases. As for ice-class ships, the load-carrying capacity is apparent on some level for designers and navigators. For non-ice class ships, however, the reserve strength after yield is not evident in collision with ice. It is crucial for both structural reasons and damage stability of the vessel.

International Maritime Organization (IMO) defines damage length requirements for various types of ships in various conventions and codes. It is necessary to study the damage extent in collision scenarios to realize whether amendments are necessary for vessels that might navigate in polar water. In this research, the structural performance of various merchant ships and offshore support vessels has been investigated under collision with ice. Finite element simulation with complex fracture models was implemented in this study.

The simulations indicated that the collision with bergy bits causes severe damage to the structure on non-ice class ships. Parameters such as ice shape in the high-pressure zone, ice geometry (mass distribution), and impact angle dramatically affect the results.

It was concluded that for the merchant vessels investigated, the damage stability requirements specified in MARPOL are conservative (except for tankers whose length does

not exceed 150m), and there is no need to include any additional damage case scenario. For offshore supply vessels, results indicate that the damage cases are not as conservative as they should be, and amendments to the current IMO regulations are necessary. In addition, it is shown that the empirical formulas available in the literature can estimate the steady-state fracture phase in the sliding collision. This finding could be used to construct the probability distribution function for damage extent in collision with ice.

Acknowledgements

This research could not be completed without the support of the research team members and industry funding partners.

I would like to thank my supervisor, Dr. David Molyneux, for giving me the opportunity to work on this project and for his constant support and valuable suggestions and guidance through my research. It was not possible for me to find a correct research path without his help.

I would like to thank my co-supervisor, Dr. Bruce Quinton, for providing me with advice on FE simulations, helping me to troubleshoot my FE models, and giving me access to his on-campus computer and cluster.

This research was funded by the National Science and Engineering Council of Canada (NSERC) DND/CRD project “Operational Capabilities of Low- and Non-ice class Vessels in Ice” project. The industrial sponsors of this project are Vard Marine Inc., the American Bureau of Shipping (ABS), and Defence Research & Development Canada (DRDC). This research would not be completed without their contribution, and we acknowledge their supports. I would like to thank Dr. Claude Daley, Andrew Kendrick, James Bond, and Dan Oldford for contributing to my research.

I would like to thank my friends and colleagues, Lt Matthew Lee Robbins, Jordan Norman, and Andrew Greenham, for their help. We had terrific discussions that assist me profoundly in solving my problems in the research.

I would like to thank my lovely mother for her support and motivation throughout my life. She always encourages me to follow my dreams, and I would not be here if not for her.

Lastly, I would like to thank my amazing wife, Zahra, for supporting me through my graduate studies. I had to study and work on my thesis every day, and she helped me withstand the difficulties. Without her kindness, patience, and understanding, I would never have been able to finish my studies.

Table of Contents

Abstract	ii
Acknowledgements	iv
Table of Contents	vi
List of Tables	xi
List of Figures	xiii
Chapter 1 Introduction.....	1
1.1 Background	1
1.2 Problem statement.....	3
1.3 Thesis structure	5
1.4 Research outcomes and significance	6
Chapter 2 Literature Review.....	7
2.1 Introduction.....	7
2.2 Classifications and national standards	7
2.3 Collision mechanics	9
2.4 Ship-ice impact analysis: FE approach	12
2.5 Summary	17

Chapter 3	A Review of the Ship and Iceberg Collision Statistics and Possible Ship-Ice Collision Scenarios	18
3.1	Introduction.....	18
3.2	Review of NRC database on iceberg-ship collisions since 1950.....	18
3.2.1	Database structure	19
3.2.2	Location of damage in the hull	20
3.2.3	Number of accidents with respect to the types of ships.....	22
3.2.4	Types of damages	24
3.2.5	Distribution of types of damages with respect to the types of vessels 25	
3.3	Ice type for the collision simulation.....	31
3.4	Bergy bit mass and speed.....	36
3.5	Summary	38
Chapter 4	Fracture Modeling and Ice Mechanics.....	39
4.1	Introduction.....	39
4.2	Ductile fracture	40
4.3	Stress state and ductile fracture.....	41
4.4	Continuum damage mechanics (CDM) and stress triaxiality (according to [54] unless otherwise stated).....	44
4.5	Fracture modeling in LS-DYNA	49

4.6	Ice Mechanics	53
4.7	Summary	55
Chapter 5	Methodology and Numerical Model	56
5.1	Introduction.....	56
5.2	Vessel's models	56
5.2.1	Single hull bulk carrier with transverse framing.....	57
5.2.2	Double hull bulk carrier with transverse framing	59
5.2.3	Double hull oil tanker with longitudinal framing	60
5.2.4	Offshore Support Vessel (OSV) with transverse framing	62
5.3	Finite element setup	64
5.3.1	Element type	64
5.3.2	Element quality	64
5.3.3	Boundary conditions	65
5.3.4	Impact scenarios.....	68
5.3.5	Ship speed and mass	69
5.3.6	Fracture criteria	70
5.3.7	Ice material.....	71
5.3.8	Contact setup.....	71
5.3.9	LS-DYNA cards (additional keywords)	72

5.3.10	Solver	72
5.4	Mesh convergence	73
5.5	Benchmark study and validation.....	79
5.6	Summary	79
Chapter 6	Results and Discussions- Part I: Single Hull Structure.....	81
6.1	Introduction.....	81
6.2	Impact with the large contact area	82
6.3	Impact with large contact area with rigid indenter	89
6.4	Impact with the small contact area.....	92
6.5	Effect of the transverse bulkhead on damage extent	100
6.6	Effect of impact angle on the damage extent.....	105
6.7	Simulation with Cone	107
6.8	Effect of mass ice distribution on damage results	111
6.9	Summary	122
Chapter 7	Results and Discussions- Part 2: Structural Response of Double Hull Structures	123
7.1	Introduction.....	123
7.2	Double hull structure with transverse framing.....	123
7.3	Double hull structure with longitudinal framing	128

7.4	Offshore supply vessel with transverse framing.....	132
7.5	Summary	139
Chapter 8	Application of Smearing Technique and Simplified Formulations in Ship-Ice Collision	140
8.1	Introduction.....	140
8.2	Smearred structure with a small contact area.....	140
8.3	Wedge cutting simulations.....	144
8.4	Effect of the hole on the structure behaviour.....	150
8.5	Summary	152
Chapter 9	Conclusions and Recommendations for Future Work	153
9.1	Highlights of findings	153
9.2	Conclusion	156
9.3	Research limitations and future works.....	158
	Bibliography	160

List of Tables

Table 3-1 Damage location of iceberg-ship collisions on ship hull.....	21
Table 3-2 Damage location of iceberg-ship collisions on ship hull (excluding unknown cases).....	21
Table 3-3 Number and percentage each type of the vessels engaged in iceberg impact for non-ice class ships.....	23
Table 3-4 Number and percentage each type of the vessels engaged in iceberg impact for ice-class ships.....	24
Table 3-5 Number and percentage each type of damages caused by iceberg collision for non-ice class ships.....	24
Table 3-6 Number and percentage each type of damages caused by iceberg collision for ice-class ships.....	25
Table 3-7 Distribution of various damages for each type of the vessels damaged by an iceberg for non-ice class ships	26
Table 3-8 Distribution of various damages for each type of the vessels damaged by an iceberg for ice-class ships	27
Table 3-9 Damage dimensions available in NRC database	30
Table 3-10 Iceberg size categories [42]	34
Table 3-11 Douglas Sea Scale [44].....	35
Table 3-12 Recorded Iceberg dimensions and mass in iceberg survey [48].....	37
Table 4-1 Triaxiality and Lode angle parameter for classic for various stress states [57]	43
Table 4-2 Modified fracture strain for various L/t.....	51

Table 4-3 Material properties for steel [58].	52
Table 5-1 Panamax Vessel main particulars	57
Table 5-2 Handymax Vessel main particulars	59
Table 5-3 Double hull oil tanker main particulars	61
Table 5-4 Typical OSV's main particulars	63
Table 5-5 Element quality parameters in FE models	65
Table 5-6 Ice material parameters [67]	71
Table 6-1 Impact scenarios results' summary (large contact area)	84
Table 6-2 Impact scenarios results summery (large contact area with rigid indenter)	90
Table 6-3 structural response during sliding impact for 6000-tonne case (refer to Figure 6-14)	94
Table 6-4 Results summary for impact with the small contact area	98
Table 6-5 Impact velocity for various collision scenarios	105
Table 7-1 Average contact force for 1500-tonne ice impact for various vessel's speed	128
Table 7-2 Summary of rupture length for various impact locations	128
Table 7-3 Double hull requirements for oil tankers delivered on or after 6 July 1996 [6]	132
Table 7-4 Damage extent for OSVs according to MSC Resolutions 235(82)	133
Table 8-1 Parameters used to calculate steady-state cutting force with Equation 27	146
Table 8-2 Average contact force comparison among various approaches	150

List of Figures

Figure 1-1 Possible shipping routes in arctic waters [1].....	2
Figure 2-1 Various arctic and sub-arctic rules design ice load [1]	8
Figure 3-1 Ship-ice impact scenario according to IACS requirements for polar class ships [40].....	22
Figure 3-2 Distribution of various damages for each type of the vessels damaged by an iceberg for non-ice class ships	27
Figure 3-3 Distribution of various damages for each type of the vessels damaged by an iceberg for ice-class ships	28
Figure 3-4 Damage length to length of the vessel histogram according to NRC database	29
Figure 3-5 Ice concentration interpretation [41].....	31
Figure 3-6 Ship navigation scenarios in ice [1]	32
Figure 3-7 (a) Standard X-band Radar, (b) Enhanced X-band Radar [41].....	34
Figure 4-1 Typical ranges of elongation at fracture for different materials [51].....	39
Figure 4-2 Typical ductile material stress-strain curve [51].....	41
Figure 4-3 Damage and fracture mechanics relationship [54].....	44
Figure 4-4 Effective and resisting area for damage variable definition [54].....	46
Figure 4-5 Young's modulus variation by developing damage in Copper (Lemaitre as cited in [53])	46
Figure 4-6 Young's modulus of intact (E) and damaged (E*) material [54].....	48
Figure 4-7 Stress-strain curve for steel based on Equation 23.....	53

Figure 4-8 Various design approaches for ice-structure collision design [63]	54
Figure 5-1 Single hull bulk carrier model extent and scantlings	58
Figure 5-2 Double hull structure with transverse framing: scantlings and model extent ..	60
Figure 5-3 Double hull structure with longitudinal framing	62
Figure 5-4 OSV structural scantlings and model extent	63
Figure 5-5 Boundary conditions for various structural arrangements	67
Figure 5-6 Bergy bit sliding collision scenario	68
Figure 5-7 Initial velocity vectors for ship and ice	69
Figure 5-8 High-density elements to include ship's total displacement	70
Figure 5-9 Ice model curve defined for crushable foam material [66]	71
Figure 5-10 Mesh convergence analysis for the actual structure	74
Figure 5-11 Fracture patterns for various mesh sizes	75
Figure 5-12 Mesh convergence analysis for smeared structure	76
Figure 5-13 wedge cutting experiment by Astrup [68] as cited in [69]	76
Figure 5-14 Mesh sensitivity analysis for ice impact on the structure with large contact area (1500-tonne bergy bit)	77
Figure 5-15 Mesh sensitivity analysis for ice impact on the structure with small contact area (1500-tonne bergy bit)	78
Figure 6-1 (a) Ice geometry (top view), (b) Ice FE model	82
Figure 6-2 Internal energy for various bergy bit impacts (large contact area)	83
Figure 6-3 Contact force for various bergy bit impacts (large contact area)	83
Figure 6-4 Deformation shape for 6000 tonnes bergy bit impact	85
Figure 6-5 Velocity of ice during simulation for all ice masses	85

Figure 6-6 Ice movement for 6000 tonnes bergy bit impact.....	86
Figure 6-7 various ice wedge dimensions used in simulations.....	87
Figure 6-8 Contact force for various wedge dimensions (4500-tonne ice).....	88
Figure 6-9 normalized rupture energy based on 1500 tonnes case.....	89
Figure 6-10 Rupture pattern for 6000 tonnes bergy bit	90
Figure 6-11 Internal energy for various rigid indenter impacts	91
Figure 6-12 Contact force for various bergy bit impacts	91
Figure 6-13 Impact scenario with the small contact area.....	92
Figure 6-14 Contact Force for 6000-tonne case	93
Figure 6-15 Internal energy for various bergy bit impacts (small contact area).....	97
Figure 6-16 Contact force for various bergy bit impacts (small contact area)	98
Figure 6-17 Ice resultant velocity during the simulation	99
Figure 6-18 Crack development in ice due to sharp edges of the ruptured structure	100
Figure 6-19 Transverse Bulkhead positions for simulations	101
Figure 6-20 Transverse bulkhead arrangement (position 2) and scantling.....	101
Figure 6-21 Rupture in the transverse bulkhead (1500-tonne case)	102
Figure 6-22 Contact force for models with transverse bulkhead and without a transverse bulkhead.....	103
Figure 6-23 Ice velocity for simulations with transverse bulkhead and without transverse bulkhead (1500-tonne with small contact area)	104
Figure 6-24 Contact force for various impact angles (1500-tonne bergy bit)	106
Figure 6-25 cones' geometries with angles of 30° and 45°	107

Figure 6-26 Contact force for impact of 1500-tonne bergy bit with various ice tip shapes	109
Figure 6-27 Contact force for impact of 4500-tonne bergy bit with various ice tip shapes	109
Figure 6-28 Internal Energy for the impact of 1500-tonne bergy bit with various ice tip shapes	110
Figure 6-29 Internal Energy for impact of 4500-tonne bergy bit with various ice tip shapes	110
Figure 6-30 Deformation pattern for 1500-tonne impact cases for both ice cones.....	111
Figure 6-31 Ice-vessel interaction in actual (top scheme) and simplified ice wedge	112
Figure 6-32 Ice modified geometry with a realistic center of mass.....	113
Figure 6-33 Ice velocity in Y-direction for 1500-tonne case for different center of masses	114
Figure 6-34 Ice wedge at 0.6 s (1500-tonne bergy bit) (a) with new geometry for the attached weight (b) initial model	114
Figure 6-35 Bergy bit shapes recorded in ice impact large scale experiment [48].....	116
Figure 6-36 Ice model with the center of mass away from the collision point.....	117
Figure 6-37 Von-Mises stress before and after ice fender contacted the structure (3000- tonne bergy bit)	118
Figure 6-38 Structural deformation at the end of the simulation (3000-tonne bergy bit)	119
Figure 6-39 Ice rotation and separation from the structure at the end of the simulation (3000-tonne bergy bit)	120

Figure 6-40 Contact force for ice collision with long cylinder shape (3000-tonne bergy bit)	121
Figure 7-1 Contact force for various ice sizes impacts with double hull structure with transverse framing	124
Figure 7-2 Internal energy for various ice sizes impacts with double hull structure with transverse framing	125
Figure 7-3 Double side structure of a container vessel after collision (taken by the author)	126
Figure 7-4 Rupture and deformation in the structure (9000-tonne bergy bit)	126
Figure 7-5 Contact force for 1500-tonne ice impact for various vessel's speed	127
Figure 7-6 Ice trajectory for impact on stiffener (1500-tonne bergy bit)	129
Figure 7-7 Contact force for various impact location (1500-tonne bergy bit)	131
Figure 7-8 Internal energy for various impact location (1500-tonne bergy bit)	131
Figure 7-9 In-plane load caused by ice faces	132
Figure 7-10 Internal energy for various bergy bit's masses collision with an OSV	134
Figure 7-11 Contact force for various bergy bit's masses collision with an OSV	135
Figure 7-12 Inner shell rupture in 1000-tonne bergy bit impact	135
Figure 7-13 OSV model with transverse bulkhead	136
Figure 7-14 Internal energy for collisions with various ice masses (Structure with BHD)	138
Figure 7-15 Contact force for collisions with various ice masses (Structure with BHD)	138
Figure 7-16 Internal energy for collisions for 1000-tonne bergy bit with and without BHD	139

Figure 8-1 Equivalent plate thickness for stiffened plate [69].....	141
Figure 8-2 Smearred structure with equivalent plate thickness	141
Figure 8-3 Internal energy for smearred structure (small contact area).....	142
Figure 8-4 contact force for smearred structure (small contact area).....	142
Figure 8-5 Comparisons among various frame effectiveness in contact force (1500-tonne scenario).....	144
Figure 8-6 wedge cutting parameter definition for Equations 7 and 8	145
Figure 8-7 Hole and wedge schematic.....	146
Figure 8-8 Contact force for various simulated wedge cutting.....	148
Figure 8-9 comparisons of contact force in wedge cutting and ice impact with the small contact area	149
Figure 8-10 Geometry of the simulation with the initial opening	151
Figure 8-11 Contact force for various structural arrangement (1500-tonne bergy bit) ...	152

Chapter 1 Introduction

1.1 Background

The Arctic waters have always been a tempting area of the world for shipping and oil and gas companies. There are oil and gas resources present, and shipping lines look at this region as an alternative path for shipping from East Asia to Europe and North America. The northern part has a harsh environment for marine operation and extraction of petroleum, and this makes it expensive and, in some seasons, impossible for operation.

Climate change and global warming have caused many changes in the earth's environment. Arctic regions are among the most sensitive areas in the world and have been going through dramatic changes. Summer ice in September has been reduced dramatically in the last decades. Although this may create some long-term problems for the planet, for shipping and oil companies, this means new shipping lines will be opened for trade, and further oil and gas explorations may becoming feasible.

Figure 1-1 shows the proposed shipping lines through arctic waters, among which the North-West Passage (NWP) is of high importance for Canada.

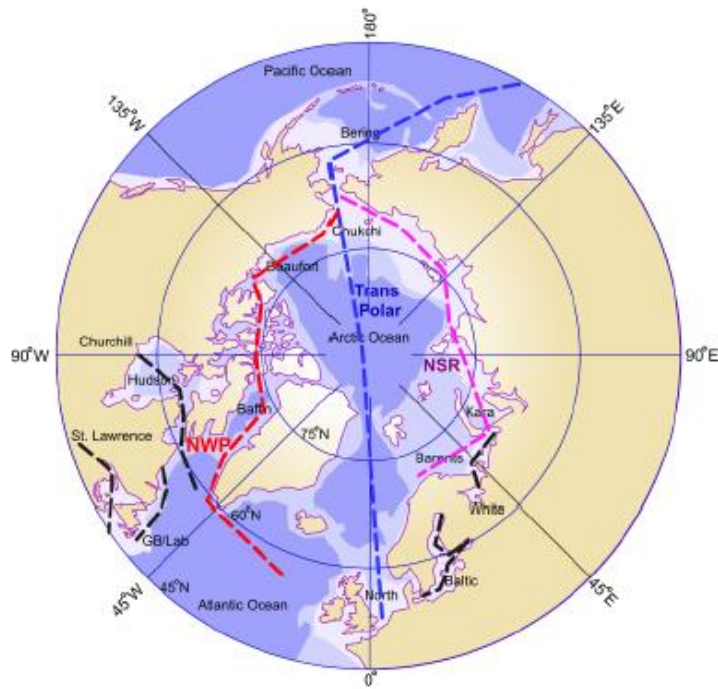


Figure 1-1 Possible shipping routes in arctic waters [1]

Some estimations indicate the multi-year ice in the arctic waters will vanish in the near future. Johannessen et al. [2] predicted ice-free seasons in arctic by the end of this century, and Holland et al. [3] anticipated such scenario by 2040 (as cited in [4]). This implies that the northern routes would be safer for shipping and other commercial activities such as tourism and oil and gas explorations. Consequently, the possibility of ice and ship collisions will escalate due to increases in shipping traffic.

Ice class vessels have the capacity to withstand the ice impact, and the survivability index of these vessels is remarkably higher compared to non-ice class ships. Although the design methodology is different for various structural design standards (IACS rules, Baltic rules, etc.), the ice load has been considered in the design phase, even for low ice-class ships. As for non-ice class ships, even small bergy bits in rough sea conditions could cause severe

damages to the structure. Therefore, the assessment of non-ice class ships' performance in collision scenarios with ice is worth investigating.

1.2 Problem statement

Available design standards for ice-class ships are based on a limited number of collision scenarios. Ramming and glancing impact are common collision scenarios for ice breakers, and Baltic class ships are designed to navigate in a channel of broken ice.

Marine traffic growth in Arctic waters will lead to a higher possibility of non-ice class ships colliding with ice. Collision with ice would be different than the collision scenario for ice-class ships for non-ice class ships in open waters. Non-ice class ship collision with ice is most likely occur in open waters with a piece of ice that is not large enough to be detected by radar. There is a possibility to use the available formulas for glancing impact, such as Popov's method to calculate the impact force and use the force to estimate the structural response.

Collision with the forepeak structure could cause severe damage to the structure, but it is unlikely to lead to extensive flooding of the vessel's compartments. Sliding collision in the mid-body of ships, where large cargo holds are located, is critical from watertight integrity and damage stability perspective. Due to the complexity of sliding collisions, there is no available design standard, and therefore, it is necessary to study the effect of sliding collisions on the structural performance of non-ice class ships. The novelty of the present research is the investigation of the structural response in the sliding impact scenario.

From the shipping industry's point of view, it becomes a question of whether it is possible to use non-ice class ships (or light ice-class ships) in specific regions where sea ice and glacial ice fragments may present. Allowing ships to access these areas could have remarkable benefits for shipping companies if they can use their non-ice class ships in new routes with some considerations.

One of the critical issues in polar navigation is damage stability and survivability. The expected extent of damage is a controlling parameter in the ship's watertight compartment arrangement. International Maritime Organization (IMO) conventions such as SOLAS [5] and MARPOL [6] deal with damage stability of various types of vessels, e.g., passenger ships, cargo vessels, and oil tankers. Also, IMO's Polar Code [7] provides a deterministic approach that gives a damage length as a portion of ship length to be contemplated in the damage stability for certain types of ships.

The question is whether the damage length prescribed by the Polar Code for collision with ice is a reasonable value for non-ice class ships that might encounter with ice in the emerging shipping routes. If the extent of damage is larger than the values in the Polar Code, it is essential to investigate the size of the damage in ice collision with damage scenarios in other IMO conventions and codes. Previous research has been focused on short glancing impact; however, the sliding impact could have severe repercussions (as seen in the Titanic accident based on the number of flooded compartments [8]).

Single side ships are vulnerable to extensive flooding after the rupture in the hull; thus, the focus of the simulations is single side ships. Three double hull structures are also investigated to cover the common structural configurations for merchant ships.

1.3 Thesis structure

This thesis is comprised of nine chapters to address all aspects of the research. In Chapter 1, the background and problem statement, in addition to research significance, are presented.

Chapter 2 provides a literature review on ship-ice collision mechanics and the application of the FE technique in analyzing ship and ice impact.

Chapter 3 consists of a detailed review of the ship and iceberg collision statistics. Moreover, an acceptable range for ice size is selected based on an assumed impact scenario.

Chapter 4 describes ductile fracture and the methodology to implement it in FE simulation. The material model and fracture criterion that were used as input in LS-DYNA is presented in this chapter.

In Chapter 5, the process of creating FE models from ship geometries to a FE model is discussed. Important FE features such as element size, boundary conditions, ice load, etc., are presented in this chapter.

Results and discussions for various structural arrangements and simplified models are presented in Chapters 6 to 8.

Finally, in Chapter 9, the conclusions, recommendations for future research and limitations are included.

1.4 Research outcomes and significance

In the previous research, the structural response of non-ice class ships to collisions with ice has not been studied, and it is of high importance for shipping companies, classification societies and flag states to know the structural capacity of non-ice class ships. This research seeks to discover the fracture behaviours of merchant ships in a particular collision scenario that has not been investigated so far.

In addition, it is intended to utilize the results of the FE simulation to discuss the current damage stability requirements and decide on whether any alteration is needed to include ice damage cases for damage stability calculations.

Finally, for probabilistic models, it is necessary to use simplified formulas for plate rupture. Assessing the accuracy of current empirical formulas in estimating ice-ship collision rupture force is another outcome of this research.

Chapter 2 Literature Review

2.1 Introduction

Naval architects and offshore engineers have to deal with uncertainties in design loads such as those caused by ocean waves. These uncertainties increased noticeably for projects in Arctic waters as a result of low temperature and ice impact possibilities. International safety organizations, countries with interest in arctic water and companies tried to overcome these uncertainty over the past decades from which the design standards have developed.

Design standards are divided into two groups, offshore structure's standards and ship's standards and regulations. Offshore structure design standards are comparatively different than the rules that common in ship design and consequently in this chapter the focus is on ship structural standards.

Previous research has been focused on short glancing impact; however, the sliding impact could have severe repercussions (as seen in Titanic accident). In this research, it is aimed to investigate the sliding collision between ice and side structure of non-ice class vessel with the help of finite element (FE) simulation. This literature review divided into three sections: classification and standards, collision mechanics, and ship-ice impact simulation with FE tools.

2.2 Classifications and national standards

Ship structural design is currently based on the international and national standards and regulations. These standards categorize into two main groups as listed below [1]:

1. Arctic Rules

- ASPPR Rules
- Russian Rules
- IACS Polar Rules
- Classification Society Rules

2. Sub-Arctic Rules

- Baltic Rules
- Classification Society Rules

For each group, a different impact scenario with ice is contemplated for ice load calculations. As discussed by Daley [1], the Arctic rules are based on heavy ramming forces on the fore shoulders and the impact lasts for less than a second. Glancing impact is relevant for vessels that operate independently in heavy ice conditions. Baltic rule is only applicable for ship operations in a channel made by an ice breaker. Thus, the sliding impact has not been included in the current standards.

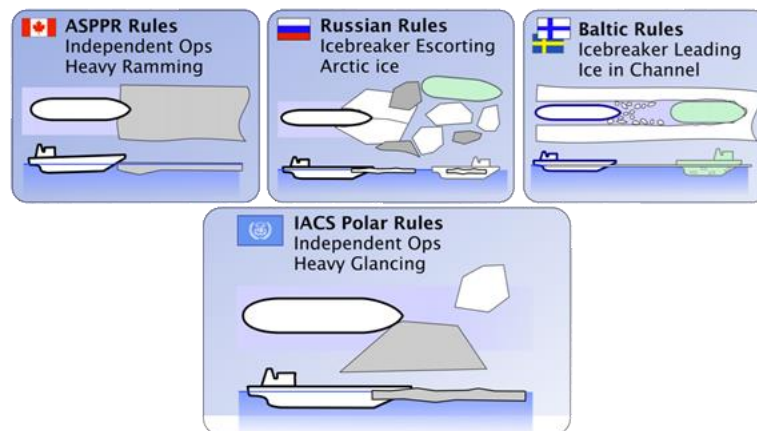


Figure 2-1 Various arctic and sub-arctic rules design ice load [1]

This approach is practical for ice-class ships, but the ice-class ships' design approach is different from ordinary vessels. Polar vessels are designed based on the plastic design approach, and ordinary vessel design methodology is according to elastic design.

The mentioned differences and lack of any current design standard is an indication that there is a necessity to study the sliding impact in more detail.

2.3 Collision mechanics

Ship collision is a complex phenomenon that includes many parameters such as hydrodynamic effects, motion of two (or even more) objects and their interactions and structural failure and fracture. Including all of these parameters in one simulation requires remarkable efforts and computational capacity that is impossible for many research and engineering application. Generally, the collision of ship to ship or ship to ice consists of two parts, (1) external mechanics and (2) internal mechanics. Internal mechanics focuses on the behavior of a structure subject to application of accidental loads that could be collision force due to the impact of another marine structure, ice or seabed.

External mechanics deal with the hydrodynamic effects, interaction and motion of the objects. As for ice collision, it is necessary to have information on the amount of energy that dissipates due to the motion of the ship and ice. In addition, the energy that dissipates because of ice crushing should be calculated in order to calculate the available energy that causes structural damage. It should be noted that there are two assumptions for applying such an approach. Firstly, the added mass could be considered constant and then the duration of collision is short [9].

The work done by Popov et al.[10] was one the first attempts to solve the external mechanics of ice and ship collision. As it is discussed by Daley [1] Popov's model was based on Kheysin theory [11] and it was updated by Daley [12]. This model simplified the collision into one-dimension problem that is noticeably easier to derive analytical formulation for. In this approach, the collision is short with constant added masses (for surge, heave, sway, roll, pitch and yaw), and no friction (details of Popov approach is presented in [1]). It is worth mentioning that other research also showed that the effect of friction in impact energy is quite small and can be neglected [13].

Matskevitch [14], [15] formulate the ice load in an eccentric collision scenario in the form of linear and non-linear closed forms. It was observed that in this collision scenario, the impact load would be decreased compared to a head-on collision. In [14], an approximate closed-form of maximum impact force due to the eccentric impact has been proposed that is conservative compared with numerical analysis. According to these references, eccentric collision occurs more often than head-on collision and should be considered when probability analysis is conducted to assess the safety of the structure.

As it is noted by Liu and Amdahl [16], the 6DOF motions of two objects in the collision are to be considered since rotations of ice (yaw, pitch, and roll) influence the dissipated energy that directly changes the dimensions of the rupture area. According to [16], previous research (such as [14], [15]) did not consider this parameter. This is also a valid point for the research of Pedersen and Zhang [17]. Therefore, Liu and Amdahl [16] proposed a 3D formulation for ship collision, with external mechanics based on Stronge [18]. They formulated dissipated energy for striking and sliding cases for 2D and 3D applications. The

point is that the 3D model is important when the collision is taking place in the forepart of the vessel. That is the reason why Pederson and other researchers worked on 2D formulations. The collision between ships is more severe when it happens in the midship area where the side structure is vertical, and 2D assumptions are acceptable and reasonable. Liu and Amdahl [16] compared the results for 2D simulation with Pedersen and Zhang's work [17], and it was similar. For the 3D case, the results of the analytical simulation were compared with Tabri et al. [19]. The interesting point is that the result for analytical and experimental tests is similar to the prediction of 2D formulas. In other words, the introduced energy vector in the yaw direction has little impact on the total dissipated energy for this specific model test.

Liu and Amdahl [16] also applied the new formulation to the iceberg collision and concluded that the results are lower than predicted values by Pedersen and Zhang [17]. This was predictable since, in the 3D model, the motion in yaw direction will transfer a part of the kinetic energy to motion. It could be concluded that the 2D formulas are conservative in this type of analysis. Thus, based on the level of the accuracy needed for the project, one of these two methods could be applied for energy dissipation evaluation.

It is of high importance to bear in mind that the iceberg shape and mass are among the most critical uncertainties in ship-ice collision assessment. According to the literature, the work done by Fuglem and Muggeridge [20] could be referred to as a reference to deal with this issue. In this regard, Liu et al. [21] provided recommendations for adequate iceberg modeling. They demonstrated that there is no need to have exact details of the whole shape of the iceberg since only the small part of the iceberg will be contributed in dissipated

energy, and consequently, the local feature of iceberg in the place of impact is more important. They utilized a simple formulation according to Liu and Amdahl [16] (without considering the added mass for ship and iceberg) for calculation of maximum energy dissipated (E_0). It is only related to the mass and speed of the vessel and the iceberg. According to Liu et al. [21], the energy dissipated could be calculated with Equation 1:

$$E = \xi E_0 \quad \text{[Equation 1]}$$

Defining ξ is a difficult task because it is related to many parameters in a collision, such as the position of the collision, frame angle, the relative center of gravity, etc. According to [16], they consider 0.3, which is a conservative assumption. They concluded that this assumption leads to similar dissipation energy for accidental collision load as per current standards.

2.4 Ship-ice impact analysis: FE approach

Structural performance of marine structures in the collision and grounding accidents has been investigated for decades due to its importance in marine safety and environment protection. Ship collision and grounding have been studied extensively in the previous research. Another area of interest in ship collision is the ice and ship impact simulation that is of high importance for countries and companies with interests in Arctic and Antarctic waters.

In any research regarding the collision, three methods have typically been applied by researchers:

- Analytical methods
- Experimental methods
- Finite element method

Large scale experiments are expensive and generally it is challenging to control the governing parameters. As for laboratory experiments, there are difficulties to interpret the results to explain an actual large-scale problem. Due to the stated issues, finite element methods have been used in many studies in the ship structural assessment in collision and grounding. Two different approaches is common in FE simulation of collisions, because a collision has external and internal components, as a result. In the first approach, the hydrodynamic effects are included explicitly by modeling fluid around the structure. It is a common practice to separate the hydrodynamic effects from the analysis and only investigate the structural response in any load level. The presented work and literature review, is based on the second approach.

Ice collision analysis has even more challenges in experimental and numerical investigations to overcome compared to ship-to-ship collision. Ice is a complex material whose mechanical properties depend on many parameters such as age of ice, temperature, and salinity. These mentioned parameters cause high level of uncertainties in any simulation. There are limited numbers of large scale ice load measurements such as measurements done with icebreakers Louis S. St. Laurent (1977), Canmar Kigoriak (1980), USCGC Polar Sea (1982), Hobson's choice ice test (1990) (as cited by Daley [1]), Agulhas II [22], and CCGS Terry Fox [23]. Other than these large-scale tests, ice- structure

interaction tests have been limited to small-scale laboratory experiments to validate FE simulations.

Kim et al. [24] investigated the ice cone quasi-static load on a large scale grillage of a 10000-ton PC6 ice-class vessel. Nonlinear FE simulation was compared with experiment results and showed reasonable accuracy in predicting structural response. They proved the adequacy of IACS design standard and showed that the structure has a high reserve strength after design point that could be used to have lighter structure without impairing the safety of the vessel. It was described that the structure could sustain even more load if the structure has prior deformations.

Ice modeling and including correct failure criterion to model the ice behavior is crucial. Kim [25] implemented two different ice material models for different parts of an ice cone based on Gagnon's research [26], [27]. The focus of this research was on the ice pressure behavior since the plate in contact was very thick and rigid. Two different ice cone crushing experiments in small and large dimensions were carried out and the results showed that the proposed ice model could adequately capture the ice pressure distribution in the contact area, and load-displacement relationship as well. Bae et al. [28] studied the ice pressure load of level ice on parallel body (in three different locations: On the plate, stringer and web frame) of a chemical tanker in a channel made by an icebreaker. They modeled the ice with Gagnon ice model and defined three ice shapes to compare the contact shapes in structural response. The material modeling of ice and steel characteristics in low temperature were indicated as key parameters in analysis. Finally they suggested to include the effect of each structural member in crashworthiness in the design of the structure.

The effect of sliding load has not been investigated as extensively as stationary loads and glancing impact. Quinton [29] and Quinton et al. [30] simulate the effect of sliding load with a rigid indenter and ice cone, respectively. Quinton [29] showed that the structural response subjected to IACS stationary design load differs from moving load; however, the difference will not be the same for all polar ship categories (PC1 to PC7) and structural configuration (T-bar and flat bar beams). In the second paper [30], they included the effect of ice by substituting rigid indenter with an ice cone. The results were similar to [29], which indicates that the structure capacity in moving and stationary loading condition is different and the stationary load used in IACS Polar rules is not as conservative as it should be. A similar idea was presented in [31].

Kim and Quinton [32] investigated the moving ice load with both experiment and FE simulations. They concluded that the tangential ice load is comparatively lower than normal load and could be neglected. The FE model with ice model suggested in [25] simulated the ice pressure on the plate with acceptable accuracy.

In both grounding and collision with ice, the structural response is sensitive to the indenter geometry. Gao et al. [33] compared the impact force and energy dissipation in a collision accident of an FPSO with five ice indenter shapes. The ice material modeling has a noticeable role in the FE results. Crushable foam and elastic-plastic model (with element erosion) were used separately to compare the results. As for the crushable foam, the structural response is not sensitive to the shape of the ice because of the stress and volumetric strain. However, in the elastic-plastic model the results are sensitive to the shape of ice. For example, the sharp geometries crush easily compared to sphere or blunt shapes.

The sphere shape concluded to cause the most structural damages compared to other investigated shapes.

In addition to collision impact load on structure, the effect of the low temperature on structural response is critical. Park et al. [34] worked on the effect of the low temperature and aging on the ultimate longitudinal strength of a double hull oil tanker with ALPS/HULL software. They conducted tensile tests on various below zero temperature (up to -80°C) and modified steel properties in their assessment. They concluded that the ultimate longitudinal strength of the ship increases as the temperature decreases. Park et al. [35] simulated the effect of lower temperature and aging of the same vessel as discussed in [34] in collision. Due to the increased in the material strength as a result of low temperatures, the simulations showed that the lower temperature compensated the aging effect.

In grounding scenarios, ship bottom structure gets in contact with seabed. However, in Arctic waters ships might encounter to a grounded iceberg. Prabowo et al. [36] studied this scenario with FE simulation. They modeled 17,000 ton chemical tanker without any ice capacity. Three impact cases were investigated: on center girder, side girder and between girders. They concluded that in the case of grounding the worst rupture occurs in scenario where the grounding happens between girders.

Ince et al. [37] studied the ice impact on steel plate with FE and drop test. The intention of this study was to validate the ice model (KOSORI) proposed by Ince et al. [38]. The proposed model has a constitutive model for ice and a fracture process that works with a cohesive zone approach. They conducted a series of experiments with an ice cone and a rigid cone and compared the results. As it was predictable, the results varied. The FE

simulations showed that the KOSORI ice model simulated the ice and structure interaction with a good accuracy.

2.5 Summary

Increasing marine traffic in the polar waters in the future will increase the chance of ice collision with ships that are not designed to withstand such accidental limit state. From a damage stability perspective, the sliding collision and a long crack on the side plate could lead to sinkage and total loss of ship. Previous research indicated that the structure fails on a lower load level in moving load scenario compared to normal impact. The sliding ice-ship collision, however, has not been studied in-depth for neither ice-class nor non-ice class ships. Due to the importance of this topic and the lack of knowledge in this field, this research aims to investigate the load bearing capacity of non-ice class ships in sliding collision with bergy bits.

Chapter 3 A Review of the Ship and Iceberg Collision Statistics and Possible Ship-Ice Collision Scenarios

3.1 Introduction

This chapter presents a review of the National Research Council Canada (NRC) database on iceberg-ship collision. In sections 3.3 and 3.4, the impact scenario was defined and based on available data and experts' opinion, a range for ice mass was defined to be used in FE modelling.

3.2 Review of NRC database on iceberg-ship collisions since 1950

Collision with ice is one of the main hazards in arctic operation and has caused financial and environmental issues in addition to the loss of lives. Information on damage cases is scarce in this field of engineering, because in many cases, damages are limited to dents and not holes or rupture; therefore, no immediate repair or assistance would be required. This means that damages would not be reported to authorities; consequently, the lack of enough data makes it complicated to have a complete picture of the total accidents. The main intention of this research is to calculate the damage extent in ice collision; therefore, it is necessary to review the collision statistics to obtain an understanding of previous accidents.

National Research Council Canada (NRC) has created a database according to reported accidents. This database's focus is on iceberg collisions in North Atlantic off Newfoundland and Labrador. It is noted by NRC that this report neglected several incidents around Greenland and the fiords of Alaska [39]. This database is useful in understanding accidents from different angles such as the type of vessels that had accidents or the

geographical features of the accidents' locations. In this review, accidents from 1950 have been reviewed in order to come up with a clear view of the location of damages in ship structure, type of damages and distribution of various damage types with regard to the type of the ships.

3.2.1 Database structure

As noted, the database has been developed by NRC, and the purpose is to give an insight into the features of accidents from different aspects. Information such as the type of the vessel, dimensions of the vessels, location of damage, type of damage, consequences of the accident (loss of cargo and human lives and pollution), etc. This database consists of 681 accidents' information from the 17th century, and for a limited number of these accidents, the accident report is also included. However, in this review, accidents from 1950 have been considered since we aim to look at steel ships with structures and designs as similar as possible to current shipbuilding practice.

As noted, the accidents which have been reviewed are from 1950 up to now, which are 92 cases in total. It is aimed to focus on the following parts of the database:

- Location of damage in the hull
- Number of accidents with respect to the types of ships
- Types of damages
- Distribution of types of damages with respect to the types of vessels

The reason for selecting these parts of the database is that it could give an overview of the structural damages in the previous collisions. Due to the importance of non-ice class ships

in this project, with the exception of the location of damage in the hull, data for icebreakers and ice-class ships are presented separately.

3.2.2 Location of damage in the hull

Knowing the location of damages on the hull can clarify which sections on the ship hull are more vulnerable to ice impact. From this point of view, the main hull has been divided into three parts, aft, mid and fore sections as defined in the following.

Generally, classification societies consider $0.125L$ from the fore perpendicular as the forward section and consider higher scantlings for this region (for the bottom, side and deck structures). Therefore, it was assumed that the damages in the forepeak area happened in this boundary.

The aft part of the ship is defined from the transom to the forward bulkhead of the engine room. Thus, it is assumed that any damage in this region has happened in the aft part of the vessel. It is worth mentioning that this assumption is not valid for offshore supply vessels (OSVs) as the engine room is a noticeable part of the midship area. However, only one collision of OSV with an iceberg has been recorded that caused the flooding of the compartment next to the engine room, which is considered to be in the midship region.

The whole region between these two boundaries is considered as midship area. Midship area for cargo ships and oil tankers is allocated for cargo, and any damage to this part would have drastic financial and environmental consequences.

Based on the mentioned categories, the collision location has been reviewed, and the summary of the results is presented in Table 3-1. This table is based on the information on damage location and available damage description reports provided by the database.

Table 3-1 Damage location of iceberg-ship collisions on ship hull

	Aft	Midship	Fore	Unknown	Total
Number of accidents	8	9	37	38	92
Percentage	8.69	9.78	40.22	41.3	

The main problem with the result is that the majority of data is vague with respect to the position of damage in the hull. As it is clear from Table 3-1, for the majority of accidents, there is no record on the position of damage, and it has a considerable impact on the information that is available. If we do not consider this part of the data and look at the information that we could refer to them, the percentages will be as shown in Table 3-2.

Table 3-2 Damage location of iceberg-ship collisions on ship hull (excluding unknown cases)

	Aft	Midship	Fore	Total
Number of accidents	8	9	37	54
Percentage	14.81	16.66	68.52	

It is clear that the majority of accidents happened in the fore part of the vessels, with close to 70 percent of total accidents. This was predictable since IACS polar requirements have been formulated based on the glancing impact of the bow shoulder with ice, as shown in

Figure 3-1. It seems that as opposed to ship–ship collisions, the midship area is not critical with respect to iceberg collision. However, for any risk analysis, the consequence is as important as the probability of occurrence. In one case two cargo holds have been flooded, and in other case, 8 out of 11 cargo tank was damaged. Therefore, in mid-body collision, the consequences might be more severe than forepeak collision.

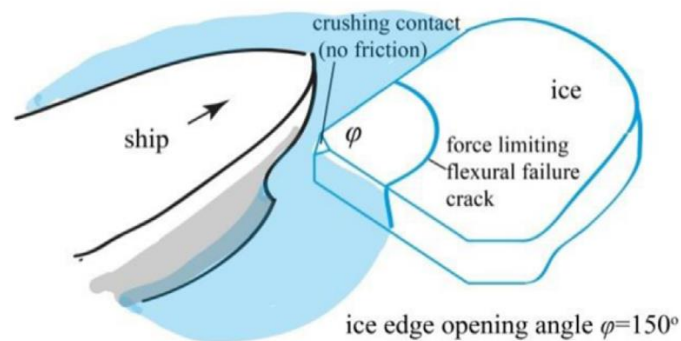


Figure 3-1 Ship-ice impact scenario according to IACS requirements for polar class ships [40]

For aft impacts, it might be caused by a delayed reaction to icebergs. In other words, the crew tried to steer away from the iceberg, but due to delay, the aft part of the ship hit the iceberg. This also might be caused by turning in an ice channel or backing in case of stopping in ice.

3.2.3 Number of accidents with respect to the types of ships

Another useful characteristic of the database is the types of vessels engaged in accidents. The overall information has been summarized in Table 3-3 and Table 3-4 for non-ice class ships and ice-class ships, respectively. There are two cases in which the type of the vessel is the catamaran, and we assumed that these were passenger ships because this type of

structure is more common in passenger ships than cargo vessels. In both categories, fishing vessels had the highest values, and in non-ice class ships, cargo ships and for ice-class ships, both cargo and passenger ships had the second-largest numbers.

Nearly a quarter of accidents happened to fishing vessels, which is around the sum of cargo ships, tankers and OSV/Tug incidents during the same period. It might stem from the fact that the number of fishing vessels navigating in the polar and near-polar area is higher than other types of vessels, in addition to lower structural design standards.

OSVs (especially those with towing class notation) and tugs are generally designed with robust and heavy main hull structures, which might be why the number of accidents is negligible for these types of ships. The other reason might be the higher maneuverability capacity of these ships than the other types of vessels that can help the master to avoid the collision.

Table 3-4 illustrates that the number of accidents for icebreakers or ice-class ships. Numbers are remarkably lower than non-ice class ships, which means that these kinds of vessels have enough structural strength for such impacts, and therefore less vulnerable to structural failure due to the ice impact.

Table 3-3 Number and percentage each type of the vessels engaged in iceberg impact for non-ice class ships

Vessel Type	Fishing Vessels	Cargo/ Container Vessels	Bulk/ Ore Carrier	Tanker	OSV Tug	Passenger Ferry	Others	No data
Number of Accidents	20	13	14	5	2	12	5	9
Percentage in Total	28.17	18.31	19.72	7.04	2.82	16.90	7.04	12.68

Table 3-4 Number and percentage each type of the vessels engaged in iceberg impact for ice-class ships

Vessel Type	Fishing vessels	Cargo/Container Vessels	Bulk/Ore Carrier	Passenger/Ferry	Icebreaker	Total
Number of Accidents	4	3	1	3	2	13
Percentage in Total	30.77	23.08	7.69	23.08	15.38	

3.2.4 Types of damages

Table 3-5 compares the number of various damages that have been reported for the accidents in this period. Similar to other presented data, a noticeable percentage of damages is not precise. One might assume that because these damages were minor and the damage reports were not being reported adequately.

Table 3-5 Number and percentage each type of damages caused by iceberg collision for non-ice class ships

Type of damage	Dent	Crack	Puncture	Hole	Large Hole	Crush	Sinkage	No data	No damage
No. of Occurrence	7	8	8	8	11	3	17	17	1
Percentage	7.61	8.70	8.70	8.70	11.96	3.26	18.48	18.48	1.09

Table 3-5 is of high importance because it shows that in half of the collisions, the ship's watertight integrity has been impaired. This has led to the sinking of the vessels in 22 percent of accidents. It should be noted that in the NRC database, there is no clear definition

for the defined categories of damages that might be necessary for the next step to make these categories more clear.

Table 3-6 gives the same information presented in Table 3-5 for ice-class ships. Although the number of accidents is remarkably lower than non-ice class ships, damages were noticeable. About 60 percent of accidents ha led to different levels of impact on the watertightness of compartments.

Table 3-6 Number and percentage each type of damages caused by iceberg collision for ice-class ships

Type of damage	Dent	Hole	Large Hole	Crush	Sinkage	Unknown	Crack/ Puncture/ No damage
No. of Occurrence	2	2	1	1	3	3	0
Percentage	16.67	16.67	8.33	8.33	25.00	25.00	0.00

3.2.5 Distribution of types of damages with respect to the types of vessels

The other important item to consider is the types of damages with respect to the types of vessels. As it has been presented in Table 3-7 and Figure 3-2, fishing vessels have the highest number of sinking among other types of ships. As previously stated, the design standard for fishing vessels is relatively lower in comparison with other vessels, especially in damage stability (damage stability calculation is not mandatory for fishing vessels). The critical point about cargo ships is that the high number of sinking accidents. It might be because the keel-laying date of all of sank vessels (with the exception of one vessel for which the keel-laying date is not clear) is before the date that SOLAS made damage stability mandatory for cargo ships.

Table 3-8 and Figure 3-3 compare frequent types of damages for each type of ships in accidents reported for ice-class vessels. Sinking has happened only for fishing and passenger vessels. As stated, damage to ice-strengthened vessels is lower than non-ice class ships. However, fishing vessels and passenger ships had accidents that led to sinking and total loss. Large holes had not been reported, but the hole for fishing vessels and cargo ships are recorded in the database.

Table 3-7 Distribution of various damages for each type of the vessels damaged by an iceberg for non-ice class ships

	Fishing	Cargo/ Container	Bulk/ Ore	Tanker	OSV/ Tug	Passenger/ Ferry
Dent	2	2	0	0	0	2
Crack	0	1	2	2	0	0
Puncture	0	2	1	0	0	3
Hole	2	0	2	1	1	0
Large Hole	1	1	6	0	0	1
Crush	1	0	0	1	0	0
Sinkage	9	5	0	0	0	1

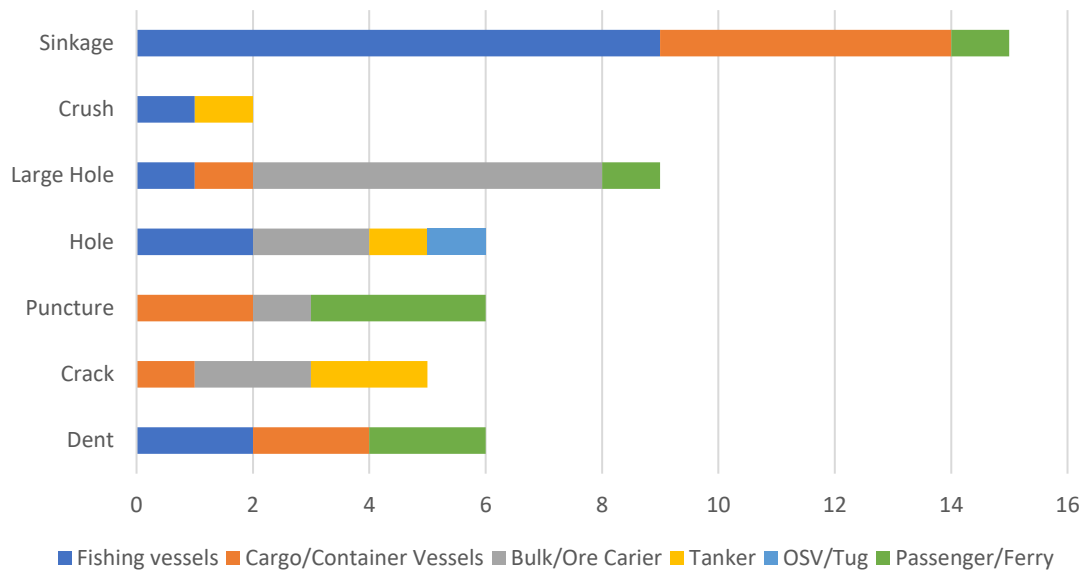


Figure 3-2 Distribution of various damages for each type of the vessels damaged by an iceberg for non-ice class ships

Table 3-8 Distribution of various damages for each type of the vessels damaged by an iceberg for ice-class ships

	Fishing vessels	Cargo/Container Vessels	Bulk/Ore Carrier	Passenger/Ferry
Dent	1	1	0	0
Crack	0	0	0	0
Puncture	0	0	0	0
Hole	1	1	0	0
Large Hole	0	0	0	0
Crush	0	0	1	0
Sinking	2	0	0	1

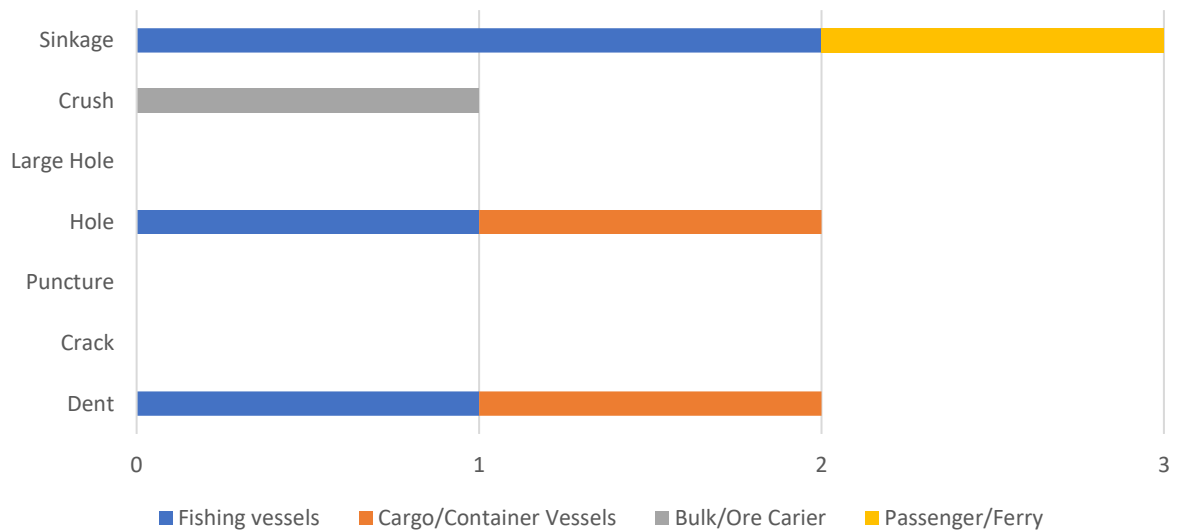


Figure 3-3 Distribution of various damages for each type of the vessels damaged by an iceberg for ice-class ships

It is noted that for the majority of accidents, the data on the damage extent is unclear. Table 3-9 illustrates the data available on the damage information for accidents. Based on Table 9, the histogram for the l/L (damage length/length of the vessel) has been created and shown in Fig.4. it is similar to lognormal distribution with high standard deviation and skewness; however, it is evident that much more data is required for more accurate estimation. It could be seen that the $0.02L$ range has the highest frequency among other ranges. It could also be seen that the $0.06L$ covers almost all accidents listed. Polar code requirement for damage stability calculation is specified the damage extent as follows [7]:

“The longitudinal extent is 4.5% of the upper ice waterline length if centred forward of the maximum breadth on the upper ice waterline, and 1.5% of upper ice waterline length otherwise, and shall be assumed at any longitudinal position along the ship's length.”

These I/L ratios are similar to what is shown in Figure 3-4, even though this histogram is based on the limited number of available data. The probability that the damage length to vessel length exceeds 4.5% of the vessel length is 27%. This is unrealistically high that stems from the limited number of recorded accidents.

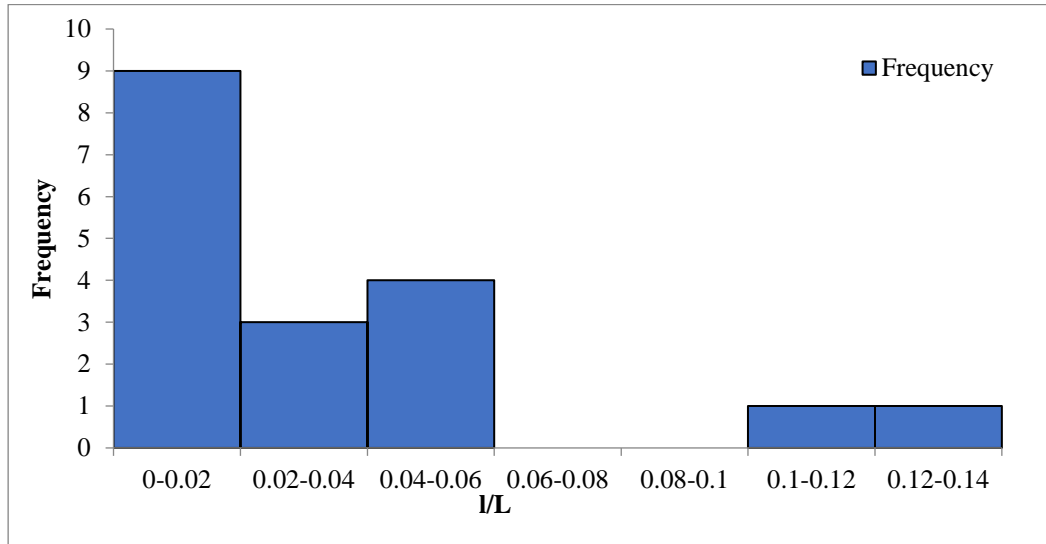


Figure 3-4 Damage length to length of the vessel histogram according to NRC database

Finally, it should be noted that these limits (even 0.06L) are lower than other mandatory requirements for damage extent for damage stability calculations. For instance, the required damage extent for OSVs according to amendments to the guidelines for the design and construction of offshore supply vessels, 2006 (resolution MSC.235(82)) is 0.1L for vessels with a length of 43m and upward (keel-laying date after 22 November 2012). However, for modern designed non-ice class ships that might encounter ice impact, there is a need to assess the probable structural impacts and their consequences (from structural and damage stability points of view) in order to adequately address this issue.

Table 3-9 Damage dimensions available in NRC database

Interaction Event ID (NRC Code)	Vessel Type	Damage Location	Damage Type	D _L * (m)	D _H ** (m)	L*** (m)	Ice Class
7	Fishing trawler	Aft	Sinkage	---	1	56.1	Yes
17	Tanker	Fore	Crack	6	6	272	No
18	Ore / Bulk / Oil Carrier, Tanker	Fore	Small puncture	0.3	0.3	281.1	No
19	Bulk Carrier	Fore	Large hole	3	0.5	222.49	No
20	Container	Fore	Large hole	9.6	---	231.6	No
21	Bulk Carrier	Fore	Large hole	45	6	229.5	No
22	Ore / Bulk / Oil Carrier, Tanker	Fore	Cracks	7	3	250	No
23	Offshore Research & Survey	Midship	Hole	4.5	---	85.04	No
30	Passenger / Cargo	Unknown	Unknown	0.4	0.04	32.72	Yes
41	Passenger / RoRo Car Ferry	Fore	Sinkage	1	---	106.99	Yes
44	Bulk Carrier	Fore	Large hole	10.5	7.5	186.5	No
46	Bulk Carrier	Fore	Large hole	4	---	---	No
50	Passenger	Fore	Large hole	4.6	2.1	160.2	Yes
59	Ore Carrier	Fore	Large hole	3	2.4	155.7	No
62	Bulk Carrier	Fore	Hole	2.1	0.1	209.5	No
67	General Cargo	Fore	Hole	1.4	0.45	135.4	Yes
653	Bulk Carrier	Fore	Unknown	24.4	3.35	213.37	No
662	Bulk Carrier	Fore	Cracks	15	9	270	No
693	Passenger	Unknown	Puncture	0.076	---	47.55	No
729	Passenger	Fore	Large hole	2.5	0.8	195.7	No
*Damage Length ** Damage Height *** Length of Vessel							

A review of the NRC database showed that available data for damaged vessels is limited for non-ice class ships. Consequently, statistical analysis would not be an appropriate method to estimate the damage length in collision with ice. Therefore, simulations are required to study the fracture length in the hull. Ice shape, size, and velocity are the main

parameters necessary for the FE simulations. In the following sections, the discussions about the selection of ice features and impact scenarios are presented.

3.3 Ice type for the collision simulation

According to the [41], non-ice class ships cannot navigate in areas with a high concentration of ice. However, these vessels could navigate with low speed in open pack ice concentrations of 6/10 or less without being in contact with all ice in the path. Figure 3-5 compares the various ice concentration conditions. Even in low ice concentration conditions, navigators constantly watch for possible ice threats and maneuver with caution. Reducing the speed and changing course to prevent the collision and limit the collision force are some of the strategies that are implemented in ice navigation.

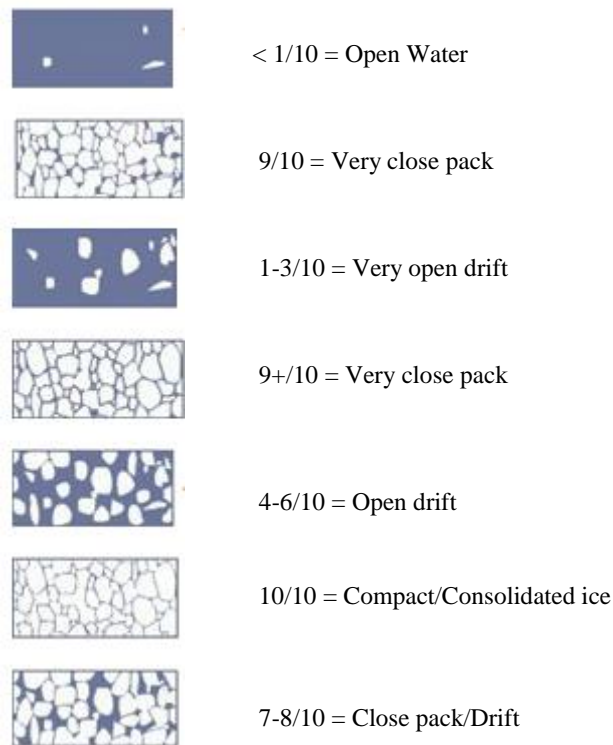


Figure 3-5 Ice concentration interpretation [41]

Figure 3-6 depicted various maneuvering in ice based on ice concentration. These maneuvers are for the cases that the navigators are aware of ice, and they continuously avoid it or try to limit the collision force.

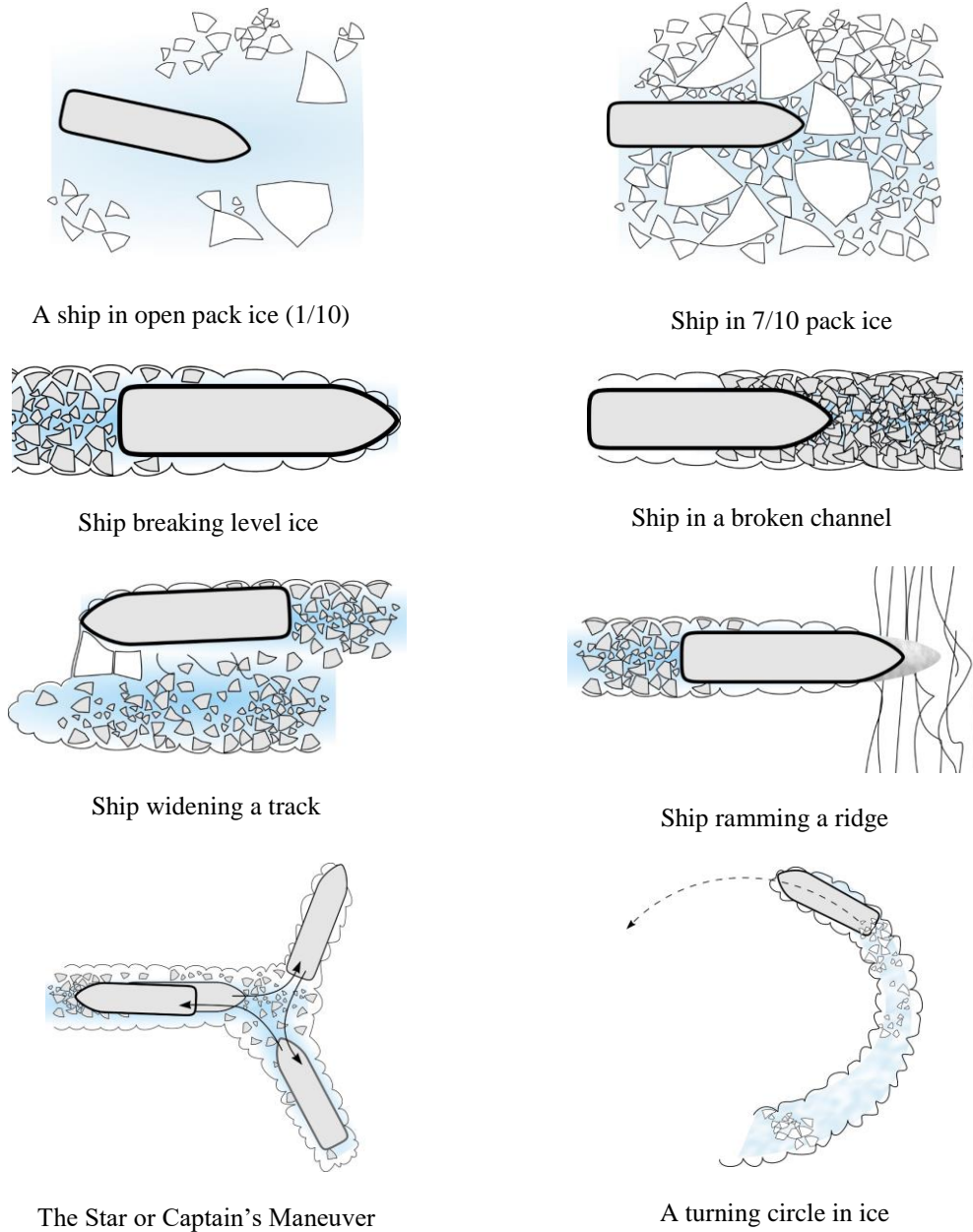
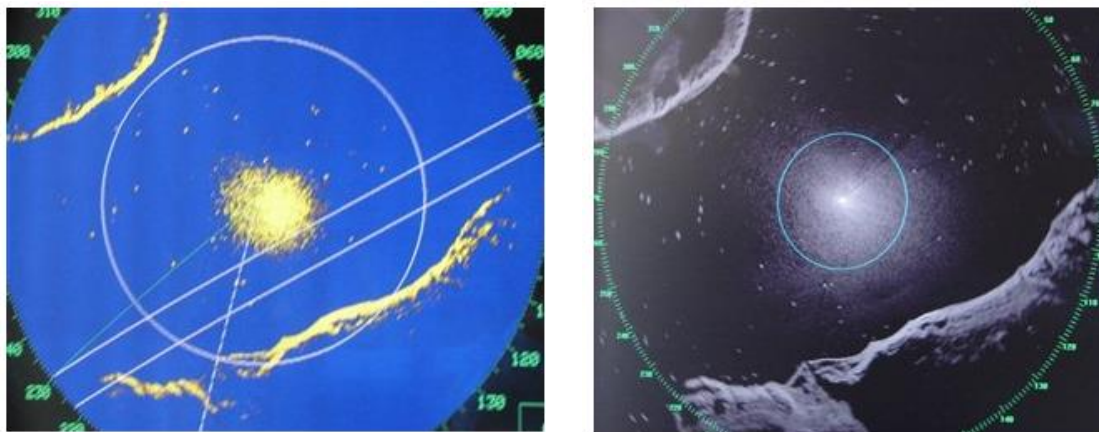


Figure 3-6 Ship navigation scenarios in ice [1]

The collision scenario in this research, however, is different than the cases shown in Figure 3-6. In this research, collision with bergy bits in open water is studied. In this scenario, it is assumed that the ice would not be detectable before the collision, and consequently, the officers cannot alter the course or reduce the speed.

Ice detection is an important part of mariners' responsibility in arctic shipping. The success rate in detecting ice depends on many parameters such as the light, visibility, sea state, and size of ice. Icebergs have a high freeboard that makes them visible both visually and on the radar. However, if the visibility is low, the radar will be the only means to detect ice. Radar capability in detecting icebergs depends on factors such as the shape and size of the above-water part and the existence of ice or sea clutter. Despite the difficulties in detecting icebergs, it could be assumed that ship officers are able to see glacial ice larger than the bergy bit (refer to Table 3-10 for iceberg size definitions). Furthermore, the advancement in radar technologies such as enhanced marine radars, which are optimized for navigation in ice-covered areas, will decrease the risk of collision with massive icebergs. Figure 3-7 compares the quality and precision of standard X-band radar with enhanced X-band radar.

It should be noted that enhanced radar does not exist onboard non-ice-class ships; thus, we cannot consider the advances in enhanced radars for non-ice-class ships. There are also various attempts to detect ice with satellite image processing, mostly applicable for ice-fast waters and do not apply to open sea navigation.



(a)

(b)

Figure 3-7 (a) Standard X-band Radar, (b) Enhanced X-band Radar [41]

Table 3-10 Iceberg size categories [42]

Category	Height above WL (m)	Length (m)
Growler	<1	<5
Bergy bit	1–4	5–14
Small berg	5–15	15–60
Medium berg	16–45	61–122
Large berg	46–75	123–213
Very large berg	>75	>213

The most crucial characteristic of an iceberg is the height above the waterline. As discussed in [43], bergy bits are difficult to detect in rough seas because the above-water size is not large. Consequently, the risk of collision to bergy bits is high. Table 2 categorized the sea states based on the average wave height. It is evident that even in a moderate sea state, the

bergy bits could be hidden in wave clutter. Oceanex shipping company reported at least two collisions with bergy bits offshore Newfoundland that took two out of three container ships out of service. Such accidents indicate that the possibility and the consequences of such accidents can be significant for islands in Canadian waters.

To sum up, in this research, bergy bit with various masses are chosen as an appropriate ice size group that has a high probability of causing severe damages to non-ice class ships. In the following section, a discussion regarding the mass selection of the bergy bit in collision scenarios is presented.

Table 3-11 Douglas Sea Scale [44]

Sea State	Wave Height (m)	Definition
0	0	Calm, Glassy
1	0-0.1	Calm, Rippled
2	0.1-0.5	Smooth
3	0.5-1.25	Slight
4	1.25-2.5	Moderate
5	2.5-4	Rough
6	4-6	Very Rough
7	6-9	High
8	9-14	Very High

3.4 Bergy bit mass and speed

Iceberg mass and contact shape are the main features required to conduct FE simulations for collision scenarios. The target bergy bit for this research is glacial ice with a maximum waterline length of 14 m. The mass of an ice piece is a function of the shape and density of ice.

There have been various attempts to implement the probabilistic approach to define ice loads, such as Jordaan et al. [45], Fuglem et al.[46], Fuglem et al.[20], Taylor et al. [47]. However, in this research, a predefined range of ice masses was used in FE simulations.

The variation in ice density can be ignored due to the limited range of ice density, and a typical density of 900 kg/m³ is reasonable. Contrary to density, bergy bits have many forms and shapes; thus, it is difficult to calculate the mass accurately. As discussed by Ralph et al. [48], the mass of an iceberg is calculated with Equation 2:

$$m = \left(\frac{\rho_i \rho_w}{\rho_w - \rho_i} \right) fLWH \quad [\text{Equation 2}]$$

Where;

ρ_w : Seawater density (kg/m³)

ρ_i : ice density (kg/m³)

L, W, and H: above water length, width, and height (m)

f: block coefficient

Block coefficient is 1 for cubic shape, 1/3 for a pyramid with a rectangular base, and $\pi/6$ for hemisphere or semi-ellipsoid with an average of 0.3 for icebergs in Grand Banks [48]. Table 3-12 shows the reported bergy bits, which are in the target dimension range of this research.

Table 3-12 Recorded Iceberg dimensions and mass in iceberg survey [48]

No.	L (m)	W (m)	H (m)	Mass (tonnes)
1	14	---	---	915
2	11.3	---	1.8	671
3	16.6	11.3	3.1	1698
4	12.1	7.9	1.4	391

The mass has been calculated with Equation 2 for cases with available L, W, and H values. In other cases, a different empirical formula has been used ($m=aL^3$, $a=300 \text{ kg/m}^3$). Based on the above discussion, a 1500-tonne bergy bit is an acceptable value for the mass of the bergy bit. In addition to the available data in the literature, project partners were asked for input to decide on the upper limit of ice mass. Experts in the American Bureau of Shipping (ABS) harsh environment technology center suggested that the upper limit of the bergy bit for collision is reasonable to be set as 9000 tonnes. Therefore, ice mass range was selected to be between 1500 and 9000 tonnes in the simulations.

It is discussed by Amdahal [49] that there is no agreed shape for collision geometry, and various shapes were adopted in the previous research. The problem is that the velocity of a

bergy bit is site-specific, and it depends on ice size and shape and many environmental parameters such as wind, wave features, and depth of the water. For larger icebergs, the wave-induced motion has a minor effect on impact energy. Smaller bergs have lower mass, but their impact velocity due to wave-induced motion is larger, and consequently, the impact energy would be noticeable [50].

For simplicity, the ice velocity of 3 m/s was chosen as it was used in the previous research. The hydrodynamic behaviour of ice and structure while approaching is another challenge that was not included in this study.

3.5 Summary

A review of available damage data on the NRC database showed that the recorded data is limited and can't be used to find an appropriate damage extent in collision with ice scenarios for non-ice class ships. Despite the lower probability of collision in the mid-body of ships, the consequences might be drastic and worth investigating. Collision in the mid-body region is a sliding impact that was not studied in-depth like glancing impact. It was also concluded that the non-ice class merchant vessels such as bulk carriers, cargo ships and oil tankers had accidents in the past. As a result, structural arrangements that could represent these vessels are to be studied.

Based on the assumed impact scenario, a bergy bit with mass ranged between 1500 tonnes and 9000 tonnes was chosen.

Chapter 4 Fracture Modeling and Ice Mechanics

4.1 Introduction

Ductile materials undergo large plastic deformation before failure, which is a valuable mechanical property for engineering applications. Materials that are known to have a sudden failure with elongation less than 5% are categorized as brittle [51]. As shown in Figure 4-1, metals and alloys have a wide range of elongation, and it is 22% for ordinary steel in the shipbuilding industry [52].

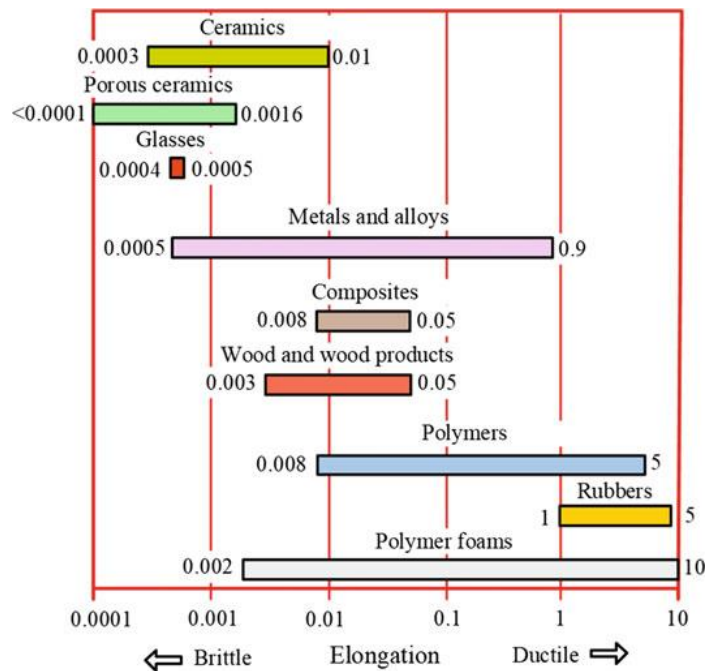


Figure 4-1 Typical ranges of elongation at fracture for different materials [51]

Generally, four mechanisms lead to the separation of atomic bonds and consequently material damage: cleavage, growth and coalescence, glide plane decohesion, and void growth due to grain-boundary diffusion. Unlike cleavage, in which the stress concentration without plastic deformation leads to damage, growth and coalescence and glide plane

decohesion occur in large plastic deformation [53]. Therefore the material characteristics are critical in the mode of fracture from the microscopic perspective. Damage in the material occurs as mechanical properties change due to the growth of cavities at the microscopic level. Damage is categorized phenomenologically into the following groups [53]:

- Ductile Damage
- Brittle Damage
- Creep Damage
- Fatigue Damage (low cycle, very low cycle, high cycle, and very high cycle)
- Creep-Fatigue Damage
- Spall Damage

Due to differences in material characteristics, the fracture formation and growth for ductile materials are different from brittle materials. Consequently, ductile fracture theories are to be implemented for ductile materials in FE simulations. In this section which is based on [54], the ductile fracture will be discussed.

4.2 Ductile fracture

Structures are designed to endure under a wide range of loads, and failure is defined as the inability of a structure to withstand a defined design load. The common material in the ship building industry is mild steel that is a ductile material. The stress-strain curve for mild steel is similar to Figure 4-2.

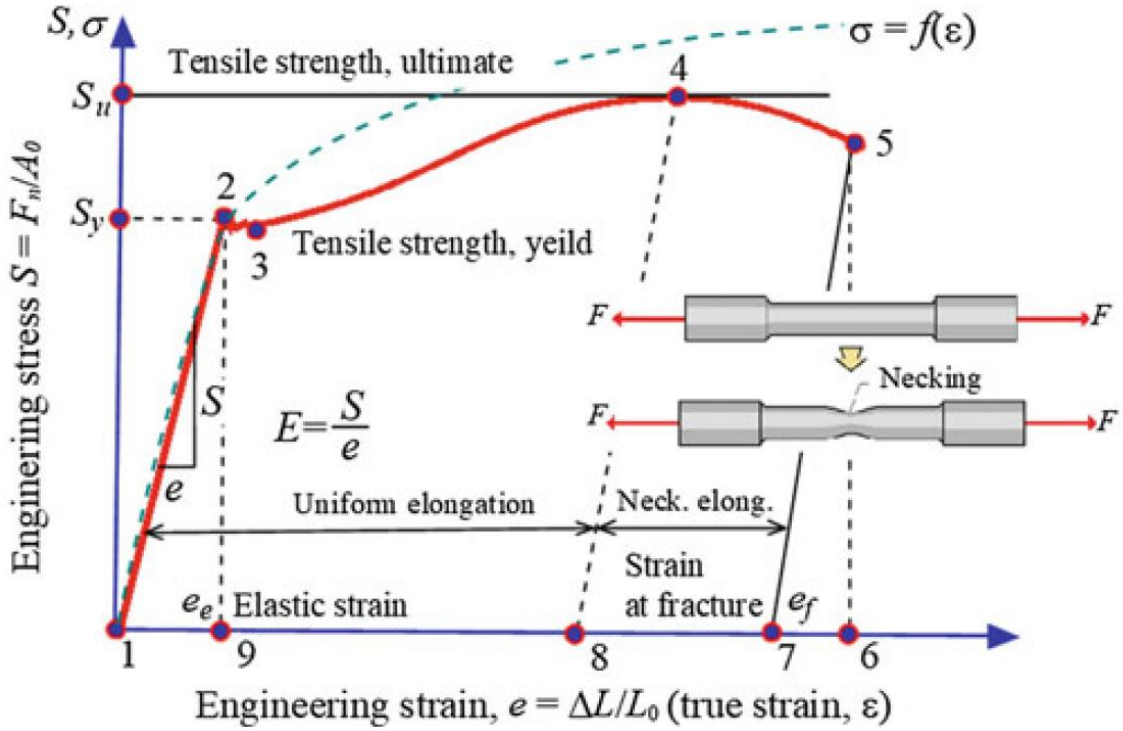


Figure 4-2 Typical ductile material stress-strain curve [51]

4.3 Stress state and ductile fracture

Fracture in ductile material has shown to be dependent on the stress state in the structure [55]. It means that the fracture threshold varies at every instance and for every single element during simulation. Two parameters control the fracture strain in ductile material: stress triaxiality and lode angle parameter [56]. To explain these two parameters, it is necessary to define the basic stress parameters (the following equations are from [56]).

$$p = -\sigma_m = -\frac{1}{3}tr([\sigma]) = -\frac{1}{3}(\sigma_1 + \sigma_2 + \sigma_3) \quad [\text{Equation 3}]$$

$$q = \bar{\sigma} = \sqrt{\frac{3}{2}[S]:[S]} = \sqrt{\frac{1}{2}[(\sigma_1 - \sigma_2)^2 + (\sigma_2 - \sigma_3)^2 + (\sigma_3 - \sigma_1)^2]} \quad [\text{Equation 4}]$$

$$r = \left(\frac{9}{2}[S] \cdot [S] : [S]\right)^{\frac{1}{3}} = \left[\frac{27}{2}\det([S])\right]^{\frac{1}{3}} = \left[\frac{27}{2}(\sigma_1 - \sigma_m)(\sigma_2 - \sigma_m)(\sigma_3 - \sigma_m)\right]^{\frac{1}{3}} \quad [\text{Equation 5}]$$

Where:

σ_1 , σ_2 , and σ_3 are principal stresses

[S] is deviatoric stress tensor ($[S]=[\sigma]+p[I]$)

Stress triaxiality is defined as the ratio of hydrostatic pressure to equivalent stress:

$$\eta = \frac{\sigma_m}{\bar{\sigma}} \quad [\text{Equation 6}]$$

Lode angle θ , is defined as follows:

$$\xi = \left(\frac{r}{q}\right)^3 = \cos(3\theta) \quad [\text{Equation 7}]$$

ξ is the normalized third stress invariant that is between -1 and 1. By normalizing the Lode angle, the Lode angle parameter is defined as follows:

$$\bar{\theta} = 1 - \frac{2}{\pi} \arccos \xi \quad [\text{Equation 8}]$$

The Lode angle parameter is between -1 and 1. Any stress state can be defined with stress triaxiality and Lode angle parameter. Various stress states with their stress triaxiality and Lode angle parameter are listed in Table 4-1.

For detailed and accurate fracture modelling, a fracture locus is to be defined based on these two parameters like those suggested in [57]. However, as Cerik and Choung [38] discussed, ductile fracture for grade A steel, which is the most common steel in ship building, can be considered independent of the Lode angle parameter. Side structures of merchant ships are constructed with mild steel except for strakes in the vicinity of the deck and bottom. Therefore, it is possible to construct a fracture criterion only based on triaxiality for collision simulations with ice because collision with ice often occurred over the mid-depth of side structure.

Table 4-1 Triaxiality and Lode angle parameter for classic for various stress states [57]

Specimen type	Analytical expressions for stress triaxiality	The Lode angle parameter
Smooth round bars, tension	$\frac{1}{3}$	1
Notched round bars, tension (Bridgman, 1952)	$\frac{1}{3} + \sqrt{2} \ln\left(1 + \frac{a}{2R}\right)$	1
Plastic plane strain, tension	$\frac{\sqrt{3}}{3}$	0
Flat grooved plates, tension (Bai et al., 2006b)	$\frac{\sqrt{3}}{3} \left[1 + 2 \ln\left(1 + \frac{t}{4R}\right)\right]$	0
Torsion or shear	0	0
Cylinders, compression	$-\frac{1}{3}$	-1
Equi-biaxial plane stress tension	$\frac{2}{3}$	-1
Equi-biaxial plane stress compression	$-\frac{2}{3}$	1
Plastic plane strain, compression	$-\frac{\sqrt{3}}{3}$	0
Notched round bars, compression	$-\left[\frac{1}{3} + \sqrt{2} \ln\left(1 + \frac{a}{2R}\right)\right]$	-1
Refer to [57] for parameter definition.		

4.4 Continuum damage mechanics (CDM) and stress triaxiality (according to [54] unless otherwise stated)

Applied loads on structures lead to cracks and microscopic defects in the material. Microcracks developed by increasing tensile load results in fracture in ductile materials. The distribution of defects in a material affects the fracture response and mechanical properties of the material, like strength and stability. From an engineering perspective, defects are introduced in continuum mechanics and thermodynamics with variable damage parameters. The field of continuum damage mechanics includes the effect of defects by adjusting the mechanical and physical properties of a material based on the defect distribution in the material. It worth mentioning that in fracture mechanics, crack is assumed to be a discontinuity (as new boundaries), and material properties (constitutive equations) remain constant. Figure 4-3 depicted the relationship between the mentioned approaches to defects and cracks in the material.

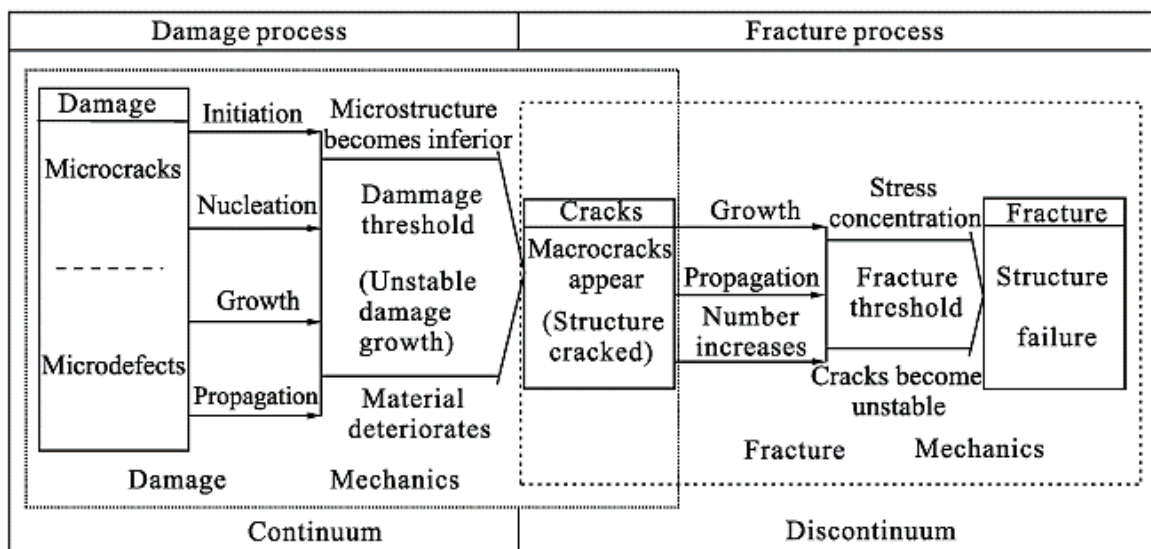


Figure 4-3 Damage and fracture mechanics relationship [54]

Damage mechanics is the study of damage in the material on micro-level; however, in continuum damage mechanics, the effect of micro-defects on material macro characteristics is investigated. The damage variable is a crucial parameter in CDM and material fails if the damage variable exceeds a threshold.

Damage variables can be defined in several ways, and the classic form of damage variable is as follows:

$$\Omega = \frac{A-A^*}{A} \quad \text{[Equation 9]}$$

Where;

A^* is the effective resisting area, and A is the overall area of the element (Figure 4-4). When the damage variable is equal to zero, it means that the material is undamaged and when it reaches the critical value, Ω_C , material is considered to experience fracture (Ω_C has a range between 0.2 and 0.8 for metals). As discussed in [53], defining the effect of damage on material strength by decreasing the cross-section area is not always accurate. Therefore, other forms of damage variable have been suggested, like Equation 9 by Lemaitre as cited in [53] (E^* is the young modulus of damaged material).

$$\Omega = 1 - \frac{E^*}{E} \quad \text{[Equation 10]}$$

Equation 10 states that Young's modulus of the material decreases by developing damage in the material. Figure 4-5 depicts how Young's modulus of Copper 99.9% changes as plasticity develops in the material.

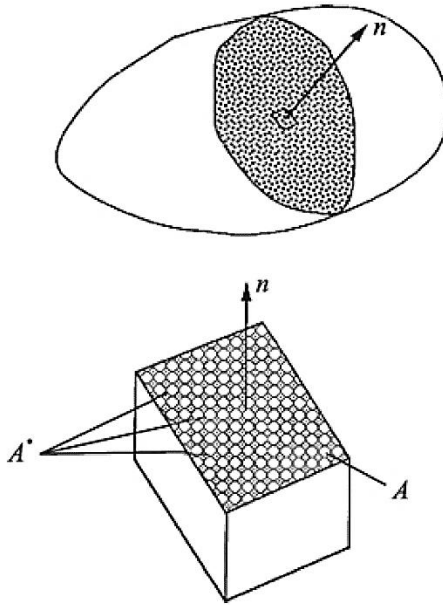


Figure 4-4 Effective and resisting area for damage variable definition [54]

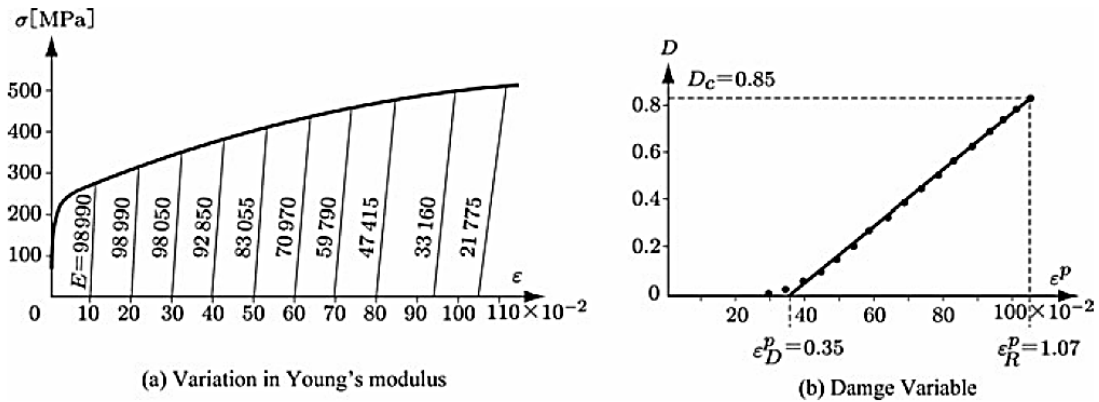


Figure 4-5 Young's modulus variation by developing damage in Copper (Lemaitre as cited in [53])

The damage variable is used to modify the Cauchy stress tensor, σ , to the effective stress tensor in the damage state. Because in damaged and intact material, the force value is constant and based on Equation 10, the stress tensor in the damaged case can be calculated with Equation 11.

$$\{\sigma^*\} = \frac{\{\sigma\}}{1-\Omega} \quad [\text{Equation 11}]$$

Equation 11 assumes that the damaged stress tensor changes with a scalar damage variable, which is not an accurate assumption for anisotropic materials.

Two hypotheses to describe constitutive equations for isotropic damage are strain equivalence and stress equivalence.

In strain equivalence hypotheses, the $\sigma - \varepsilon$ in damaged condition can be assumed to be similar to the undamaged state, but the effective stress (σ^*) tensor is to be used instead of Cauchy stress (σ) with Equation 12:

$$\{\sigma\} = [D^*]\{\varepsilon\} \quad [\text{Equation 12}]$$

Where D is the elasticity matrix and D* is the damaged constitutive matrix that could be calculated according to Equation 13.

$$[D^*] = (1 - \Omega)[D] \quad [\text{Equation 13}]$$

The stress equivalent hypothesis is similar to strain equivalent, but the practical strain is substituted for strain (refer to [54] for formulations). Another hypothesis that is applicable for both isotropic and anisotropic damage is the strain energy equivalence. According to strain energy equivalence, the D* could be expressed as follows:

$$[D^*] = (1 - \Omega)^2[D] \quad [\text{Equation 14}]$$

Therefore, based on strain equivalence (model A) and strain energy equivalence (model B), the damage variable could be defined for one dimension as shown in Equations 15 and 16. Strain equivalence and strain energy equivalence are different assumptions that use stress-

strain relationship of undamaged material in the damaged state. For example, in strain equivalence, it is assumed that the stress-strain curve of undamaged material can be used in damaged condition but the effective stress, $\{\sigma^*\}$, have to be used instead of Cauchy stress.

$$\Omega_A = 1 - \frac{E^*}{E} \quad [\text{Equation 15}]$$

$$\Omega_B = 1 - \sqrt{\frac{E^*}{E}} \quad [\text{Equation 16}]$$

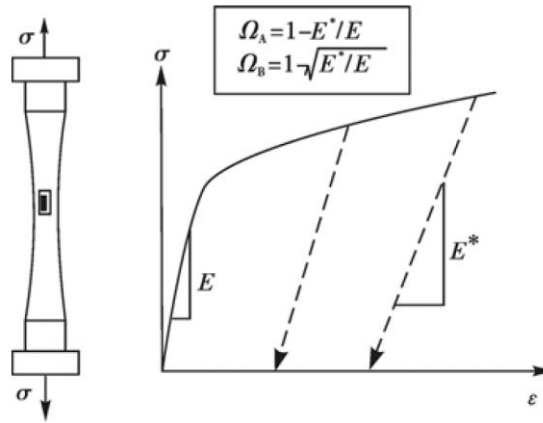


Figure 4-6 Young's modulus of intact (E) and damaged (E^*) material [54]

According to dissipation inequality for isotropic damage (see Equation 17), the total energy dissipation rate is a combination of mechanical (plastic dissipation and internal dissipation) and thermal energy dissipation.

$$\underbrace{\{\sigma\}^T \{\dot{\epsilon}_p\}}_{(1)} - \underbrace{Y\dot{\Omega} - R\dot{\gamma}}_{(2)} + \underbrace{\{q\}^T \{g\}}_{(3)} \geq 0 \quad [\text{Equation 17}]$$

Where:

(1) Plastic dissipation

- (2) Variation of internal variables
- (3) Thermal dissipation

$-Y\dot{\Omega}$ represents the dissipated energy due to the damage in the material. Y indicates the variation of elastic strain energy as a result of damage development. It is proved in [54] that for a one dimension case, the value of Y for model A and model B hypothesis can be derived as follows:

$$Y_A = \frac{\bar{\sigma}^2}{2E(1-\Omega)^2} \left[\frac{2}{3}(1+\nu) + 3(1-2\nu)\left(\frac{\sigma_m}{\bar{\sigma}}\right)^2 \right] \quad [18]$$

$$Y_B = \frac{\bar{\sigma}^2}{2E(1-\Omega)^3} \left[\frac{2}{3}(1+\nu) + 3(1-2\nu)\left(\frac{\sigma_m}{\bar{\sigma}}\right)^2 \right] \quad [19]$$

According to Equation 18 and Equation 19, the released energy associated with damage growth ($Y\dot{\Omega}$) is a function of the stress triaxiality. Thus, any FE simulation that aims to capture fracture in a structure should consider a fracture criterion that is defined based on the stress triaxiality.

4.5 Fracture modeling in LS-DYNA

Crashworthiness analysis is a complex field of engineering that has application in many engineering branches. Collision and grounding are the main sources of marine accidents that often result in structural failure and hull rupture.

A common approach in fracture modelling is with the aid of element deletion. In other words, finite elements are deleted when a defined criterion exceeds a threshold. As for impact simulation, effective plastic strain at failure has been widely implemented in both academic research and practical engineering. Effective plastic strain criterion can be defined in two ways:

- 1- Constant equivalent plastic strain at fracture
- 2- Varying equivalent plastic strain at fracture

In the first method, the value of the strain is constant through the simulation and it is independent from stress state. Germanischer-Lloyd (GL) criteria is one of the most used methods for constant fracture strain technique. As noted, the value of fracture strain is constant, and it could be modified with methods such as Barba's law for various mesh sizes and thickness [58]. The key issue with this approach is that the fracture strain is independent of the stress state.

For the second method, the value of the stress is dependent on the stress state. Any stress state could be defined with two parameters, stress triaxiality and lode angle parameters. Fracture criteria such as Rice-Tracey and Crockcroft-Latham (RTCL) are based on stress triaxiality. Other more sophisticated fracture loci have been developed in the preceding years for different materials such as [55]–[57]. Recently, Cerik and Choung [59] developed a fracture locus for mild and high strength steel (HST) steels that are common in ship building. The problem with these fracture locus is that they are generally calibrated with fine solid mesh elements that make it challenging to implement for large shell elements. Despite some efforts in solving this issue [60], [61], there is no reliable way to calibrate available fracture locus for large shell elements.

In this research, the RTCL criterion, which is a combination of Rice-Tracey and Crockcroft-Latham, is used. Equations 20 and 21 [62], show the dependency of the fracture strain on the stress triaxiality. LS-DYNA has a special material card to define and include the RTCL fracture model in simulation.

MAT_MODIFIED_PIECEWISE_LINEAR_PLASTICITY_RTCL is an option of MAT_123 with RTCL fracture criterion built-in function.

$$\Delta f_{damage} = \frac{1}{\varepsilon_0} f\left(\frac{\sigma_H}{\bar{\sigma}}\right)_{RTCL} d\bar{\varepsilon}^p \quad [\text{Equation 20}]$$

$$f\left(\frac{\sigma_H}{\bar{\sigma}}\right)_{RTCL} = \begin{cases} 0 & \frac{\sigma_m}{\bar{\sigma}} \leq -\frac{1}{3} \\ 2 \frac{1 + \frac{\sigma_m}{\bar{\sigma}} \sqrt{12 - 27\left(\frac{\sigma_m}{\bar{\sigma}}\right)^2}}{3 \frac{\sigma_m}{\bar{\sigma}} + \sqrt{12 - 27\left(\frac{\sigma_m}{\bar{\sigma}}\right)^2}} & -\frac{1}{3} \leq \frac{\sigma_m}{\bar{\sigma}} \leq +\frac{1}{3} \\ \frac{1}{1.65} \exp\left(\frac{3\sigma_m}{2\bar{\sigma}}\right) & \frac{\sigma_m}{\bar{\sigma}} \geq \frac{1}{3} \end{cases} \quad [\text{Equation 21}]$$

The fracture strain must be modified based on the plate thickness and element length. For this purpose, Equation 22 was implemented. The constant values have to be calibrated with the experiment. Ehlers et al. [58] provided the values for the material used in this analysis with $n=0.205$ and $\varepsilon_n = 0.67$ (ε_n is fracture strain for $L/t=1$).

$$D_{cr}\left(\frac{t}{l_e}, \frac{\sigma_H}{\bar{\sigma}} = \frac{1}{3}\right) = \varepsilon_f\left(\frac{t}{l_e}\right) = n + (\varepsilon_n - n) \frac{t}{l_e} \quad [\text{Equation 22}]$$

Table 4-2 shows the ε_0 (in Equation 20) which is required in RTCL fracture model in LS-DYNA for various plate thickness and element size.

Table 4-2 Modified fracture strain for various L/t

L/t	e_f (Equation 22)	ε_0 (LS-DYNA)
1	0.67	0.67
1.5	0.515	0.515
2	0.4375	0.4375
3	0.36	0.36

Two methods have been discussed in the literature for element deletion, (1) sudden deletion, (2) damage-induced softening. In this project, the sudden deletion has been adopted because there is no need to couple the fracture and material properties (i.e., stress and strain curve).

In addition to material fracture, the steel characteristics reported by Ehlers et al. [58] were implemented in the FE model (as shown in Table 4-3).

Table 4-3 Material properties for steel [58].

Density (kg/m ³)	Young's modulus (GPa)	Yield strength (MPa)	ν
7850	2.06	284	0.3

After the yield point, the stress-strain curve was defined with a power-law (see Equation 23). Figure 4-7 shows the stress-strain curve defined as a curve in LS-DYNA based on Equation 23.

$$\sigma = K\varepsilon^n \quad \text{[Equation 23]}$$

Where $n=0.2$, and $K=730$ [58].

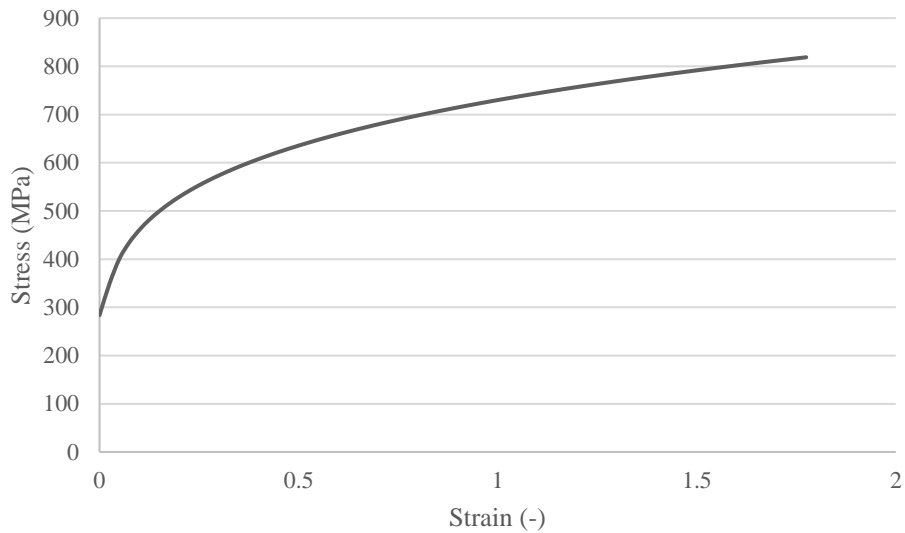


Figure 4-7 Stress-strain curve for steel based on Equation 23

4.6 Ice Mechanics

There are three approaches to consider energy dissipation in ice and structure collision: strength design, ductile design, and shared-energy design (Figure 4-8). The Shared-energy method is a more realistic approach because energy dissipates in ice crushing and structural deformation [49]. Therefore, considering ice as a rigid body (as assumed in ductile design) or assuming the ice crushing as the primary source of energy dissipation (as assumed in strength design) are not accurate approaches.

To consider both ice and structure in the energy dissipation process, ice should be defined in a form that mimics the ice failure. Ice is a complex material, and it is a challenge to define it in numerical simulation. Ice has a wide range of mechanical properties at different temperatures and salinity. As discussed by Daley [1], ice could behave differently in various temperatures, salinities and strain rates.

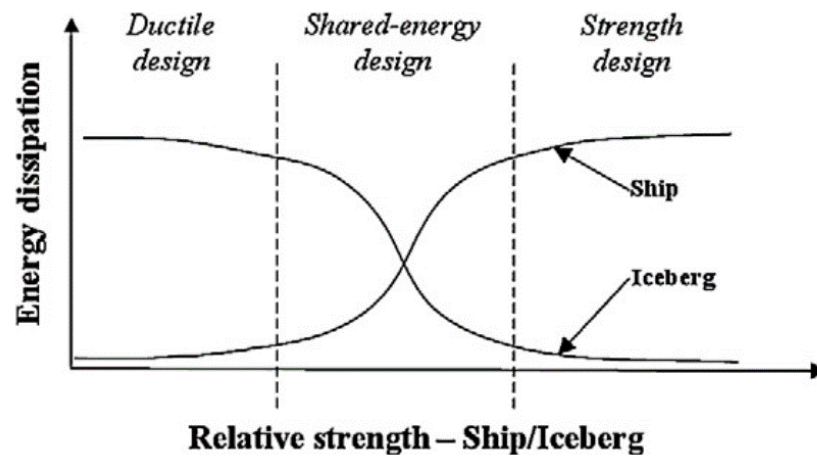


Figure 4-8 Various design approaches for ice-structure collision design [63]

Researchers attempted the ice modeling with brittle material (with erosion modeling of ice), or crushable foam. Nisja [64] compared the results for the four methods to define ice material in FE simulations:

- Crushable Foam
- Brittle Damage Model
- Holmquist-Johnson-Cook (HJC)
- Lemaitre Damage Model

The author simulated several impact scenarios, and in the case where an ice sheet collides with an offshore structure, the predicted load values by crushable foam model had the most accurate results.

In the recent years, various models are presented in the literature such as [63] and [38] to describe ice failure in collision. However, their accuracy needs to be tested in large scale collisions as it has been done for Gagnon model. Crushable foam model that was calibrated

by Gagnon does not simulate the ice behaviours such as cracking and spalling. However, the predicted ice load on the ship is showed to be in a good agreement with experiments. The reason is that the model was calibrated based on the large-scale ship and ice collision. Therefore, in this research, the Gagnon ice model as described in 5.3.7 is used. As noted, the crushable foam does not simulate ice fracture and therefore, for sliding simulation, the load level will be higher than actual collision scenario. It is assumed that the there is enough ice around the high pressure zone to maintain the high pressure zone over the simulation time. It is necessary to mention that the higher ice load is a problem for other ice models as reported by Nisja [64].

One of the problems with ice mechanic simulation is that there is no reliable ice model that could be implemented in FE simulation to accurately mimic the ice behaviour and produce a realistic ice load. Some researchers combined crushable foam with erosion technique to include ice failure in Gagnon model [33], but it is not a correct approach because Gagnon ice model calibrated for crushable foam not other erosion methods.

4.7 Summary

Ductile fracture is a complex phenomenon, and it is crucial to implement fracture criteria in the FE model as accurately as possible. Fracture models with constant thresholds are easy to set up in FE software; however, more sophisticated fracture models are required in collision simulations. In this thesis, the RTCL fracture model that is dependent on the stress triaxiality has been implemented. The fracture strain is dependent on element size and plate thickness, and these parameters are considered in defining the RTCL fracture criterion.

Chapter 5 Methodology and Numerical Model

5.1 Introduction

As stated earlier in the literature review chapter, there are three common ways to study the collision between ice and ship. Experimental methods are expensive and, in some cases, it is implausible to design the experiment. Analytical methods have limitations, and simplifications might lead to overestimation or underestimation of the actual phenomenon. The finite element (FE) method has been proven to show promising results with adequate accuracy. FE simulations have been used in almost all industries to study the crashworthiness of the structures. Due to the complex structures that are studied in this thesis, the analytical methods are not capable of capturing the whole fracture process. In addition, there is no analytical method to describe ice behaviour in sliding collisions. Therefore, the FE simulation is the only practical method to approach the raised research questions.

5.2 Vessel's models

As discussed in Chapter 3, nearly 50% of ice collision for non-ice class ships is for merchant ships and offshore vessels. This situation will be changed by increasing marine traffic in Polar waters in the near future. So far, oil exploration and military activities have been the focus of research for ice-ship collision. Therefore, in this study, the focus is on merchant ships to investigate the structural capacity of these ships. Four different vessels with various structural arrangements have been studied in the simulations:

- 84000 tonnes displacement single hull bulk carrier

- 64000 tonnes displacement double hull bulk carrier
- 64000 tonnes displacement double hull oil tanker
- 6000 tonnes displacement OSV

The main particulars and scantlings presented in this section are not for a specific vessel and represent the typical size and structural configuration of these vessels.

5.2.1 Single hull bulk carrier with transverse framing

As discussed, a single-side hull bulk carrier was chosen as the most vulnerable structure of non-ice class ships that might have a collision with bergy bits. Table 5-1 lists the main particulars of a typical Panamax vessel.

Table 5-1 Panamax Vessel main particulars

		Unit
Length BP.	217	m
Breadth moulded	32.25	m
Scantling draft	13.75	m
Depth	19	m
Displacement at scantling draft	84000	tonnes
Steel yield strength (at waterline side structure)	235	MPa
Frame spacing	840	mm

As shown in Figure 5-1, to reduce the effect of boundary conditions on the results, the model's vertical extent was selected from the hopper tank to the topside tank. The sliding impact needs to be long enough to observe the structural behaviour and capture fracture

initiation. Therefore, after several initial simulations, ten frame spacings was selected as longitudinal extent of the structure.

The structural scantling of the vessel is as follows (see Figure 5-1):

- Side shell plate thickness: 23 mm
- Hopper tank plate thickness: 18 mm
- Topside tank plate thickness: 18 mm
- Hopper tank and topside tank brackets: 14 mm
- Frame brackets: 13 mm
- Transverse frame: 400*13+150*18(T)

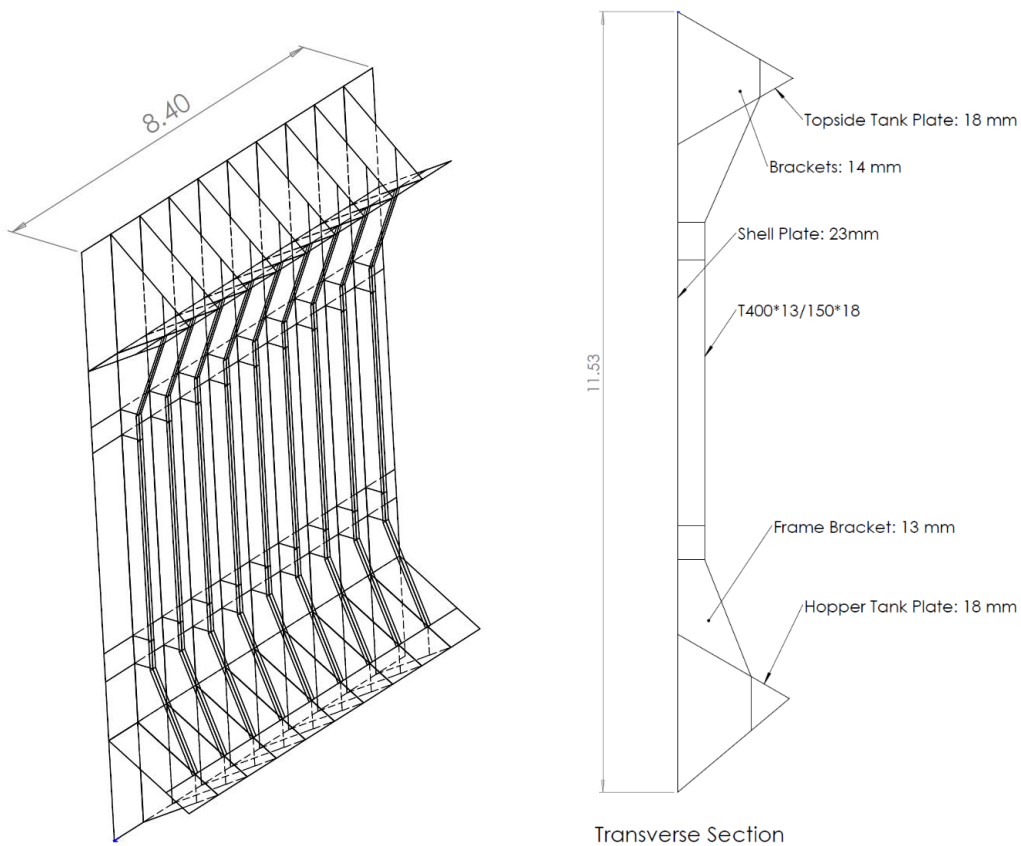


Figure 5-1 Single hull bulk carrier model extent and scantlings

5.2.2 Double hull bulk carrier with transverse framing

Double hull structures have a higher survivability index for damage stability calculations. However, the outer side of these vessels is not as sturdy as a single hull vessel and, consequently, vulnerable in collision accidents. A Handymax vessel with main particulars listed in Table 5-2 was chosen as a representative of a double hull vessel with transverse framing.

Table 5-2 Handymax Vessel main particulars

		Unit
Length BP.	183	m
Breadth moulded	32.26	m
Scantling draft	12.54	m
Depth	17.5	m
Displacement at scantling draft	65000	tonnes
Steel yield strength (at waterline side structure)	235	MPa
Frame spacing	800	mm

The structural arrangement, model extent and scantlings are shown in Figure 5-2. The structural scantling of the vessel is as follows:

- Side shell plate thickness: 15 mm
- Stringer: 12 mm
- Web frame: 11 mm
- The transverse frame (inner side and outer shell): L250*10+90*15

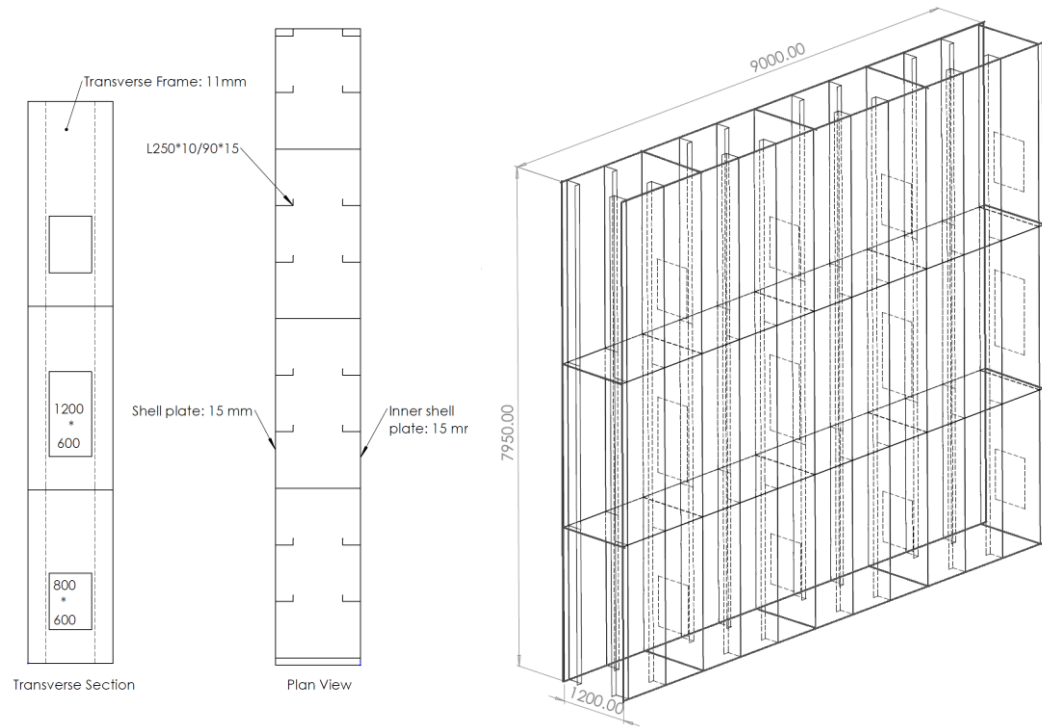


Figure 5-2 Double hull structure with transverse framing: scantlings and model extent

5.2.3 Double hull oil tanker with longitudinal framing

Double hull structures with a longitudinal framing system are a typical structural arrangement for all merchant ships. In this section, the results of simulations for a typical vessel with main particulars shown in Table 5-3 were presented. Ship speed, ice velocity, and impact angle were similar to the previous simulations in order to be able to compare the results.

Table 5-3 Double hull oil tanker main particulars

		Unit
Length BP.	183	m
Breadth moulded	32.2	m
Scantling draft	13	m
Depth	19	m
Displacement	65000	tonnes
Steel yield strength (at waterline side structure)	235	MPa
Frame spacing	700	mm

Plate thickness is the dominant parameter in fracture initiation for thin-walled structures; therefore, to assess the effect of the framing system on contact force and internal energy, the plate thickness was chosen to be equal to the double hull bulk carrier model. Longitudinal stiffeners' scantling is similar to the bulker model; however, the framing spacing of 700 mm was selected instead of 800 mm. A summary of the structural scantlings are as follows:

- Side shell plate thickness: 15 mm
- Stringer plate thickness: 12 mm
- Web frame plate thickness: 11 mm
- The transverse frame (inner side and outer shell): L250*10+90*15

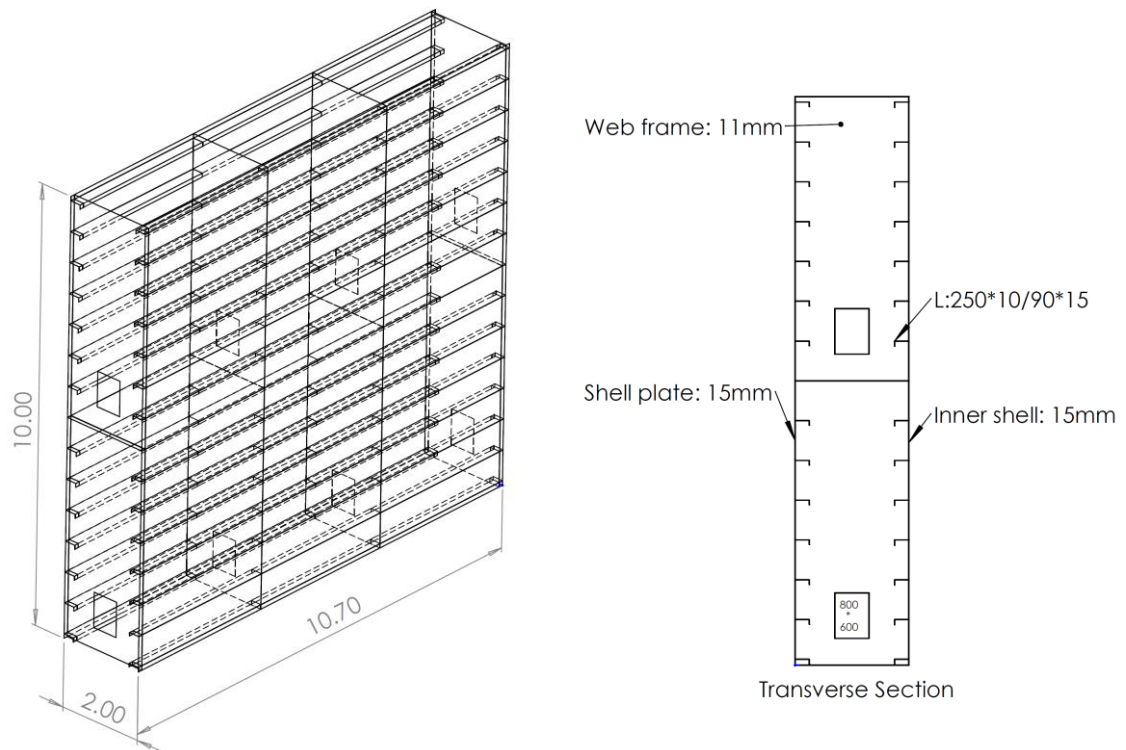


Figure 5-3 Double hull structure with longitudinal framing

5.2.4 Offshore Support Vessel (OSV) with transverse framing

Offshore support vessels (OSV) are designed for a wide range of operations and the need for maximizing payload capacity and maneuverability, means that their structures are optimized to be as light as possible. Thus, these vessels are to be investigated for the purpose of damage extent due to the ice collision. Typical main particulars of these vessels are listed in Table 5-4. These vessels are transversely framed on side shell; thus, transversely framed structure is studied for OSV simulations. Structural scantlings and FE model extent are shown in Figure 5-4.

Table 5-4 Typical OSV's main particulars

		Unit
Length BP.	70	m
Breadth moulded	16	m
Scantling draft	7	m
Depth	8	m
Displacement	6000	tonnes
Steel yield strength (at waterline side structure)	235	MPa
Frame spacing	720	mm

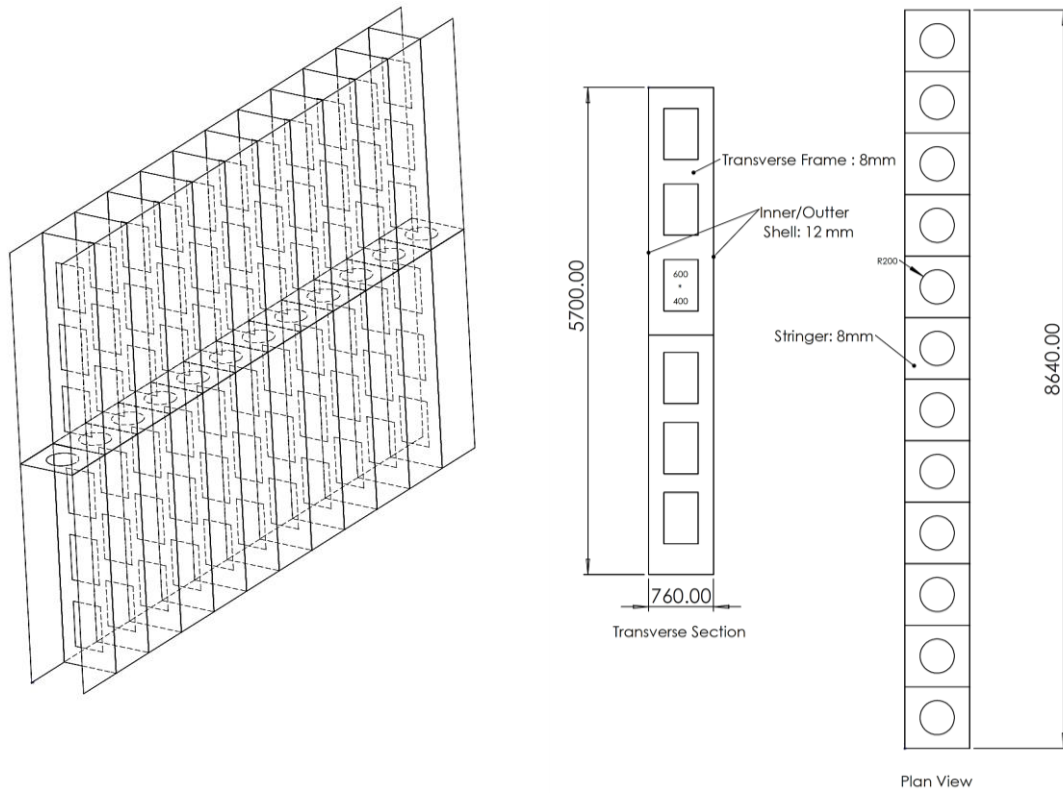


Figure 5-4 OSV structural scantlings and model extent

5.3 Finite element setup

5.3.1 Element type

In collision with ice, there are two different materials with various characteristics from an FE modelling perspective. Ship structure and ice need various approaches to model in FE model.

Ships are designed as thin-wall structures, except for some limited parts such as heavy machinery foundations. Structural thickness is minuscule compared to the width and length of members. This means that ship structures can be discretized with shell elements. Shell elements have features that make them an ideal choice for thin-wall structures. There is no need to model the structure in 3D with shell elements. This reduces the modelling and FE setup time. In addition, with the lower number of shell elements, the accuracy of the result is higher in comparison with solid elements (especially when bending is a dominant force). Therefore, shell element was used to mesh steel structure in the simulations. Element type Hughes-Liu was selected because it is a suitable element for large deformations and it has warping and hourglass control built in element formulations. Five through-thickness integration points were included and the shear factor $5/6$ was chosen.

For the ice side of the collision, the most suitable type of element is the solid element. Thus, the ice and rigid attached part to the ice are modelled with solid elements.

5.3.2 Element quality

Element quality is of high importance in FE simulations, mainly when large deformations and fractures occur. Therefore, element quality criteria are to be checked before simulations. Table 5-5 summarized the value for each element quality criterion for various

ship's models. For the ice, the solid elements have a maximum aspect ratio of 2.1. The crushable foam was used for the ice material model, and the foam material is sensitive to element quality because the foam undergoes severe deformation. Tetrahedral solid element is not an appropriate element and leads to instabilities and convergence issues. Hexahedra solid element was selected for the modelling of ice material with under-integrated constant stress formulation (ELFORM=1). Hourglassing is a common issue for under-integrated elements; thus, an hourglass energy card was included in the analysis (IHQ=6 and HQ=0.1).

Table 5-5 Element quality parameters in FE models

	Maximum aspect ratio	Warpage	Minimum Jacobian	Maximum Skew
Single hull with transverse framing	2.5	0	0.66	40
Double hull with transverse framing	2.45	0	0.74	27.8
Double hull with longitudinal framing	2.1	0	0.64	42
OSV with transverse framing	2	0	0.72	27

5.3.3 Boundary conditions

Boundary conditions have a noticeable effect on FE simulations, and they should be selected to represent the actual physical conditions. Fixed and simply supported boundary

conditions are often used in marine structures' FE simulations. It is an engineering practice to extend the model to the stiff areas of the structure to be able to apply fixed boundary condition. Deck, double bottom, stringers in the double side, and transverse bulkheads are considered as fixed boundary conditions. Therefore, the height of the models was chosen to have boundaries adjacent to stiff structural regions.

For the single hull model, the upper and lower boundaries are on the hopper and topside tank, respectively. These regions are stiff enough to be considered as a fixed boundary condition. For double hull models, the upper and lower boundaries are in way of decks that are also stiff enough to be considered as fixed boundary conditions. As for both ends of the models, because they located apart from primary structural members, the simply supported condition was selected. Boundary conditions that were applied in each model are shown in Figure 5-5.

Because the ship is moving forward, for all boundary conditions, all nodes are free to move in surge direction. Other directions of translation and rotation supposed to be zero because the mass of ship is noticeably higher than the mass of ice and energy dissipation in form of ship motion assumed to be negligible. For ice, however, there is no constrains to simulate the freedom that the ice has in real-world situation.

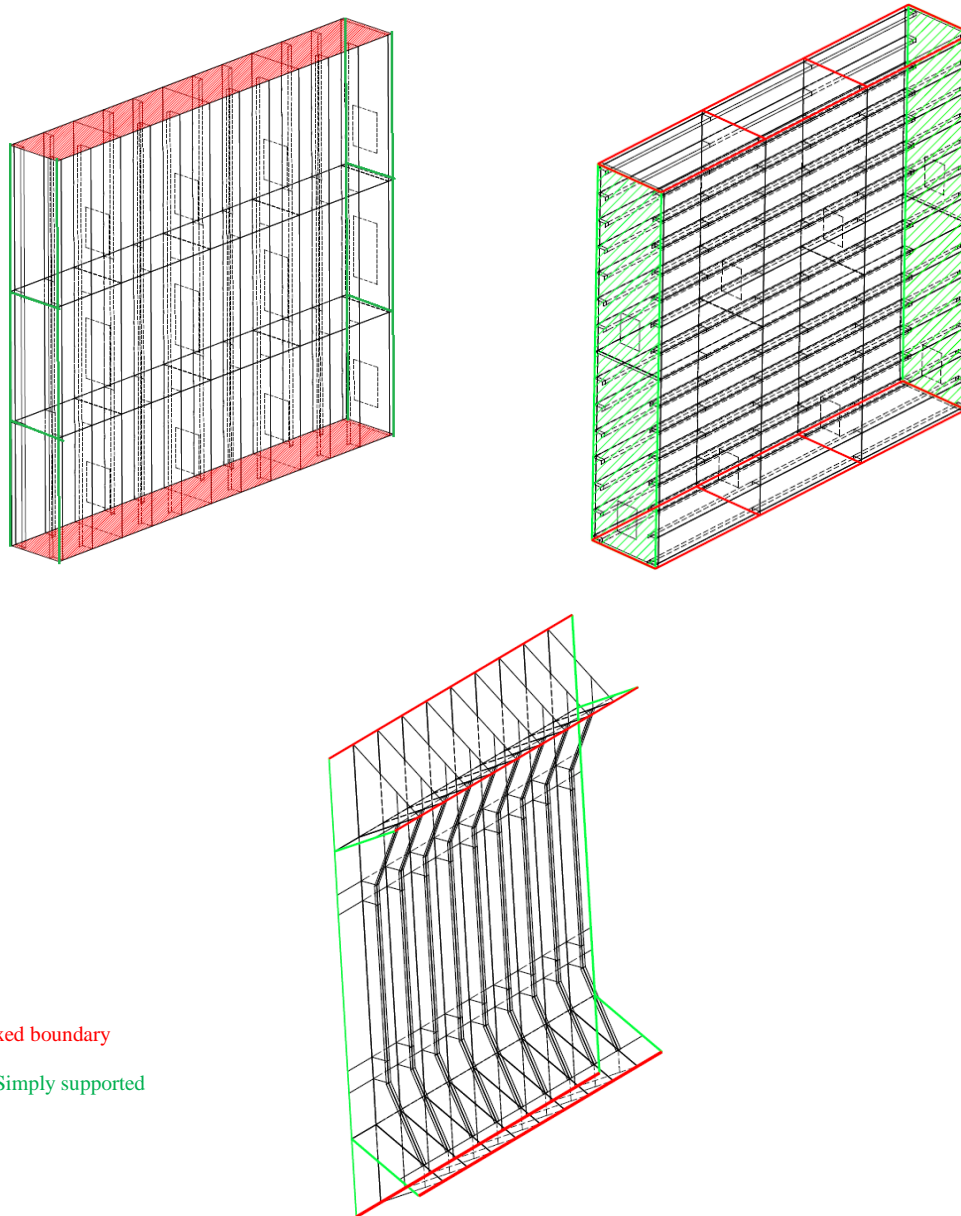


Figure 5-5 Boundary conditions for various structural arrangements

In simulations when the effect of a transverse bulkhead is investigated, all bulkhead boundaries are assumed to be fixed boundary.

5.3.4 Impact scenarios

Various impact scenarios are probable between ice and ship that depends on the type of the vessel (ice breaker, ice-class and non-ice class ship), and ice condition. For non-ice class ships that operate in open water, the most probable and dangerous scenario is the collision with bergy bits. Bergy bits are difficult to detect in rough sea conditions and wave induced velocity can be increase the impact energy to a level that leads to the rupture in shell plate.

Figure 3-6 depicts the collision scenario that is studied in this thesis. In this scenario, a bergy bit collides the mid-body of the vessel and slides along the side plate.

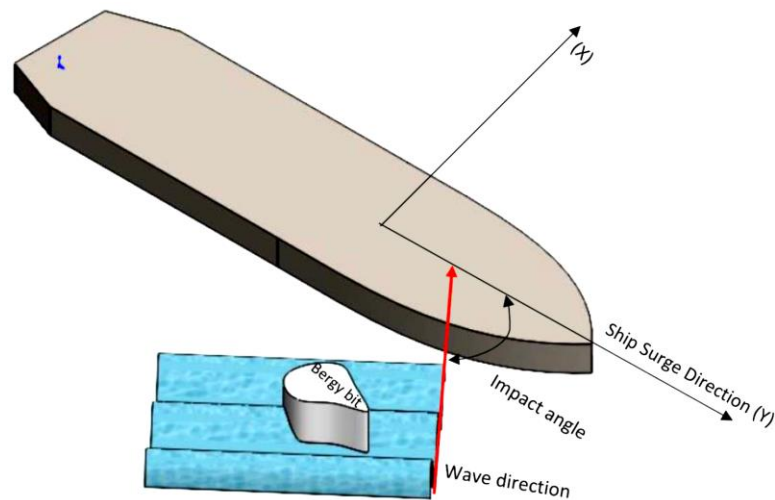


Figure 5-6 Bergy bit sliding collision scenario

Two node sets were defined for all nodes on structure and ice, and Initial_Velocity_Generation keyword was used to define initial velocity for ice and ship. As shown in Figure 5-7, ship and ice had different velocity vectors with a defined angle of impact. Other than some simulations that the effect of impact angle and velocity were studied, in all analyses the ice velocity and angle of impact were 3 m/s and 50°,

respectively. As for ship velocity, the speed assumed to be 16 knots unless otherwise stated in the result and discussion chapter.

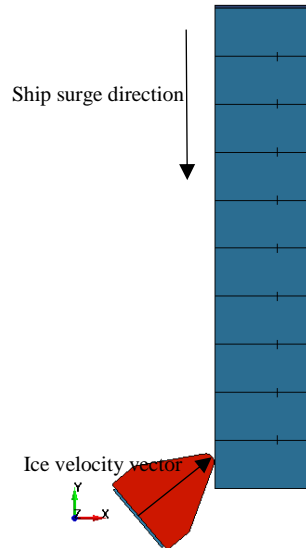


Figure 5-7 Initial velocity vectors for ship and ice

5.3.5 Ship speed and mass

Two common approaches are generally implemented by mariners in encountering rough seas. The first approach is to decrease the speed and navigate with a head-on course. The other is to maintain the speed and change the course in order to limit the slamming forces and shipping sea [65]. Generally, the speed reduction in the head-on case is the best method to control the load on the structure. However, it is difficult to maintain the speed even in the course change approach. In research done by the Japan P&I club [65], the course change is to be large in order to have a noticeable change in vessel behaviour. The value of speed reduction is vessel-specified, but a reduction of speed around 1 to 2 knots can half the number of the shipped sea [65]. For the slamming, the speed reduction should be in the range of 2~3 knots.

For all investigated cases, except for section 7.2 of the result chapter, the vessel speed assumed to be 16 knots and speed reduction due to the angle of impact was not considered. In order to account for ship momentum in the collision with ice, the total displacement of the ship was applied at the aft end of the model with a row of high-density shell elements (marked with red in Figure 5-8).

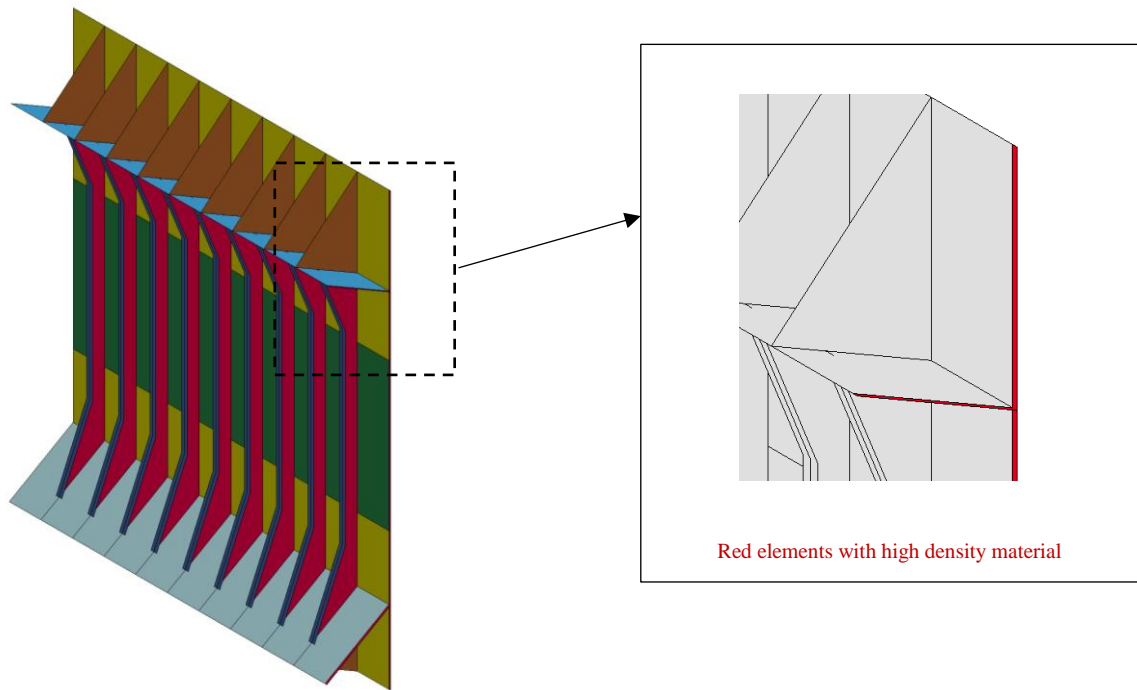


Figure 5-8 High-density elements to include ship's total displacement

5.3.6 Fracture criteria

A detailed description of the fracture model and variable inputs are presented in Chapter 4.

5.3.7 Ice material

Ice material is simulated with a crushable foam model with *MAT-063-CRUSHABLE_FOAM. Material properties, as reported by Gagnon and Derradji-Aouat [66] and Zong [67], as shown in Table 5-6 and Figure 5-9, are used in defining ice material.

Table 5-6 Ice material parameters [67]

Density (kg/m ³)	Young's modulus (GPa)	Poisson's ratio	Tensile cut-off stress (MPa)
900	9	0.003	35

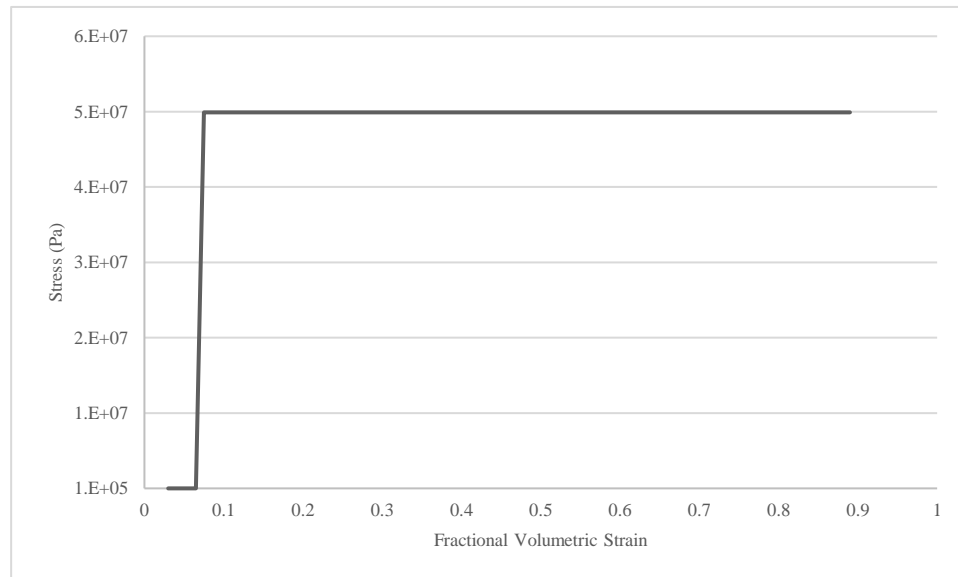


Figure 5-9 Ice model curve defined for crushable foam material [66]

A Variety of ice indenters were modelled, which are explained in detail in chapter 6.

5.3.8 Contact setup

The collision between two bodies is a problem that should be solved with a contact algorithm. Force developed on the structure as the ice with initial velocity collides with a moving structure. Contact_Automatic_Single_Surface algorithm was selected to include

both ice and structure interaction and contact between structural members after large deformation and fracture. It is necessary to active softening option in order to prevent ice from penetrating the shell plate. In order to avoid noise in the contact algorithm, static and dynamic friction coefficients were set as equal. A friction coefficient of 0.05 was decided to be used in the simulation due to the low friction between ice and steel.

Contact_Force_Transducer_Penalty keyword was added to capture force value exerted to the structure by ice.

5.3.9 LS-DYNA cards (additional keywords)

For simulations that include complex material models and fracture, additional keywords should be included in LS-DYNA. Control_Accuracy, Control_Energy, Control_Hourglass, and Control_Shell keywords were added from the LS-DYNA library to increase the accuracy of the results.

5.3.10 Solver

The explicit solver with double-precision was chosen as the FE solver for the simulations. As for explicit solver, the timestep is automatically calculated by the software with Courant–Friedrichs–Lewy (CFL) criterion. According to the CFL criterion, the maximum stable timestep is calculated by dividing the shortest path through the element to the speed of the sound in the material. Therefore, the timestep is a function of element size and material characteristics. Element size has a significant effect on timestep size, simulation time and cost. Although the size of elements dictates the timestep, due to the ice crushing, sometimes a smaller timestep is required to prevent instability in simulation. Therefore,

Control_Timestep was included with TSSFAC (Scale factor for computed time step) parameter set to lower values than the default value (0.9).

5.4 Mesh convergence

In order to find a reliable mesh density for simulations, mesh convergence analysis was conducted for both actual structures and smeared structures. Three different cases were studied for wedge cutting, ice impact with large contact area, and ice with small contact area. These simulations are time-consuming, and finding an optimum mesh size is of high importance. As it was noted, the steel failure criteria are mesh sensitive and by changing the L/t ratio of the element, the strain failure of the element changes. Therefore, in this mesh-sensitive analysis, the mesh size has been changed by altering the L/t for each structural member. In this way, each member would have a different mesh size according to its thickness.

- **Wedge Cutting**

Figure 5-10 shows the internal energy vs. wedge displacement for three mesh lengths to plate thickness. It is evident that the trend is almost similar except for the last 0.5 m of wedge displacement. However, as depicted in Figure 4, L/t=3 failure pattern is not similar to what is predicted by L/t=1. L/t=2 shows better results compared to the L/t=3. Therefore, L/t= 2 is used for the rest of the simulation.

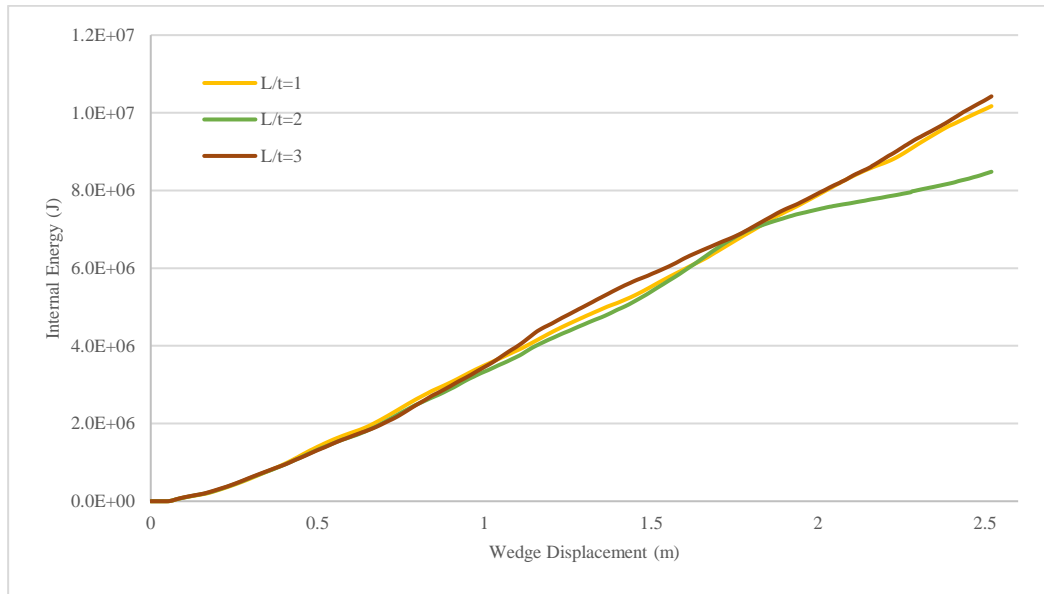
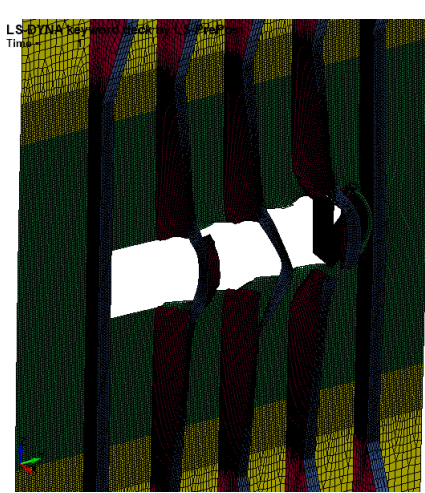
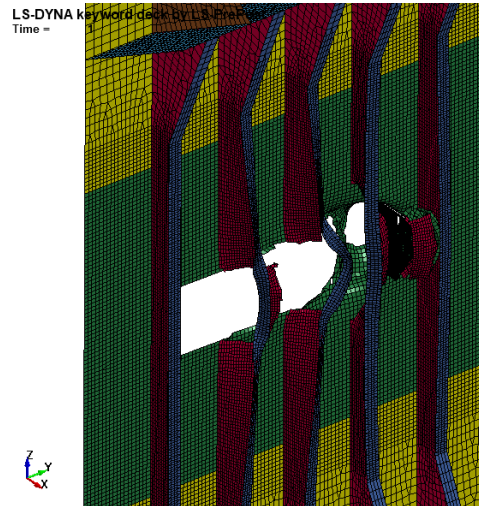


Figure 5-10 Mesh convergence analysis for the actual structure



L/t=1



L/t=2



$L/t=3$

Figure 5-11 Fracture patterns for various mesh sizes

Mesh convergence simulations for smeared structure showed a similar trend with $L/t=2$ as an appropriate mesh size (See Figure 5-12).

It should be noted that the cutting wedge simulation is very complex, and even experiments with similar material, geometries, and test setups could result in different outcomes. Figure 5-13 shows the plate cutting wedge experiment results carried out as a part of the MIT-Industry Joint Program on Tanker Safety [68] as cited in Ref. [69]. Experiment P1-15 and P2-15 had the same plate thickness (15mm), and all experimental conditions were the same, but the results are different.

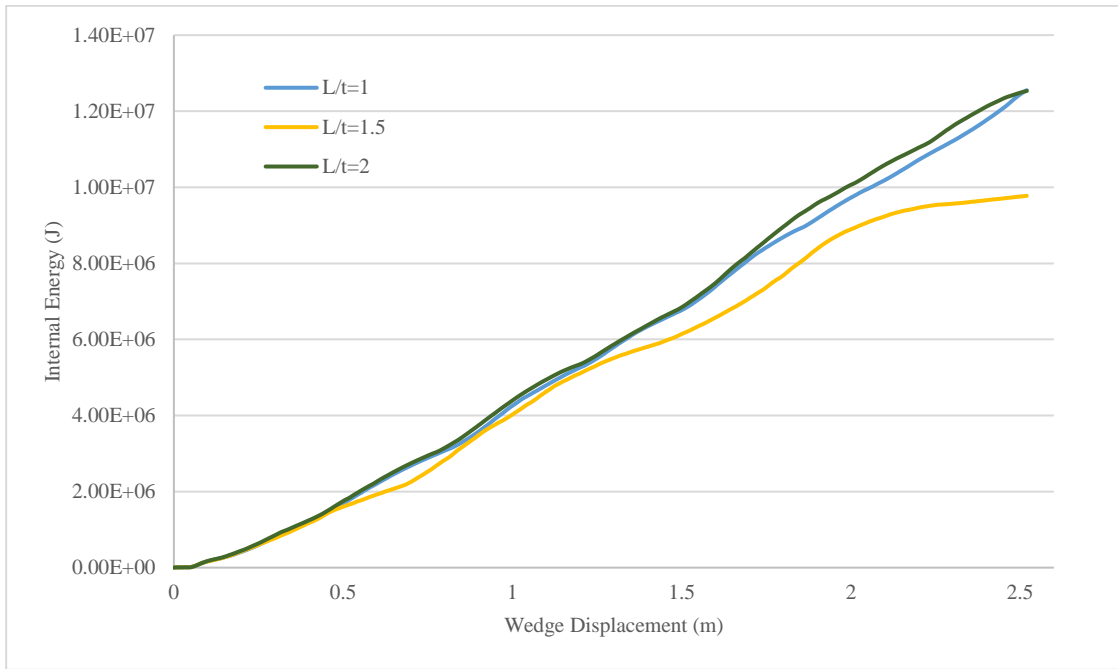


Figure 5-12 Mesh convergence analysis for smeared structure

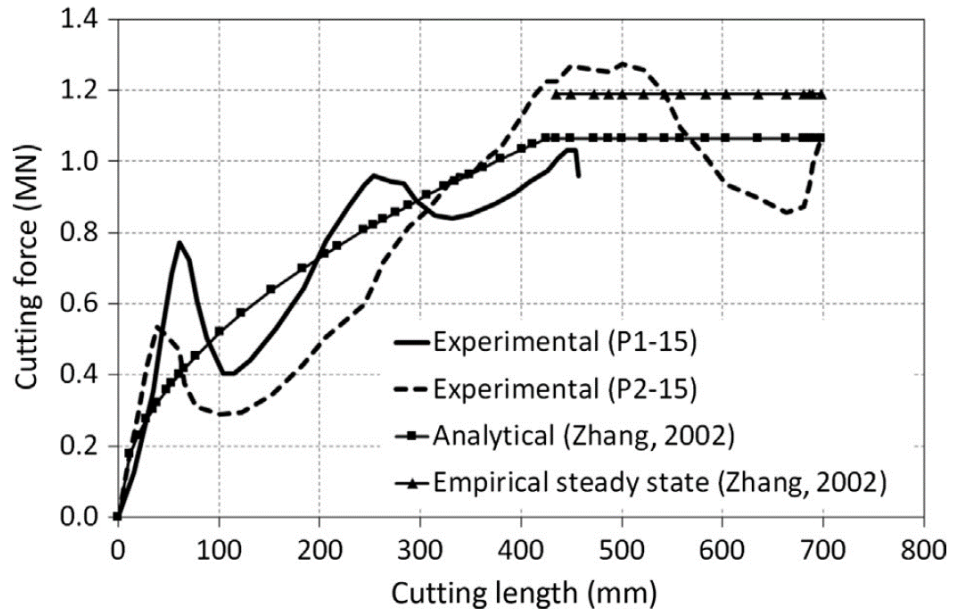


Figure 5-13 wedge cutting experiment by Astrup [68] as cited in [69]

- **Ice collision with the large contact area**

The same analysis for ice impact was carried out for 1500 tonnes bergy bit with impact angle of 50 and velocity of 3 m/s. The maximum acceptable mesh length to plate thickness ratios (L/t) is three because of the plate thickness, especially for flange of the stiffeners. For $L/t=1$ the shell element gets to its limit and it is not recommended to have shell element with $L/t=1$. According to Figure 5-14, $L/t=2$ is an accurate mesh size for the simulation of ice to ship collision. At the end of the simulation, the difference between internal energy in $L/t=2$ and $L/t=1$ is 8 percent. The differences are not significant given the complexity of the simulations. However, the $L/t=3$ is not a proper choice because the elements' thickness is high, and for the flange of stiffeners ($150*18$), the number of elements would not be enough to capture the structural response. Therefore, the $L/t=2$ would be an accurate size for the simulations with a small contact area.

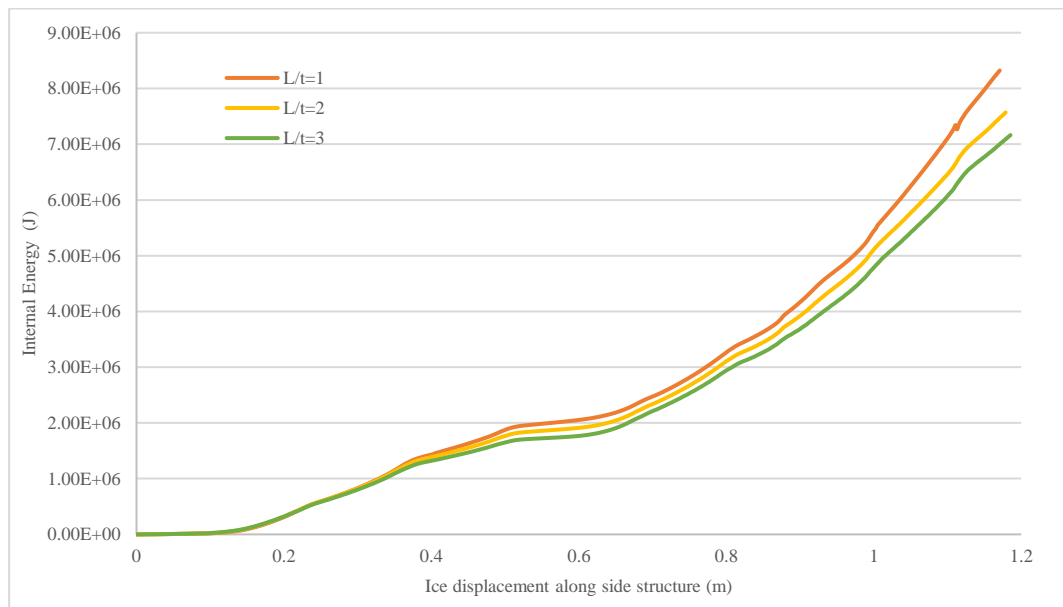


Figure 5-14 Mesh sensitivity analysis for ice impact on the structure with large contact area (1500-tonne bergy bit)

For small contact areas, based on the previous simulations for large contact areas, two lengths to thickness ratio, two and three, were investigated. Figure 5-15 compares the internal energy for the three mentioned mesh densities. At the end of the simulation, the internal energy for $L/t=2$ is 8% higher than the value for $L/t=3$. The differences are not significant given the complexity of the simulations. The $L/t=3$ is not a proper choice because the elements' thickness is high, and for the flange of stiffeners (150*18), the number of elements would not be enough to capture the structural response. Therefore, the $L/t=2$ has been chosen as a suitable size for the simulations with a small contact area. It is assumed that the same mesh size would be appropriate for the double hull structure, and consequently, the $L/t=2$ was considered for double hull simulations.

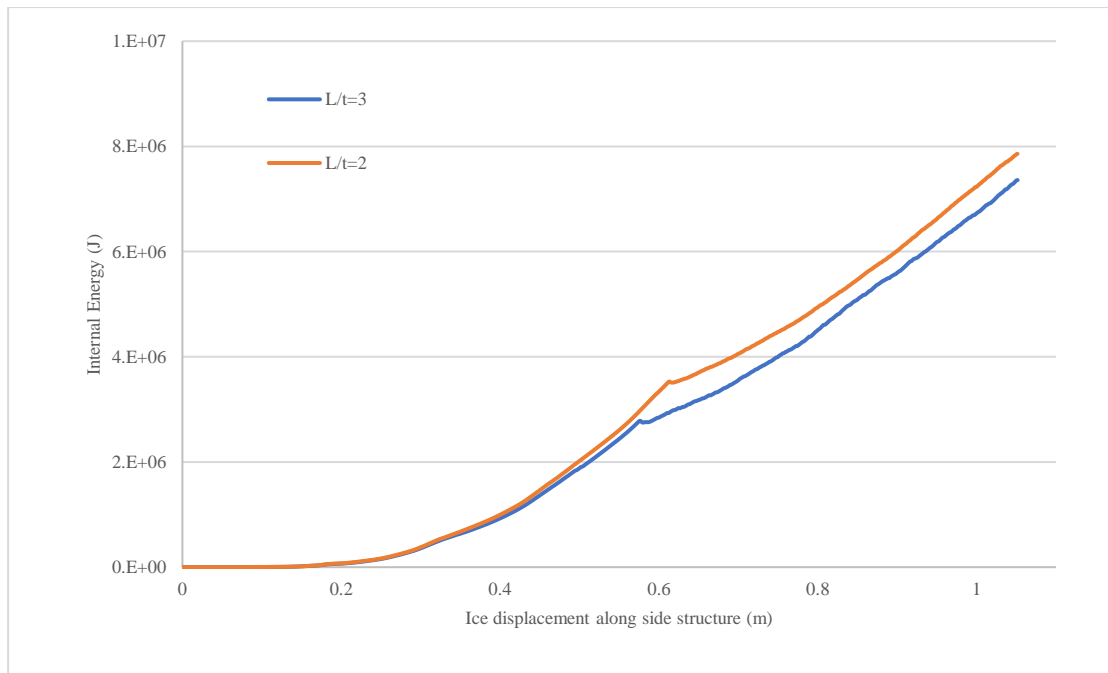


Figure 5-15 Mesh sensitivity analysis for ice impact on the structure with small contact area (1500-tonne bergy bit)

5.5 Benchmark study and validation

Finite element analysis is a complex method; therefore, any mistake in defining analysis' parameters leads to incorrect results. In this research, FE simulations consist of ice and steel structures. Although there is no experiment that benchmarks both steel and ice simultaneously, separate benchmark studies validated the ice model and steel fracture criterion used in this thesis. Gagnon's ice material was implemented in this study that was validated by field experiments and laboratory data as detailed in [66].

As for steel fracture modelling, the RTCL material properties specified in [58] were used to simulate steel fracture. In the benchmark study done by Ehlers et al. [58], three fracture criteria were studied: RTCL (Rice–Tracey and Crockcroft–Latham), GL (Germanischer Lloyd), and PES (Peschmann). Three test experiments were simulated with LS-DYNA. RTCL method had different performance in comparison to each experiment. For example, in test #3, which was the collision on the side shell plate with a bow-shaped indenter, the RTCL followed the experiment quite well, even though it overestimated the structural capacity.

The critical issue is how the criterion addresses the mesh sensitivity. All methods showed to be highly sensitive to mesh size. They concluded that the RTCL mesh sensitivity criterion was adequately addressed the mesh sensitivity. Therefore, the material properties and mesh sensitivity formula for the RTCL method were adopted in this research [58].

5.6 Summary

In this chapter, all aspects of a FE model that is required for a collision simulation of ice and ship were discussed. Geometry and scantlings of models, boundary conditions, ice

load, material properties, mesh convergence and LS_DYNA keywords were explained in detail.

Chapter 6 Results and Discussions- Part I: Single Hull Structure

6.1 Introduction

In this chapter, the results of FE results for a single hull structure are presented, and the interpretations of the results are discussed. Detailed force and internal energy graphs and tables are included for all simulations. Various controlling parameters like ice indenters' shape, collision angles, ice mass, etc. were investigated.

Ice geometry at contact with ice has a critical impact on the force level exerted on the structure. Various geometries were studied to find an ice geometry that leads to fracture in the structure. Wedge with different depths was studied, and other geometries such as sphere and irregular shapes (the results for the last two geometries are not reported). The simulations showed that to have fracture in the hull plate, the ice contact area in the first instant of collision should be small enough to cause high-pressure zone. After trial and error, the ice indenter in section 6.4 was selected and named an indenter with a small contact area. The ice indenter geometry used for most simulations is designed to simulate a localized high-pressure zone. The results are conservative, but the focus of this research is to demonstrate the fracture behaviour of the structure in extreme ice loads. It is necessary to mention that the ice contact area evolves during the simulation because of ice crushing and movement of the ice. Therefore, the term “small” refers to the contact area at the first instant of collision.

6.2 Impact with the large contact area

In the first series of simulations, a piece of ice with the shape shown in Figure 6-1 was used. The height of the ice is considered as two meters to create a large contact area. The last row of elements, which is marked with orange colour in Figure 6-1 (b), was modelled with rigid elements with high-density material characteristics to simulate the mass of the bergy bit.

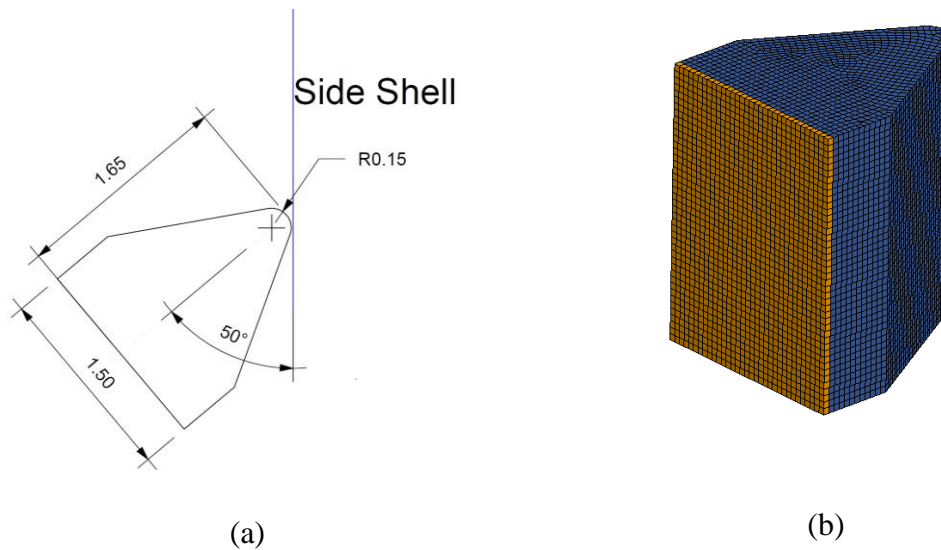


Figure 6-1 (a) Ice geometry (top view), (b) Ice FE model

This shape is a representative of a bergy bit with vertical sharp corners that is common in all types of iceberg geometries.

Five bergy bits with different masses (1500, 3000, 4500, 6000, and 9000 tonnes) with similar shapes were studied by modifying the density of the rigid end of the ice. Figure 6-2 and Figure 6-3 show the internal energy and contact force for all simulations. In none of these cases, the watertight integrity was impaired, i.e. no rupture was observed in the

structure. The structural behaviour was the same for all models, as shown in Figure 6-4, but the deformation amount was different (see Table 6-1).

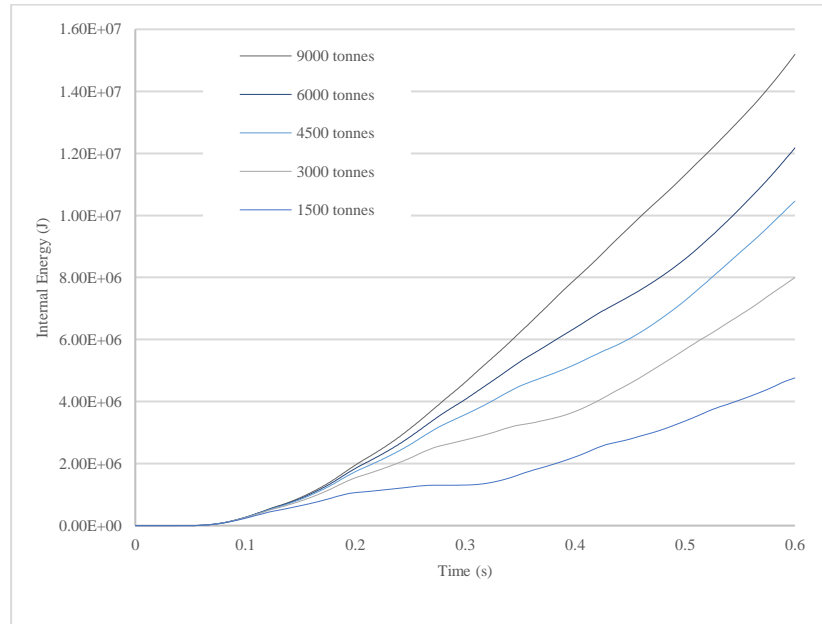


Figure 6-2 Internal energy for various bergy bit impacts (large contact area)

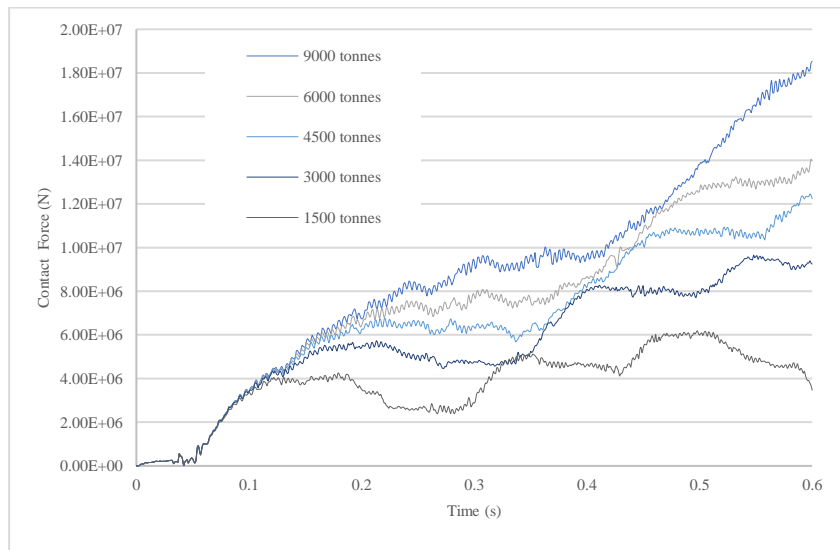


Figure 6-3 Contact force for various bergy bit impacts (large contact area)

It is evident that the mass of the bergy bit is a controlling parameter in the impact scenario with a large contact area. The large contact area caused severe deformation in the structure; however, the force distribution over a larger area prevented any rupture in the plate. It was predictable that for initiating the plate's rupture, either the bergy bit's weight is to be increased or the contact zone's shape is to be changed. As discussed in Chapter 3, a 1500 tonnes bergy bit is the upper bound of the bergy bit that might not be visible in the rough seas. Based on industry partners' feedback in the industry, a block of 9000-tonne ice could have been used as the upper limit of a possible bergy bit that might collide with a vessel in open water. The whole range was covered in the simulations, and consequently, the only parameter that could be changed is the ice's shape. Also, the bergy bit velocity is high enough and increasing the value will result in unrealistic scenarios that might not happen in real-world situations.

Table 6-1 Impact scenarios results' summary (large contact area)

Ice mass (tonnes)	Maximum dent depth (m)	Rupture
1500	0.333	No
3000	0.538	No
4500	0.526	No
6000	0.664	No
9000	0.767	No

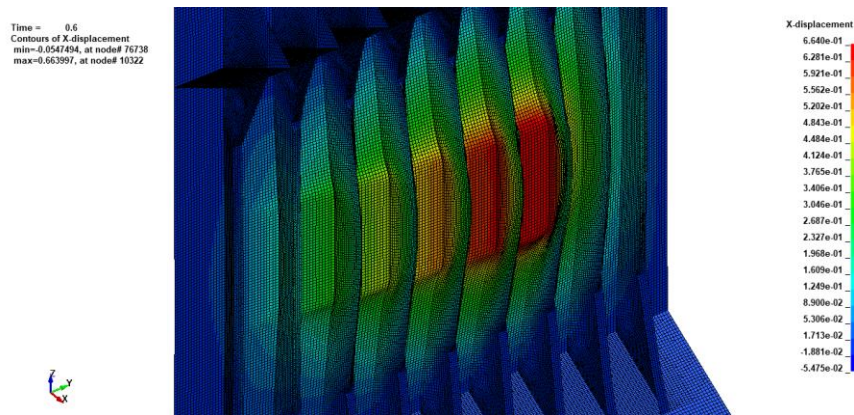


Figure 6-4 Deformation shape for 6000 tonnes bergy bit impact

The variation in the value of internal energy and how the curves diverge can be understood by tracking the ice velocity (see Figure 6-5). As the weight of ice increases, the heavier ice blocks can maintain their velocity for a longer time compared to lighter ones. As a result, the bergy bit with a higher mass could cause more damage and consequently more rupture energy, as shown in Figure 6-5.

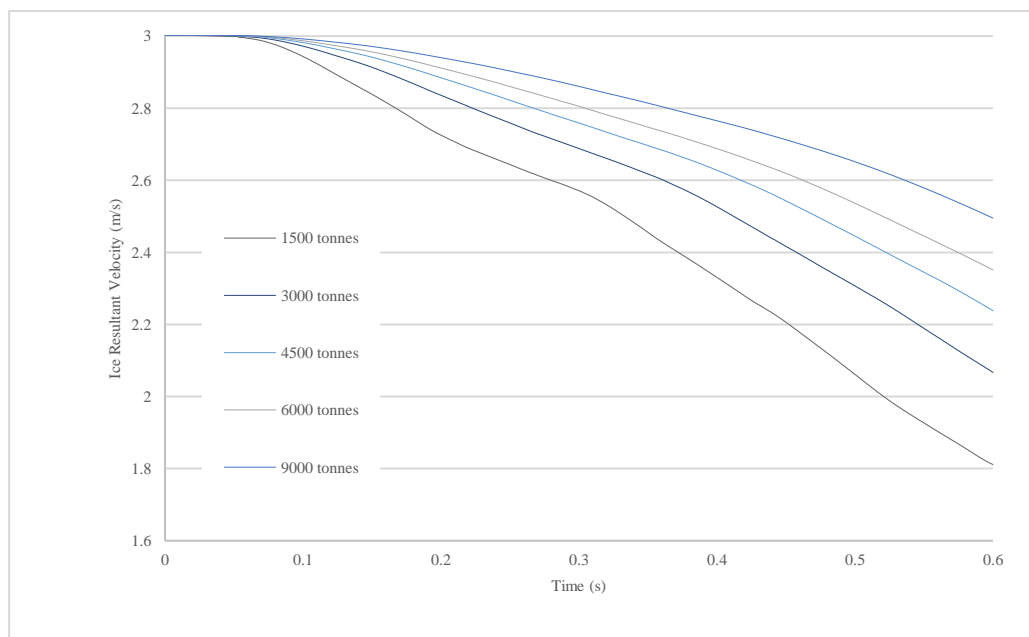


Figure 6-5 Velocity of ice during simulation for all ice masses

Figure 6-6 shows the ice movement during the simulation. It is important to note that the ship's momentum caused the ice to change direction and start to separate from the structure at the end of the simulation. The same behaviour was observed in other simulations, which means no rupture will be developed if the simulation continued for more than 0.6s.

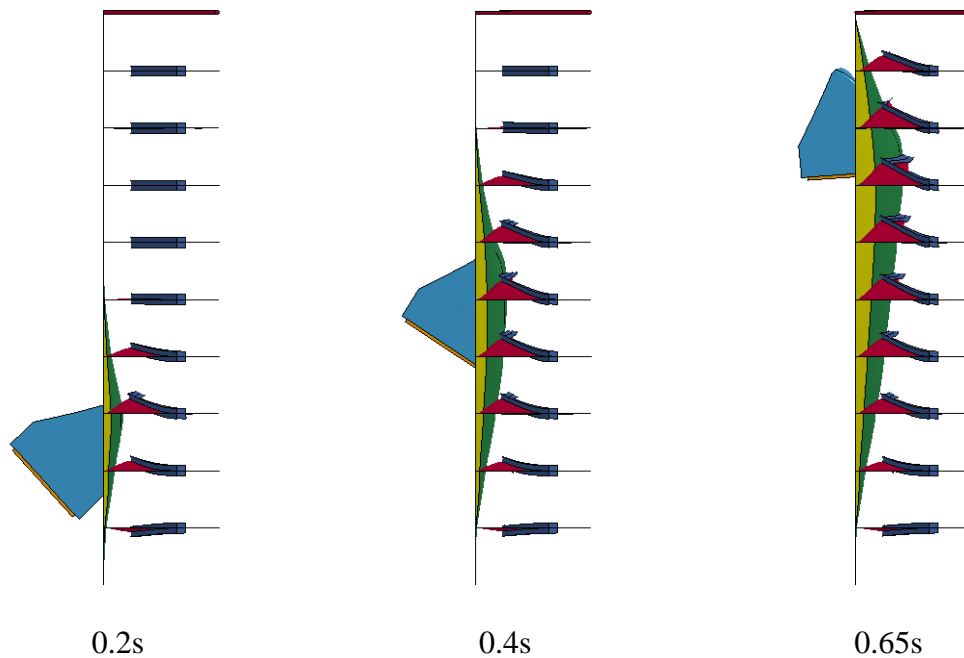


Figure 6-6 Ice movement for 6000 tonnes bergy bit impact

As mentioned, the contact area has a significant influence on force magnitude and damage intensity. The effect of the contact area on the results was investigated by simulating the impact with three smaller wedges, as shown in Figure 6-7. All wedges have the same tip geometry with various heights, and the vertical position of wedges is adjusted so that the wedges impact the middle point of the plate.

For wedge heights equal to 1.5m and 1m, the impacts did not lead to a rupture in the structure for all ice masses. As for the ice wedge with 0.5m height, the fracture occurred for ice masses of weight above 4500 tonnes. For the range of masses and defined velocities,

the wedge shapes of 0.5m in height and lower could be considered a threat to the structure's watertight integrity.

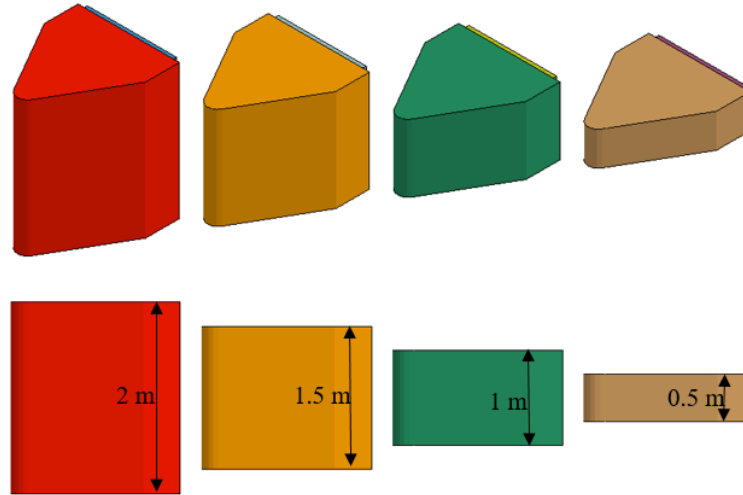


Figure 6-7 various ice wedge dimensions used in simulations

Figure 6-8 compares the contact force for a 4500-tonne bergy bit with various wedge heights. It is evident that for larger contact areas, the structure withstands the applied load; however, for 0.5m wedge height, the crack initiation and rupture growth caused a sharp decline in force level.

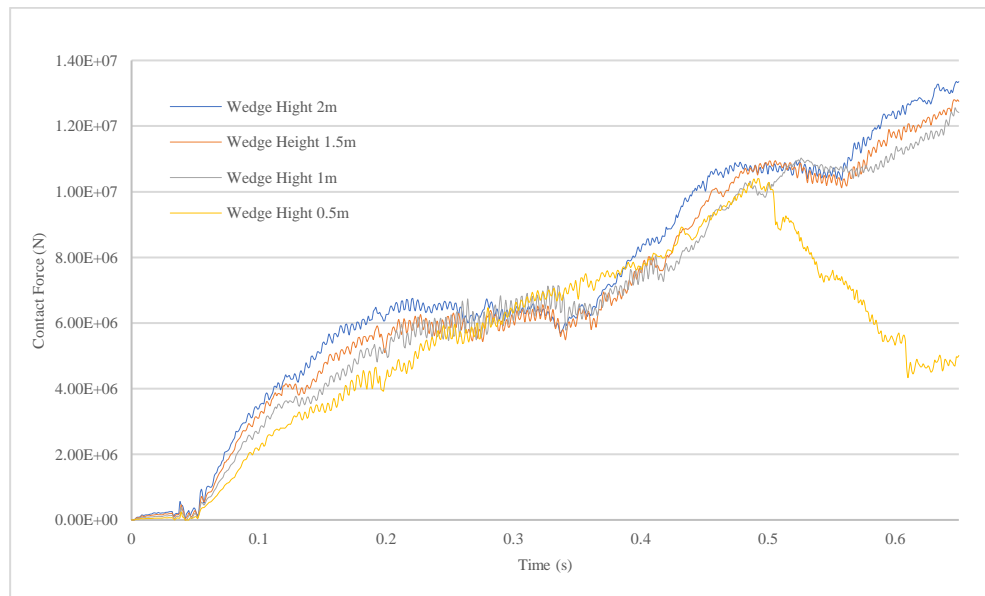


Figure 6-8 Contact force for various wedge dimensions (4500-tonne ice)

The force level is similar as shown in Figure 6-8, because the mass and velocity of both ship and ice remained constant for all simulations. By decreasing the contact area, the same force magnitude applies to a smaller area, resulting in a higher stress level.

The internal energy, which indicates dissipated energy in the form of structural deformation and rupture, is a crucial collision simulation outcome. One of the main questions about changing the mass is how it affects the rupture energy. As shown in Figure 6-9, the internal energy value at 0.6s normalized by the results of the 1500 case. By assuming a linear interpolation, the value predicted for a 12000 tonnes impact gives 3.97 (internal energy of 12000 tonnes bergy bit/ internal energy of 1500 tonnes case). This scenario was simulated, and the result was 3.78, which indicates only a 5% error (blue point in Figure 6-9). This method to extrapolate the results for larger ices can be beneficial in simplified approaches.

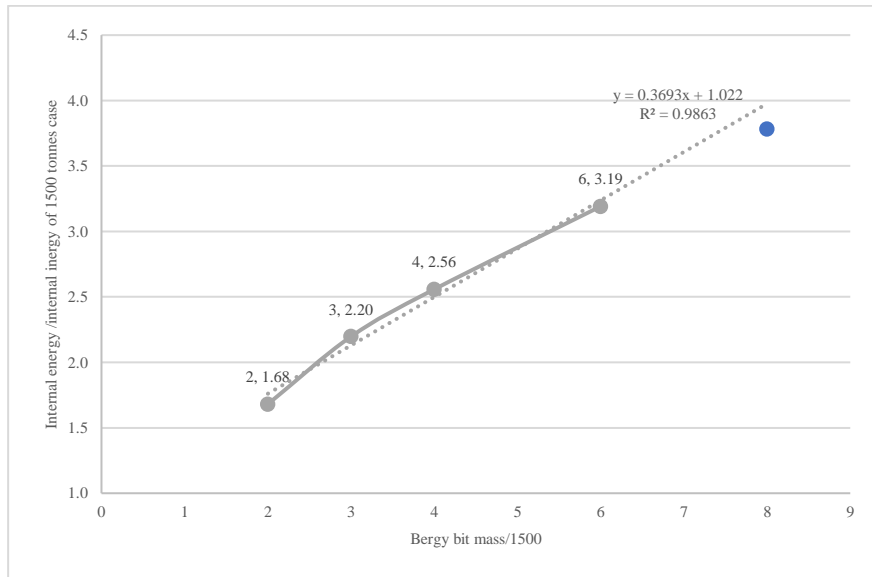


Figure 6-9 normalized rupture energy based on 1500 tonnes case

6.3 Impact with large contact area with rigid indenter

In order to assess the importance of the modelling of ice with crushable material, simulations were conducted with a rigid indenter with a similar shape, mass, friction coefficient, velocity, and impact angle (see Figure 6-1). The results were significantly different, and the impact caused extensive ruptures in the structure. The concentrated plastic strain on the upper and lower edges of rigid ice leads to plate fracture. Ice crushes and deforms under pressure, and this kind of stress and strain pattern was not observed in rigid indenter results. Therefore, the structural response shown in Figure 6-10 could not be considered realistic in an actual ice collision scenario. The summary of the results presented in Table 6-2, and the fracture pattern is depicted in Figure 6-10.

Table 6-2 Impact scenarios results summery (large contact area with rigid indenter)

Indenter Mass (tonnes)	1500	3000	4500	6000
Rupture length (m)	5.123	5.569	5.789	5.993
First contact to initial rupture (m)	1.586	1.539	1.539	1.536
First contact to initial rupture (s)	0.163	0.159	0.157	0.156
First contact to developed rupture backward (m)	1.586	1.539	1.446	1.259

Other than rupture and failure in plate and stiffeners, the internal energy and indenter force values are remarkably higher in the rigid ice impact (See Figure 6-11 and Figure 6-12). The energy that dissipated due to the ice crushing leads to lower rupture energy; moreover, the sliding impact could last over several seconds, and the delays due to ice crushing reduce the damage extent. Conclusively, the rigid indenter is not an appropriate material choice for ice sliding collision simulation.

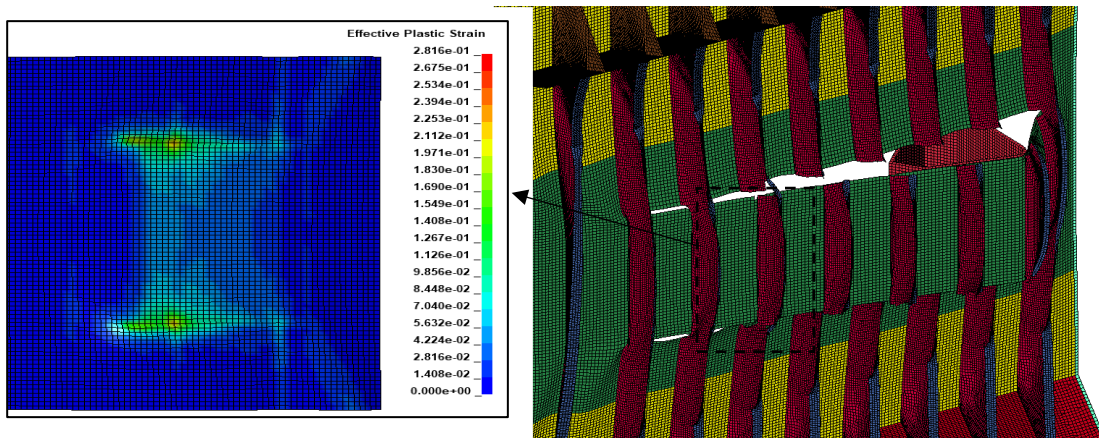


Figure 6-10 Rupture pattern for 6000 tonnes bergy bit

The results indicated that the ice material must be defined as accurately as possible, and a rigid indenter would not be an appropriate choice for sliding impact simulation.

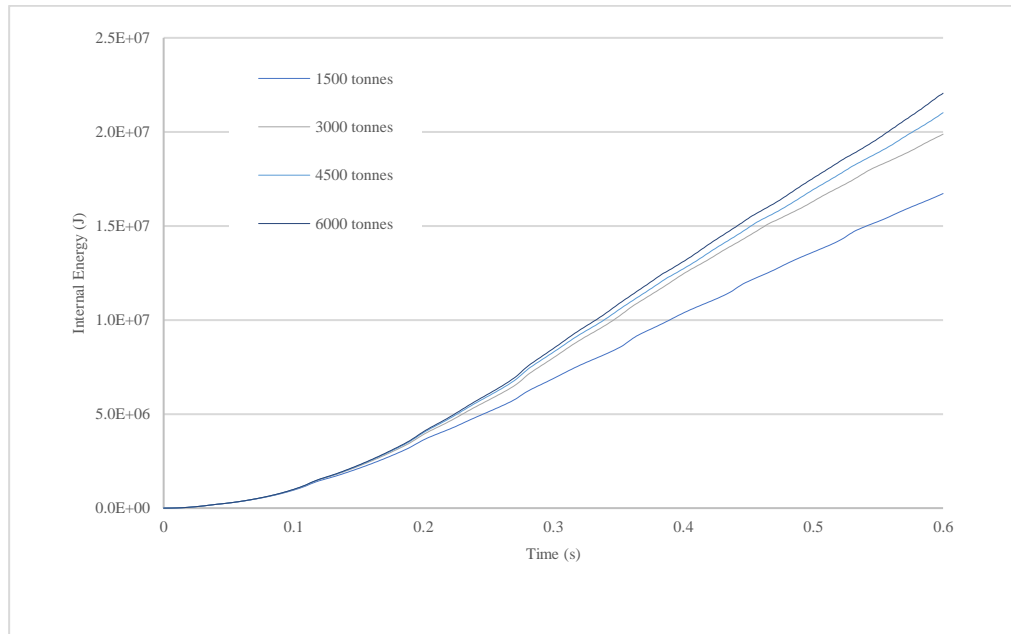


Figure 6-11 Internal energy for various rigid indenter impacts

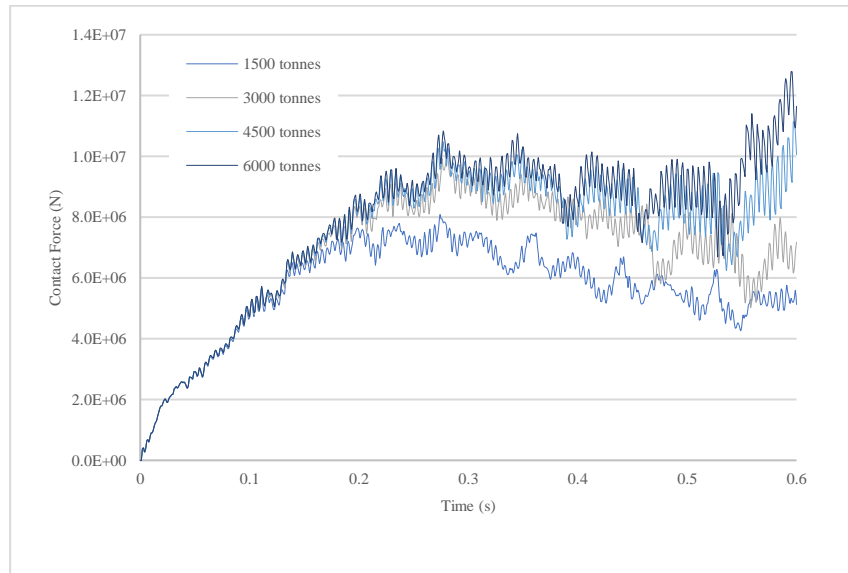


Figure 6-12 Contact force for various bergy bit impacts

6.4 Impact with the small contact area

Impact forces and resultant structural response is sensitive to indenter shape in collision simulations. Contact area and its geometry profoundly affect the contact forces; therefore, the same ice shape used in Figure 6-1 was rotated (Figure 6-13) to reduce the contact area to study the contact area's effect.

Decreasing contact area leads to a noticeable change in the structural response, as shown in Table 6-3 and Table 6-4. Selected points of simulation have been listed in Table 6-3 for the 6000-tonne impact case (Figure 6-14 shows the discussed points in Table 6-3).

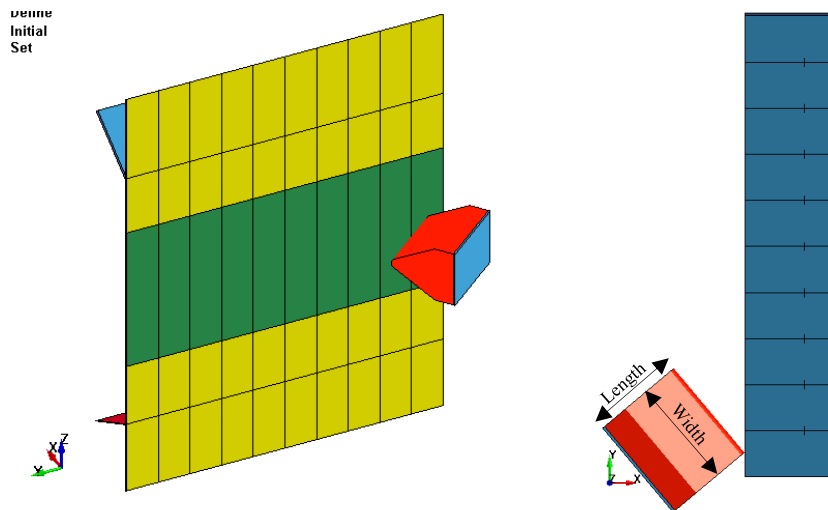


Figure 6-13 Impact scenario with the small contact area

The failure pattern is similar for all cases, and localized strain filed in the plate caused the rupture in the plate and transverse frames.

As indicated in Table 6-3, the first peak in the diagram is the plate's ultimate capacity before the fracture, primarily due to its membrane strength. The last four peaks are related to the failure of transverse frames while ice penetrates the structure.

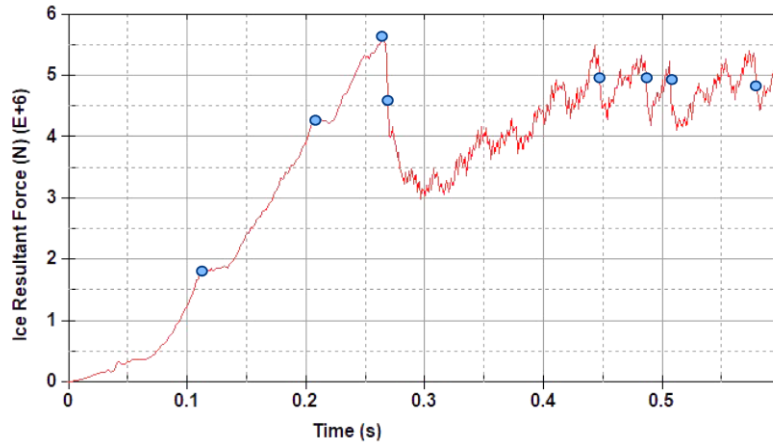


Figure 6-14 Contact Force for 6000-tonne case

Compared to the large contact area simulations, Figure 6-15 and Figure 6-16 show that the bergy bit's size is not a controlling factor in the structural response, especially as the mass increases. The reason for this observation can be seen by tracing the failure pattern during the simulation. As discussed earlier, the small contact area causes a localized strain in the plate, leading to plate failure. A small contact area results in fracture in the ice, and it is assumed that there is enough ice in an actual collision to maintain the localized ice pressure on the plate.

In other words, even small icebergs with sharp edges could rupture the plate and ship surge motion helps to develop the crack across the side shell. This point describes the graphs in Figure 6-15 and Figure 6-16, where both internal energy and contact forces are not as different as seen for large contact cases for various masses. It is evident from Figure 6-15 that the internal energy' curves converged as the weight increased. An additional ice weight of 2250 tonnes was added to capture this phenomenon.

Table 6-3 structural response during sliding impact for 6000-tonne case (refer to Figure 6-14)

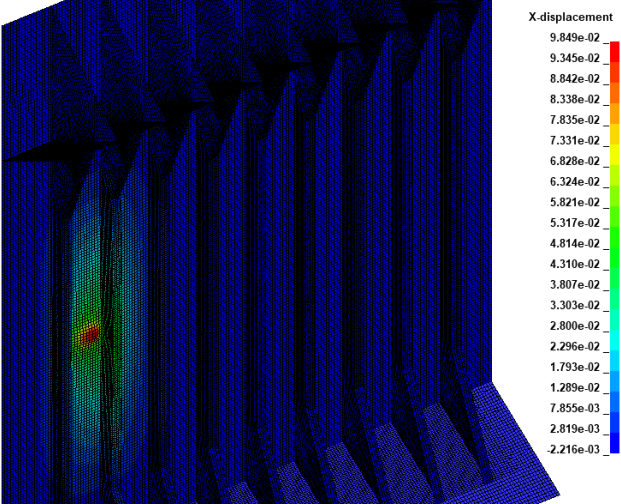
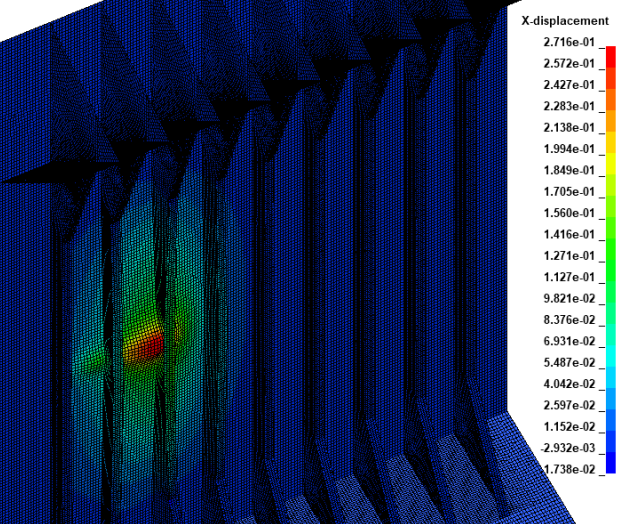
Time	Comment	
0.113	The first frame starts to deform	
0.212	The second frame deforms severely at the contact area	

Table 6-3 (continued)

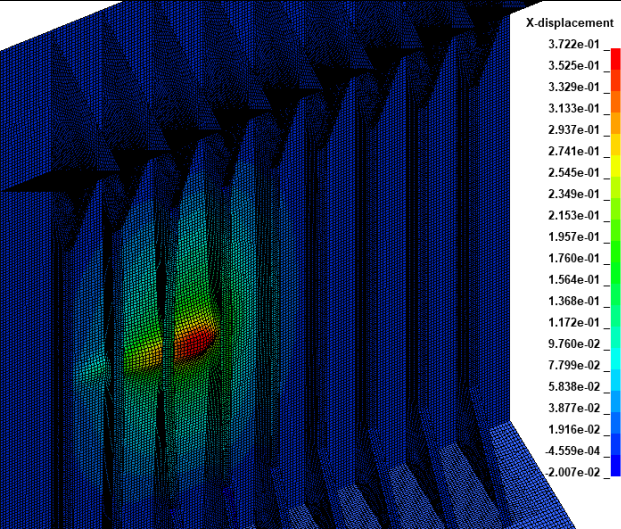
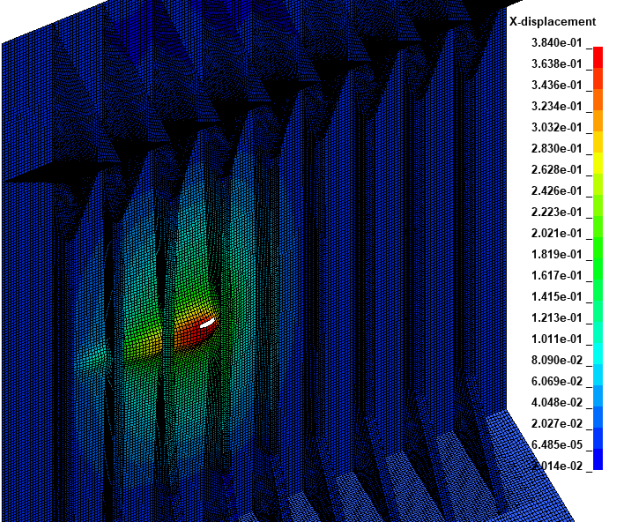
<p>0.266</p>	<p>Maximum load bearing point before a fracture initiation</p>	 <p>X-displacement</p> <ul style="list-style-type: none"> 3.722e-01 3.525e-01 3.329e-01 3.133e-01 2.937e-01 2.741e-01 2.545e-01 2.349e-01 2.153e-01 1.957e-01 1.760e-01 1.564e-01 1.368e-01 1.172e-01 9.760e-02 7.799e-02 5.838e-02 3.877e-02 1.916e-02 -4.559e-04 -2.007e-02
<p>0.27</p>	<p>Plate Rupture initiation</p>	 <p>X-displacement</p> <ul style="list-style-type: none"> 3.840e-01 3.638e-01 3.436e-01 3.234e-01 3.032e-01 2.830e-01 2.628e-01 2.426e-01 2.223e-01 2.021e-01 1.819e-01 1.617e-01 1.415e-01 1.213e-01 1.011e-01 8.090e-02 6.069e-02 4.048e-02 2.027e-02 6.485e-05 -0.014e-02

Table 6-3 (continued)

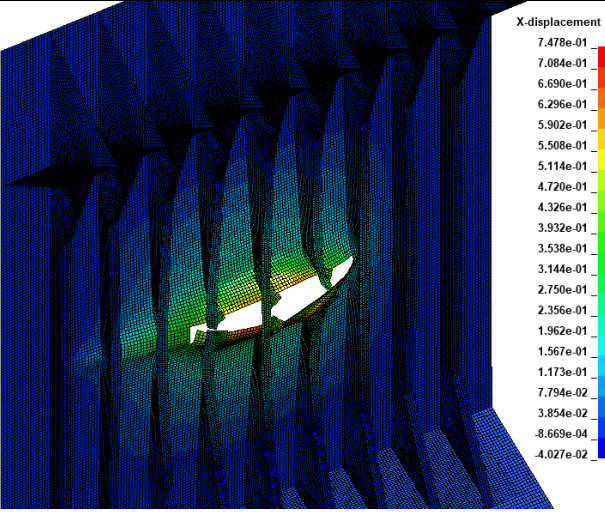
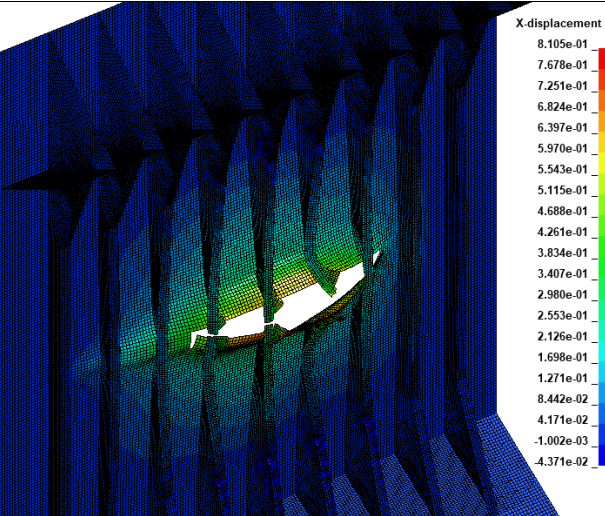
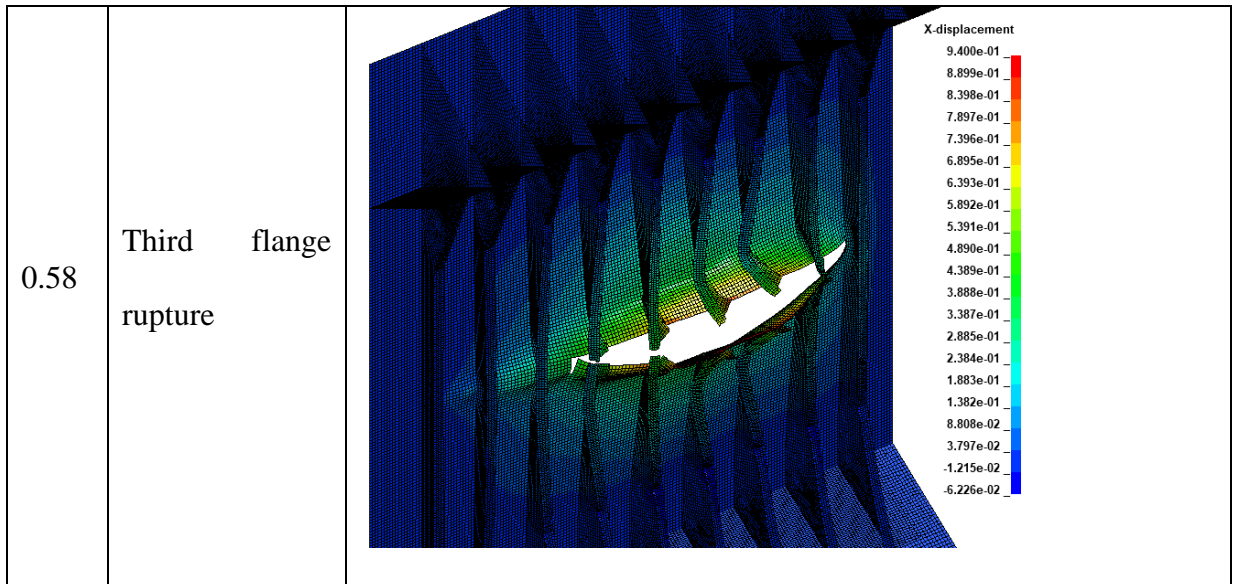
0.448	First flange rupture	 <p>X-displacement</p> <ul style="list-style-type: none"> 7.478e-01 7.084e-01 6.690e-01 6.296e-01 5.902e-01 5.508e-01 5.114e-01 4.720e-01 4.326e-01 3.932e-01 3.538e-01 3.144e-01 2.750e-01 2.356e-01 1.962e-01 1.567e-01 1.173e-01 7.794e-02 3.854e-02 -8.669e-04 -4.027e-02
0.488	Second flange rupture	 <p>X-displacement</p> <ul style="list-style-type: none"> 8.105e-01 7.678e-01 7.251e-01 6.824e-01 6.397e-01 5.970e-01 5.543e-01 5.115e-01 4.688e-01 4.261e-01 3.834e-01 3.407e-01 2.980e-01 2.553e-01 2.126e-01 1.698e-01 1.271e-01 8.442e-02 4.171e-02 -1.002e-03 -4.371e-02

Table 6-3 (continued)



In addition to the points mentioned about energy and force graphs, the data presented in Table 6-4 describes the same phenomenon. The time lag between the first contact and fracture initiation and the distance between the initial impact points to fracture initiation is similar for all cases.

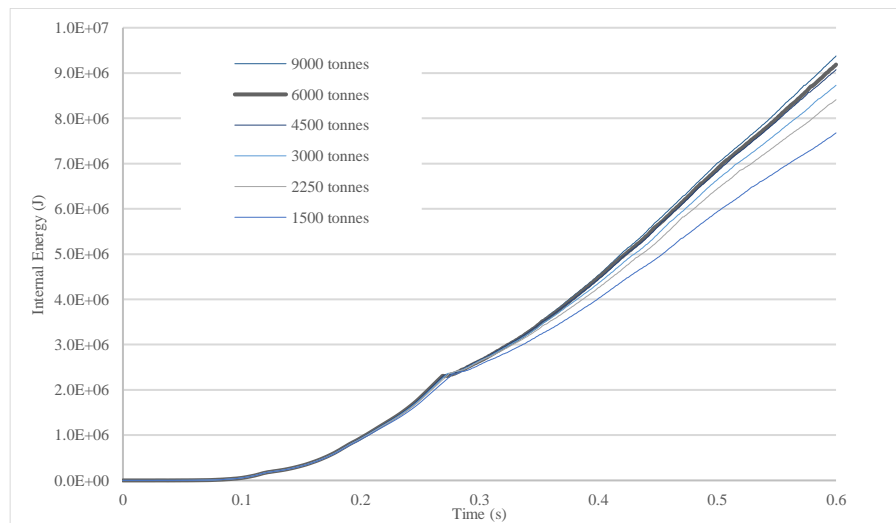


Figure 6-15 Internal energy for various bergy bit impacts (small contact area)

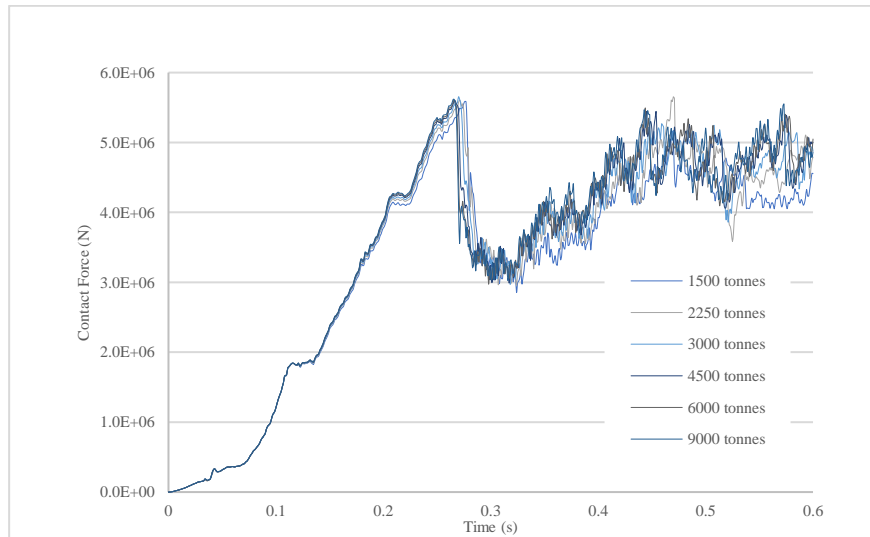


Figure 6-16 Contact force for various bergy bit impacts (small contact area)

Early failure in the plate without extensive deformation in the structure results in lower internal energy than the large contact cases. Except for 1500 and 3000 cases, other impacts had lower internal energy than the large contact area cases. This means that localized stress and strain field can result in serious rupture with lower rupture energy and contact forces.

Table 6-4 Results summary for impact with the small contact area

Ice mass (tonnes)	1500	2250	3000	4500	6000	9000
Rupture length (m)	4.47	4.54	4.63	4.67	4.77	4.82
First contact to developed rupture backward (m)	2.61	2.61	2.56	2.56	2.52	2.52
First contact to initial rupture (m)	2.753	2.706	2.706	2.66	2.61	2.66
Impact to first rupture (s)	0.278	0.0276	0.274	0.271	0.27	0.269

Even though the structural response is less sensitive to the ice's mass for sharp contact geometries, the heavier iceberg can maintain their kinetic energy longer than small ones.

This difference plays a crucial role in damage extent prediction in sliding impact. Figure 6-17 depicted the resultant velocity of the ice during the simulation. Heavier ice pieces' speed reduced slowly, which means the initiated rupture in the structure could be developed for a longer time.

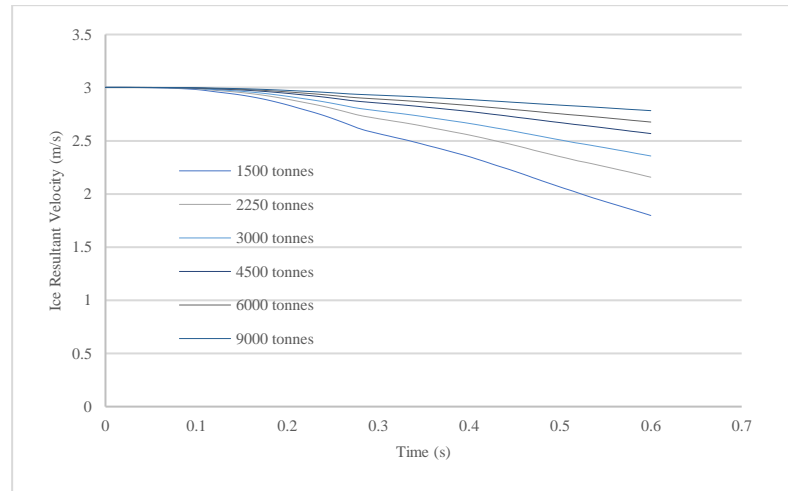


Figure 6-17 Ice resultant velocity during the simulation

Ice is a brittle material in which cracks initiate and develop in addition to crushing. When ice penetrates the hull, sharp edges of ruptured structures cause cracks in the ice (see Figure 6-18). This could lead to a shorter impact duration. The crushable foam ice model is not capable of capturing ice fracture behaviour. Consequently, when ice penetrates the hull, it keeps moving inside without any failure and crack. Unfortunately, there is no reliable ice model capable of simulating ice fracture and crack development that could be implemented in the FE model. As a result, as the sliding duration increases, the results would be less reliable.

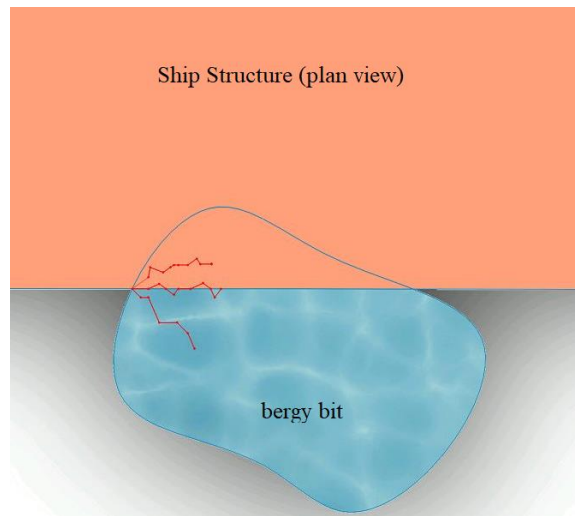


Figure 6-18 Crack development in ice due to sharp edges of the ruptured structure

6.5 Effect of the transverse bulkhead on damage extent

Transverse bulkheads are one of the main structural elements concerning strength and watertight integrity. Transverse bulkheads support longitudinal members and limit the flooding in the case of collision. One of the essential questions is that if the transverse bulkheads could withstand the ice impact load and limit the damage extent to one compartment or not. Based on the previous simulations, two positions were chosen for the BHD arrangement: before crack initiation and after a crack developed in the structure (See Figure 6-19).

Figure 6-20 illustrates the position (for position 2) and scantling of the corrugated transverse bulkhead. For the parts of the corrugated plates adjacent to the shell plate, the element ratio of two was used, and the size of mesh was increased for parts away from the critical regions.

All free edges of the bulkhead constrained as fixed due to the high rigidity of the structure.

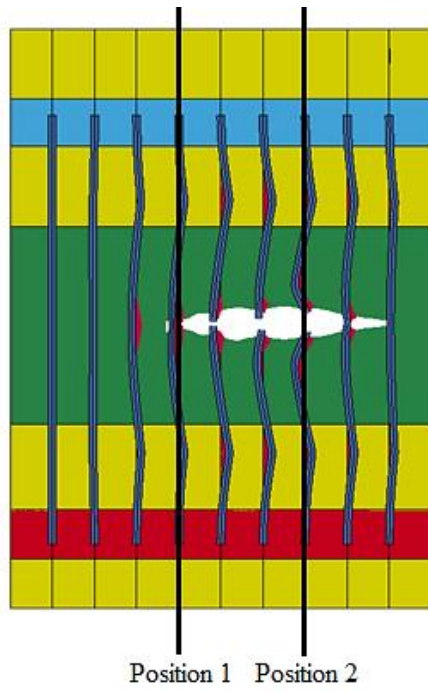


Figure 6-19 Transverse Bulkhead positions for simulations

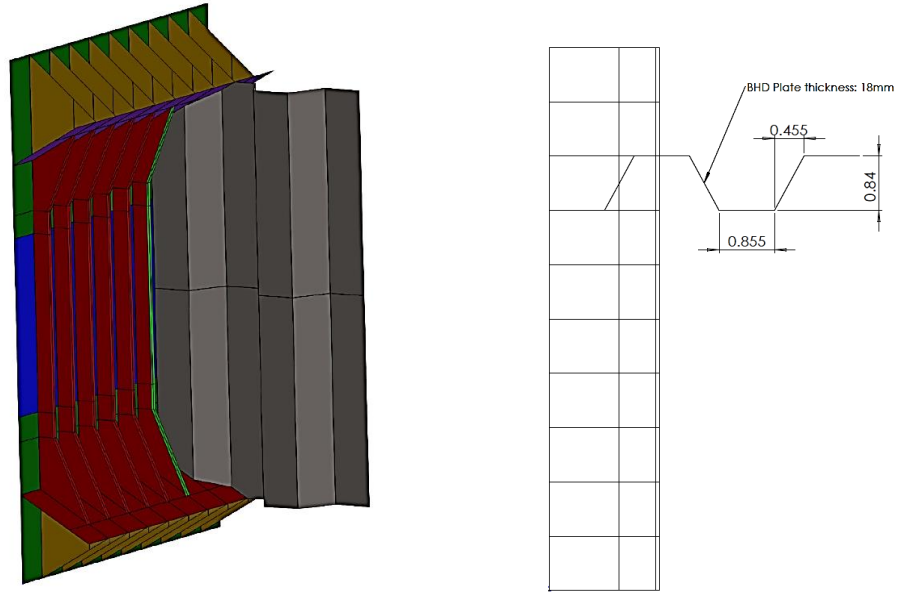


Figure 6-20 Transverse bulkhead arrangement (position 2) and scantling

Simulations were carried out for 1500-tonne bergy bit for the described positions. The analysis revealed that transverse bulkhead would not be as effective as might be thought to control the side structure's damage growth.

As shown in Figure 6-21, the bulkhead plate was deformed and crushed by the ice, and it could not stop the ice from developing rupture in the structure.

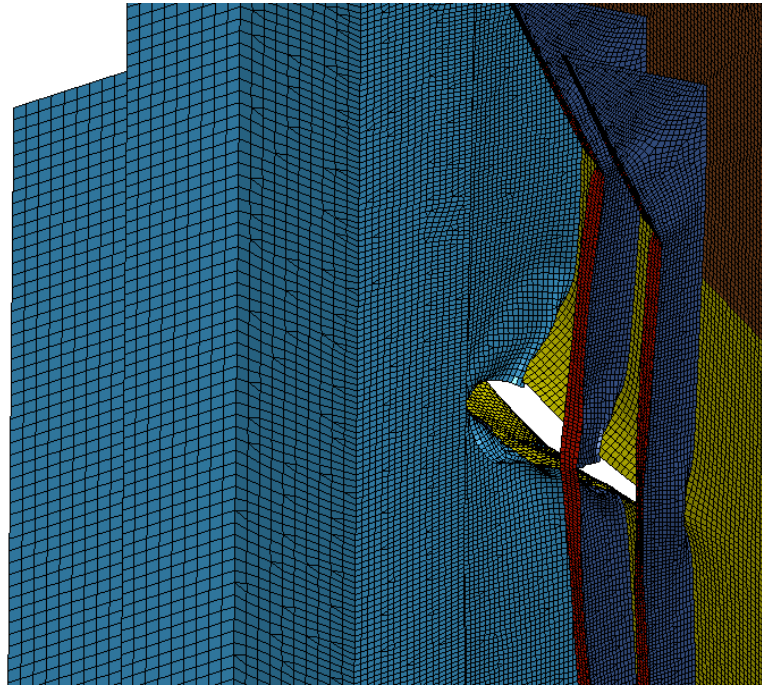


Figure 6-21 Rupture in the transverse bulkhead (1500-tonne case)

Contact force graphs shown in Figure 6-22 highlighted the effect of transverse bulkhead on the results. Broadly speaking, the response for all cases was found to be similar for all cases other than the peak force. For bulkhead located before the crack initiation, the peak contact force was observed earlier, and the force's value was higher due to the BHD's existence. The graph converged to the graph without a transverse bulkhead after the ice distance from BHD increased.

As for the transverse bulkhead located on position No.2, the graph is identical to the case without a bulkhead. After the BHD got in contact with ice, the graphs commenced diverging. The peak force was higher than the two other cases, and the reason is that the ice penetrated the hull more than in other cases. As a result, the bulkhead imposed more force on the ice in contact.

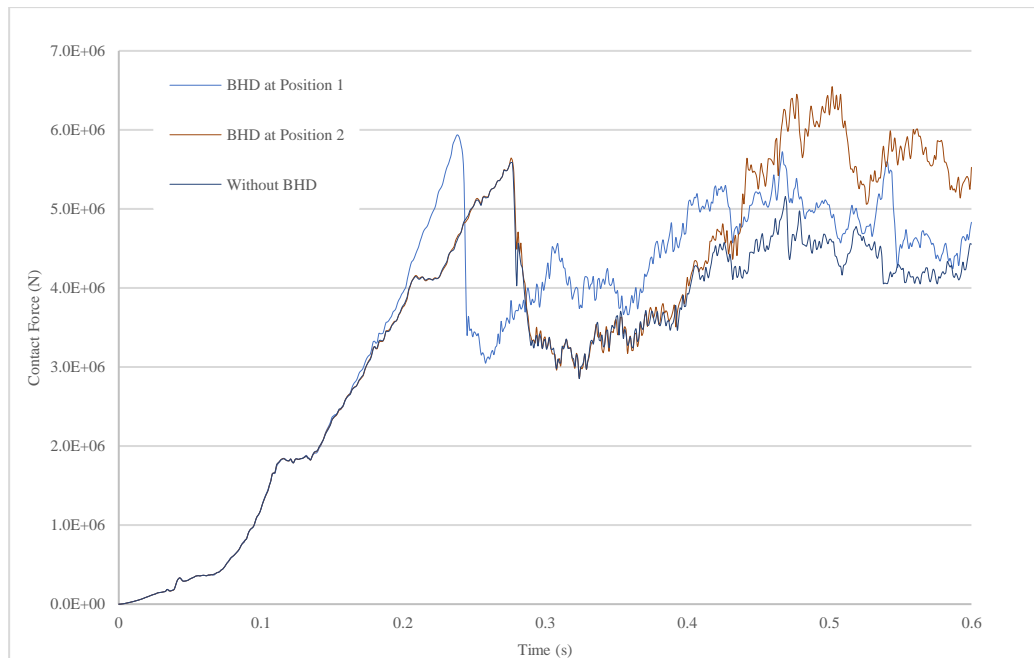


Figure 6-22 Contact force for models with transverse bulkhead and without a transverse bulkhead

The ice velocity for the mentioned three cases shown in Figure 6-23. Although the transverse bulkhead could not limit the damage in one compartment, it reduced the ice velocity. Graphs for velocity are analogous to those of contact forces. Bulkhead in position 1 caused a distinct reduction in ice velocity at the beginning of the simulation, and for bulkhead in position 2, the same reduction was captured when the BHD and ice collided. It

was detected that the ice velocity for the bulkhead located in position 2 converged to the graph of the bulkhead in position 2. The convergence of ice velocity for both cases highlighted that for estimating the damage extension, BHD's position would not be important. This finding shows that the transverse bulkhead position is not a controlling parameter for the purpose of damage extension simulation, and selecting a random location based on model length is appropriate. Even though the existence of a transverse bulkhead causes a reduction in ice velocity, the ice velocity would not change impact duration significantly.

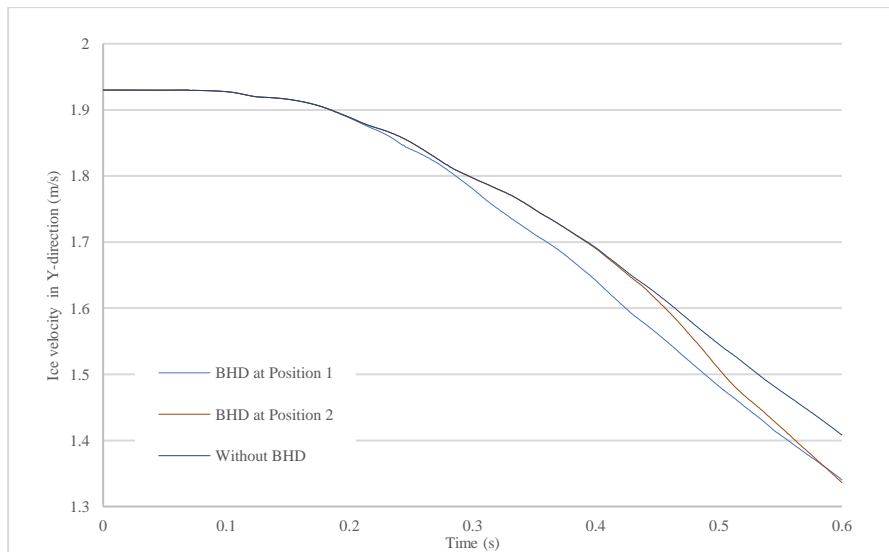


Figure 6-23 Ice velocity for simulations with transverse bulkhead and without transverse bulkhead (1500-tonne with small contact area)

As noted previously, the results indicated that the transverse bulkheads could not be effective in limiting the damage extent. These findings are crucial in damage stability calculations because they make it necessary to flood two compartments in damage stability calculations.

Deterministic damage stability calculations are based on a damage length based on the vessel's main particulars, such as length. It is necessary to decide whether the damage length should cover two compartments. Based on the presented results, the damage length should cover two adjacent compartments. For merchant ships with large cargo holds, flooding of two compartments is a severe case for damage stability calculation.

6.6 Effect of impact angle on the damage extent

Impact angle is a critical parameter in the value of the force in any collision scenario. The effect of the ice impact angle was studied by simulating various impact angles listed in Table 6-5.

Table 6-5 Impact velocity for various collision scenarios

Impact Angle (degree)	Ship surge velocity in x-direction (m/s)	Ice velocity in x-direction (m/s)	Ice velocity in y-direction (m/s)	Ice resultant velocity (m/s)
30	8.23	1.5	2.6	3.0
40	8.23	1.93	2.3	3.0
50	8.23	2.3	1.93	3.0
60	8.23	2.6	1.5	3.0
Refer to Figure 5-6 for details.				

The results showed that the impact angle is a key parameter in fracture initiation. Although the impact angle of 60° has a higher contact force than the 50° impact angle (see Figure 6-24), the impact did not cause any rupture in the structure. The fracture occurred for 40°, and 50° cases and only one element failed for 30°. It was showed that a combination of velocity in the X and Y direction is required to initiate fracture. Figure 6-24 also demonstrates that the fracture initiates earlier for 50° compared to 40°.

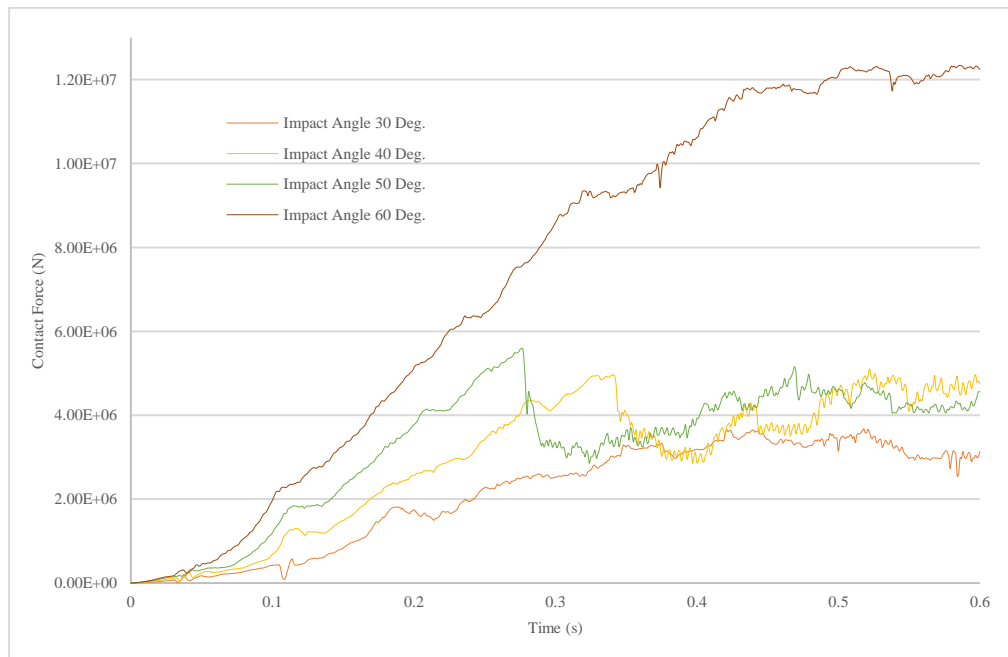


Figure 6-24 Contact force for various impact angles (1500-tonne bergy bit)

It is worth mentioning that these simulations are based on the assumption that the bergy bit moves with waves (see Figure 5-6). Two common approaches generally implement by mariners when encountering rough seas. The first approach is to decrease the speed and navigate with a head-on course. The other is to maintain the speed and change the course in order to limit the slamming forces and shipping sea [65]. Generally, the speed reduction in the head-on case is the best method to control the load on the structure. However, it is difficult to maintain the speed even in the course change approach. In research done by the Japan P&I club [65], the course change is to be significant in order to have a noticeable change in vessel behaviour. The value of speed reduction is vessel-specified, but a reduction of speed around 1 to 2 knots can half the number of the shipped sea [65]. For the slamming, the speed reduction should be in the range of 2~3 knots. Therefore, for small

impact angles, the vessel's speed is lower than the larger impact angles, which reduces the impact energy and consequent damage.

6.7 Simulation with Cone

In this section, the results of impacts with cone shape ice are presented. As discussed in the previous sections, the contact area is the dominant parameter in fracture initiation and damage growth in the collision. Two cones with angles of 45° and 30° with tip radius equal to 6cm were chosen to study cone angle effect on the structural response. The impact angle of 50° was selected for these simulations, and two bergy bit masses were investigated: 1500 and 4500 tonnes. Figure 6-25 shows the cone geometry of both cones.

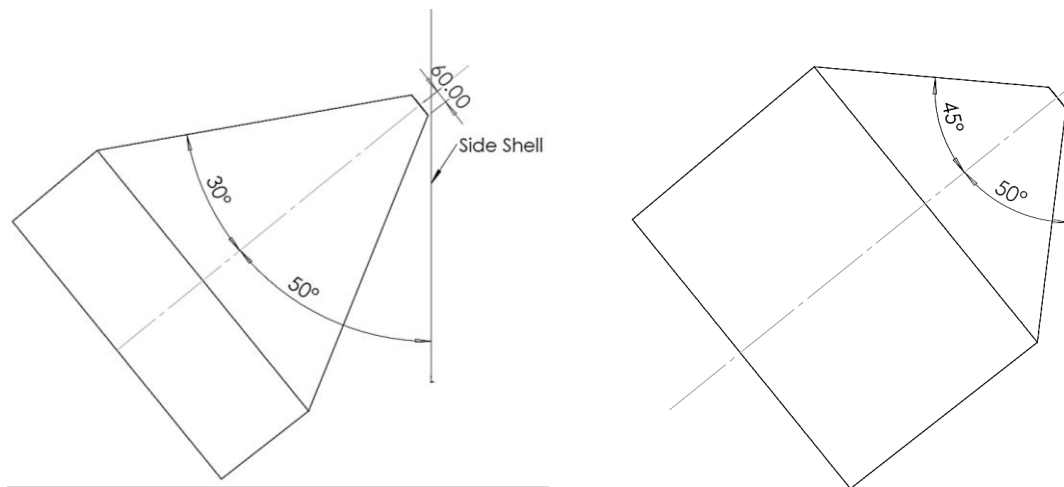


Figure 6-25 cones' geometries with angles of 30° and 45°

Figure 6-26 and Figure 6-27 compare the results for cone impacts with the ice wedge with a small contact area. It is evident that the ice geometry has a noticeable influence on the amount of force on the structure. Cone, with an angle of 45° and mass equal to 1500 tonnes,

separates from the structure sooner than in other cases. As shown in Figure 6-26, the contact force dropped rapidly after the ice commenced to separate from the structure. The large angle of the cone in 45° cone leads to no fracture in the structure even for 4500-tonne simulation.

The only case that fracture was initiated and developed was a 30° cone with a mass of 4500 tonnes. For a smaller cone, 30° cone with a mass of 1500-tonne, the ice bounced back quickly and caused no fracture despite large localized deformation in the shell plating (see Figure 6-30). In Figure 6-30, the shell plate deformation for two cones is compared, and it is shown that the cone with a wider angle caused wider deformation field and separated from the plate sooner than a sharper cone.

Sharper geometry of the 30° cone caused fracture on a lower force level in comparison with the ice wedge (small contact area). A 1500-tonne ice-wedge caused a fracture in the plate; however, the 1500-tonne ice cone did not initiate rupture despite the sharper contact region. It is concluded that a combination of several factors control whether the rupture initiates in the plate. Smaller contact areas and resulting localized strain fields are crucial to fracture initiation; however, the ice tip should have a geometry that stays in contact with the plate long enough to initiate the crack. The internal energy of the mentioned impacts is presented in Figure 6-28 and Figure 6-29.

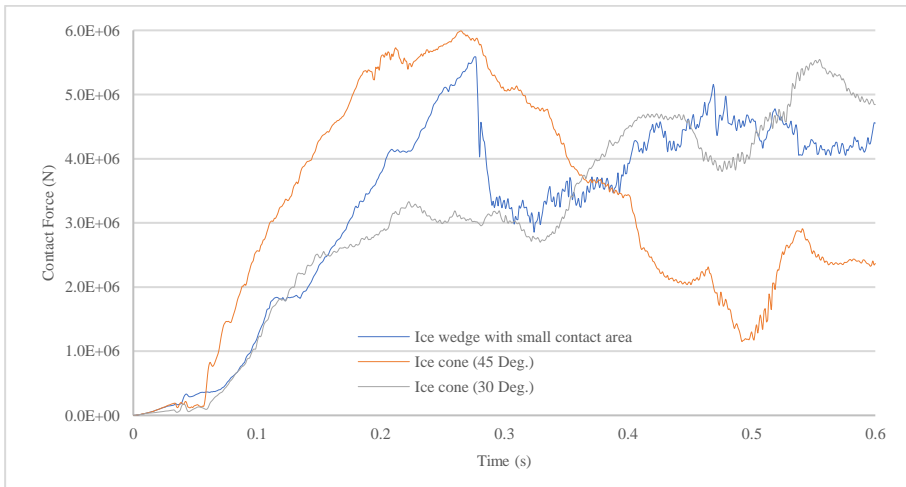


Figure 6-26 Contact force for impact of 1500-tonne bergy bit with various ice tip shapes

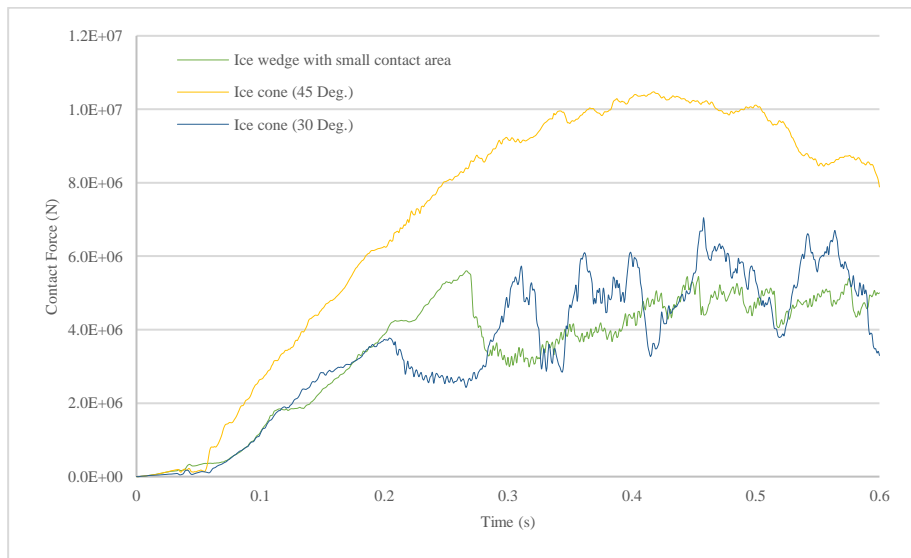


Figure 6-27 Contact force for impact of 4500-tonne bergy bit with various ice tip shapes

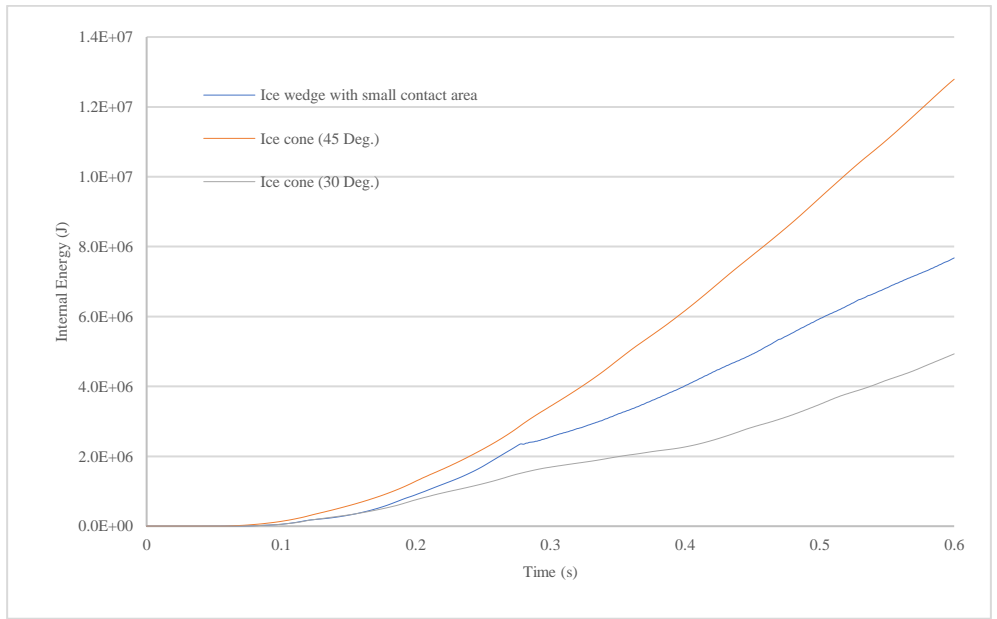


Figure 6-28 Internal Energy for the impact of 1500-tonne bergy bit with various ice tip shapes

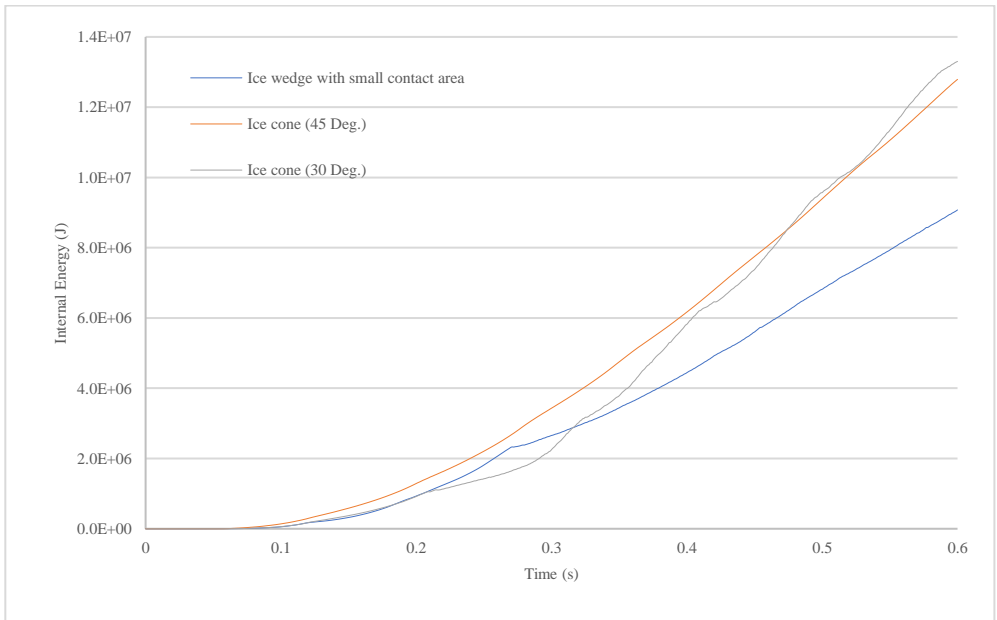


Figure 6-29 Internal Energy for impact of 4500-tonne bergy bit with various ice tip shapes

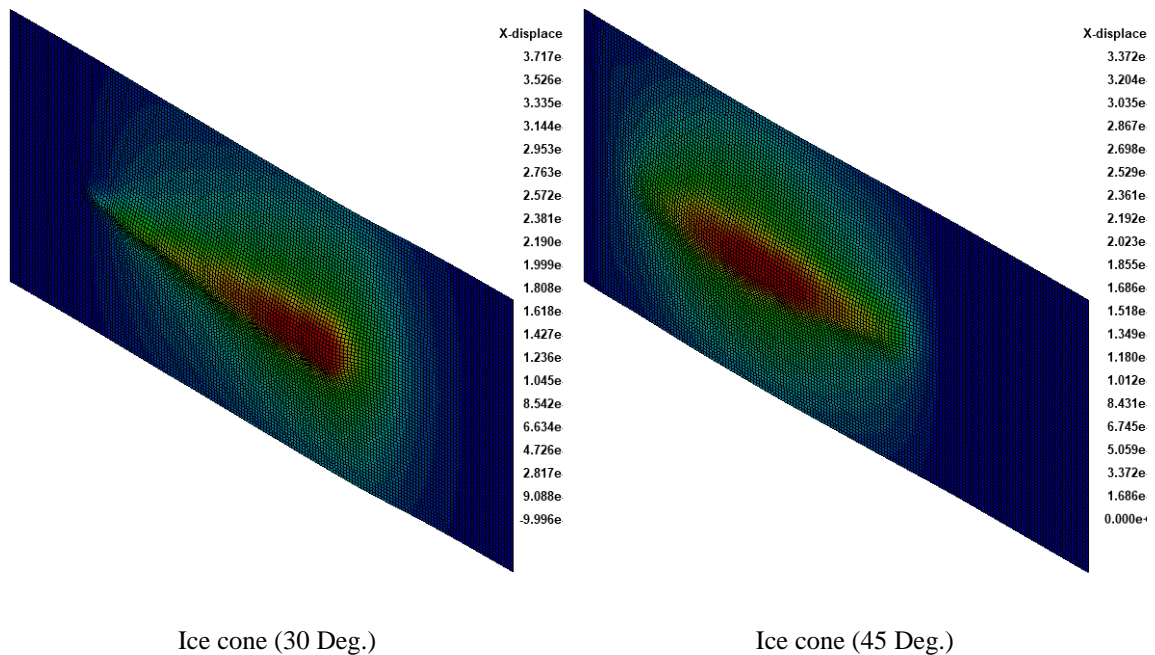


Figure 6-30 Deformation pattern for 1500-tonne impact cases for both ice cones

6.8 Effect of mass ice distribution on damage results

In the previous sections, the mass of ice was applied at the end row of elements of the ice-wedge or ice cone. In reality, however, the ice geometry and center of mass are shape sensitive, and it affects the ice-fluid interaction.

Figure 6-31 schematically compares the ice-ship interaction for irregularly shaped ice and simplified ice wedge. In an actual collision scenario, when a bergy bit collides a vessel whose mass is several times larger, a large portion of kinetic energy dissipates by ice movement (rotations and movements in six degrees of freedom). In a simulation conducted for a 3000-tonne bergy bit, the ice-wedge fully penetrated the hull.

As noted earlier, the complete method to include all parameters in a simulation is to couple both external and internal mechanics, i.e. fluid-structure interaction. The computational

capacity required for a simulation that involves fluid-solid interaction and fracture would be enormous. Therefore, the fluid interaction was not included in this research.

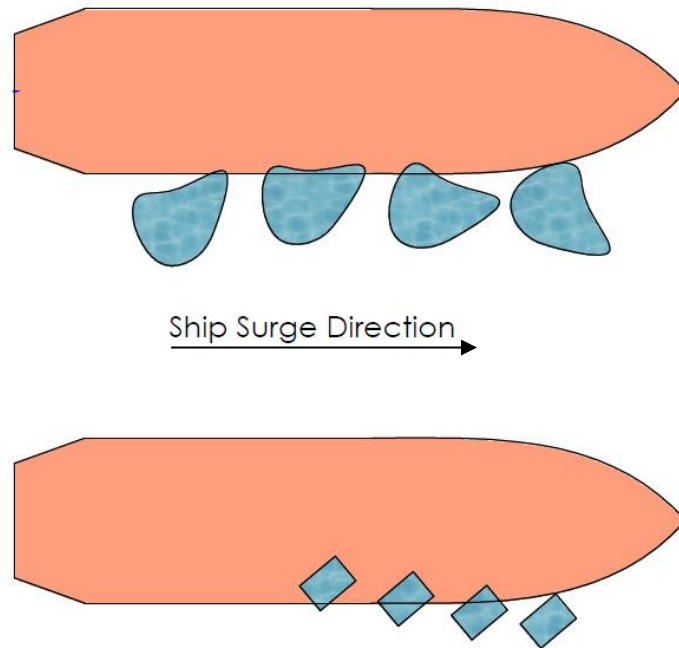


Figure 6-31 Ice-vessel interaction in actual (top scheme) and simplified ice wedge

A simplified approach to make the simulations more realistic is to define the center of mass as realistic as possible. It is possible to define a mass point at a distance from the collision point and connect all nodes to a single point to mimic mass distribution. However, this approach does not capture the effect of other parts of the ice getting in contact with the structure. Thus, the effect of mass ice distribution was investigated by considering ice as a sphere with a sharp wedge similar to the small contact area simulations.

A sphere with a mass of 1500 tonnes has a radius of 7.35 meters, and in the actual situation, the bergy bit rotates around the center of the sphere. Therefore, the ice was connected to a

hollow cylinder meshed with high-density solid elements (see Figure 6-32) to move the center of mass to the center of the sphere. A larger rotation arm induces higher momentum to the ice and increases the rotation of ice which behaves like a damper to reduce the ice velocity faster than previous simulations.

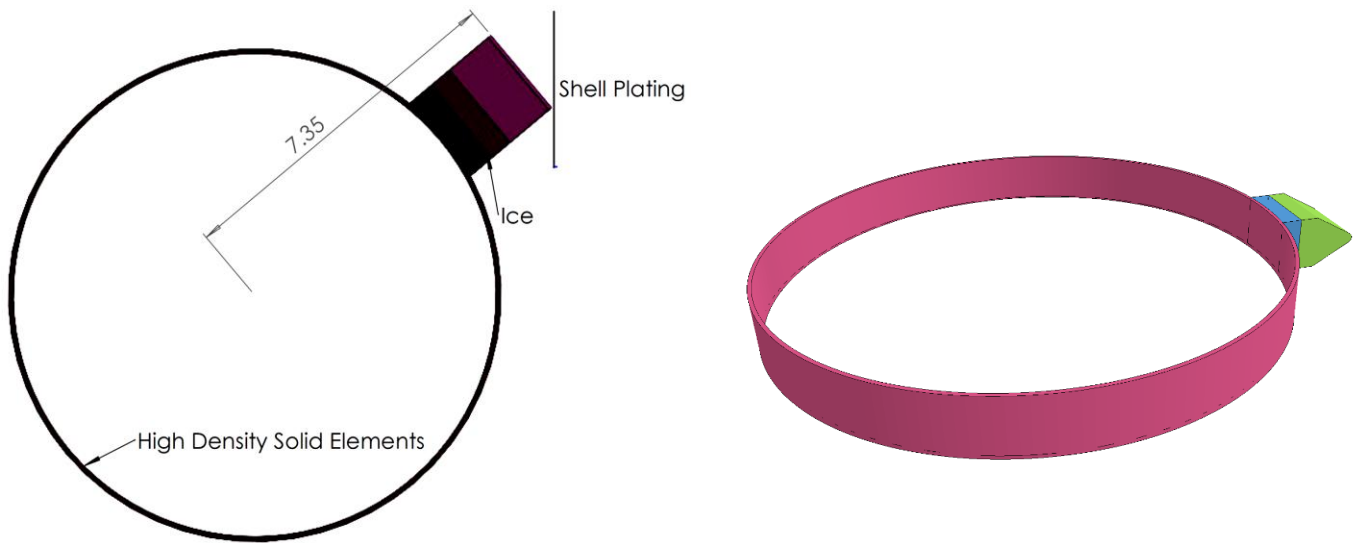


Figure 6-32 Ice modified geometry with a realistic center of mass

The damaged length for both ice shapes was similar for the same simulation duration (4.47 metres for the previous simulation and 4.3 metres for ice with the adjusted center of mass). The velocity of the mentioned cases was different, as depicted in Figure 6-33. It is evident in Figure 6-34 that the modified model starts to separate from the structure sooner than the ice wedge in the initial model.

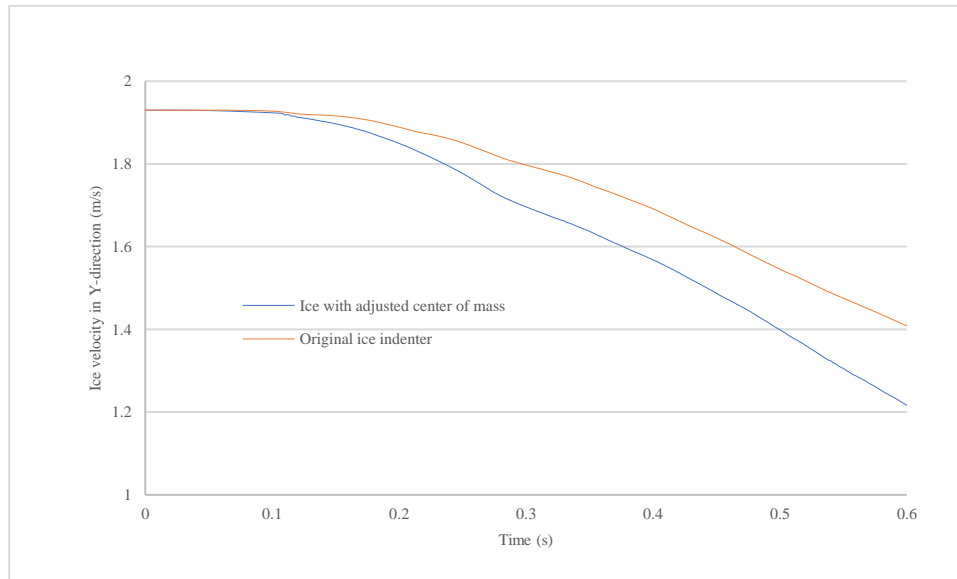


Figure 6-33 Ice velocity in Y-direction for 1500-tonne case for different center of masses

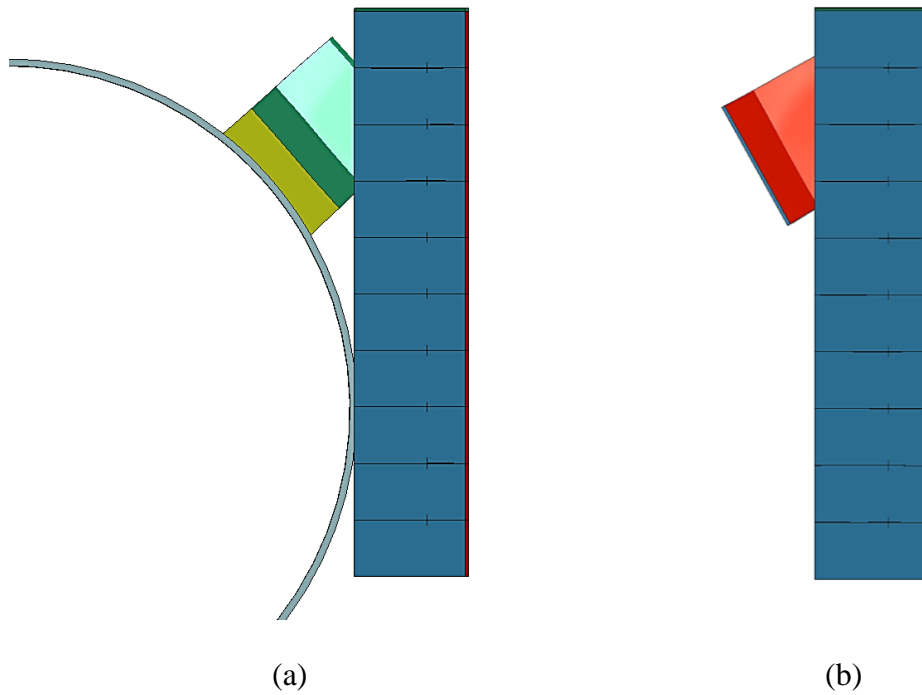
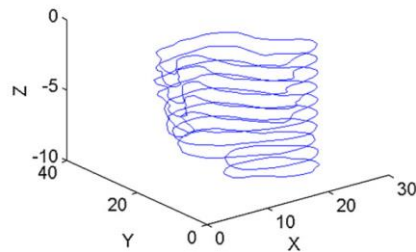


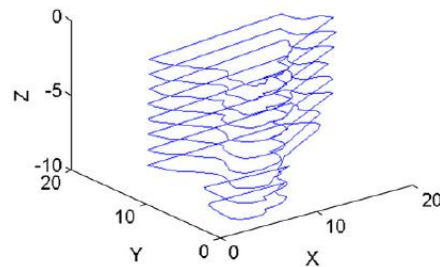
Figure 6-34 Ice wedge at 0.6 s (1500-tonne bergy bit) (a) with new geometry for the attached weight (b) initial model

A similar simulation was carried out for a 3000-tonne bergy bit, and the results confirmed that modelling ice as a wedge or cone would be a conservative way of ice modelling for sliding simulation. Other than the discussed effect of the center of mass on the results, it is necessary to mention that when the bergy bit starts to rotate, other parts of it get in contact with the ship structure. It has two consequences: firstly, the additional contact area behaves like a damper and reduces the velocity and kinetic energy of the ice. Secondly, a new contact region might extend the rupture in a different direction and increase the size of the hole on the side shell. The former occurred for a 3000-tonne bergy bit when the back end of the hollow cylinder touched the shell plate.

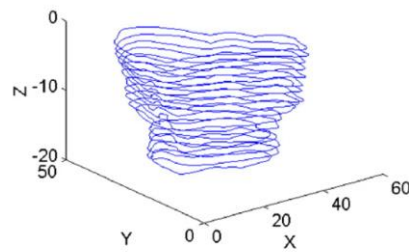
Bergy bit geometry is very intricate, and the effect of the center of mass is different for each geometry. Figure 6-35 depicts the ice shape of three bergy bits recorded in large-scale ice impact [48]. From Figure 6-35, it could be understood that the center of mass most probably will not be on the same plane as the impact point. Glancing impact occurs instantly, and considering the center of mass on the plane of collision point is a reasonable assumption. As for sliding collision, however, the actual ice center of mass is a controlling parameter.



2173 tonnes



966 tonnes



9076 tonnes

Figure 6-35 Bergy bit shapes recorded in ice impact large scale experiment [48]

A different simplified ice shape was modelled to investigate the effect of the ice center of mass when it is not on the same plane as the impact point. As shown in Figure 6-36, a cylinder with a depth of 12.6m was modelled with a rigid material to move the center of mass to a point lower than the collision plane. In the previous simulations, the rigid part of the ice contact with the side structure caused severe damage to the ship side that was unrealistic. Therefore, an ice fender was added to the cylinder to prevent rigid part contact to the side structure (Figure 6-36).

In initial simulations, the plate edges penetrated the lower ice fender that resulted in termination. Therefore, the ice cylinder moved several frames forward to avoid numerical issues. Results showed significant differences in damage to the structure and ice movement. The deeper ice model did not cause any rupture in the structure as opposed to the initial short ice cylinder.

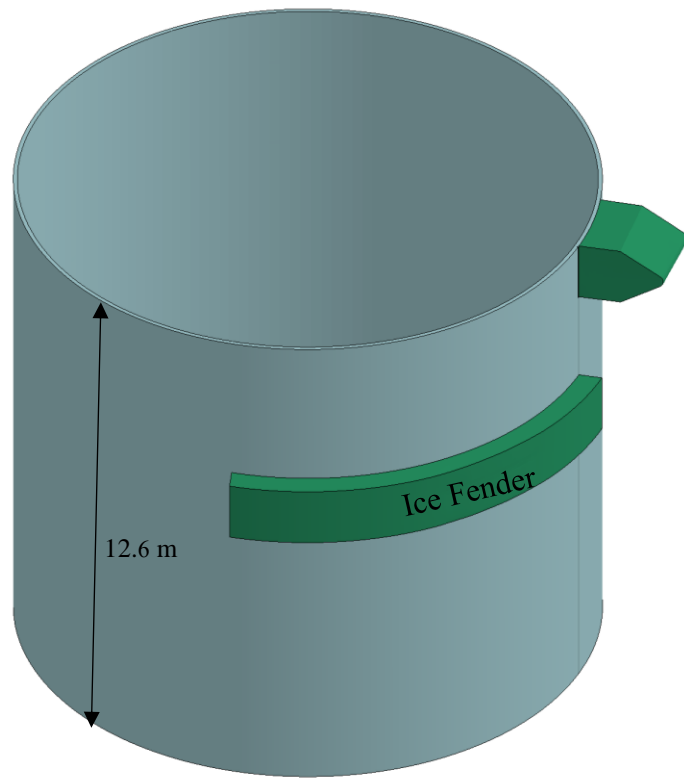


Figure 6-36 Ice model with the center of mass away from the collision point

Figure 6-37 compares the Von-Mises stress contours before and after the ice fender contacted the structure. At 0.04s, the sharp edge of the ice-wedge caused localized stress and strain filed similar to the previous simulations. However, after the ice fender became in contact with the structure, the stress level dropped at the ice-wedge contact region and continued to the end of the simulation. This case a combination of small and large contact areas in the previous sections. A large contact area caused severe deformations, but to initiate fracture a localized strain field is necessary.

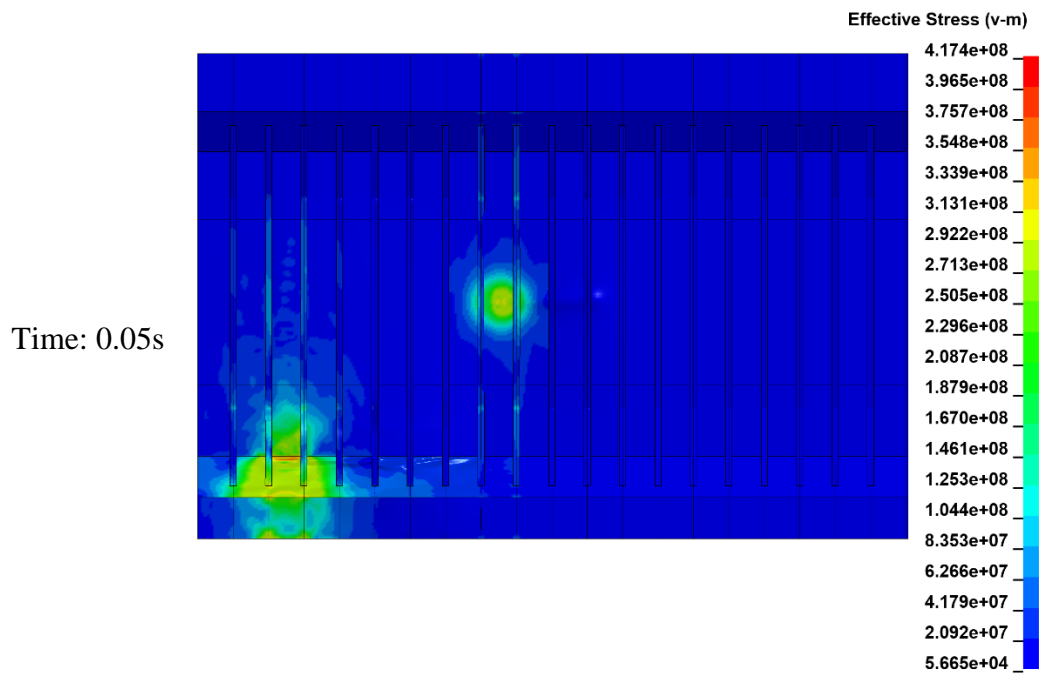
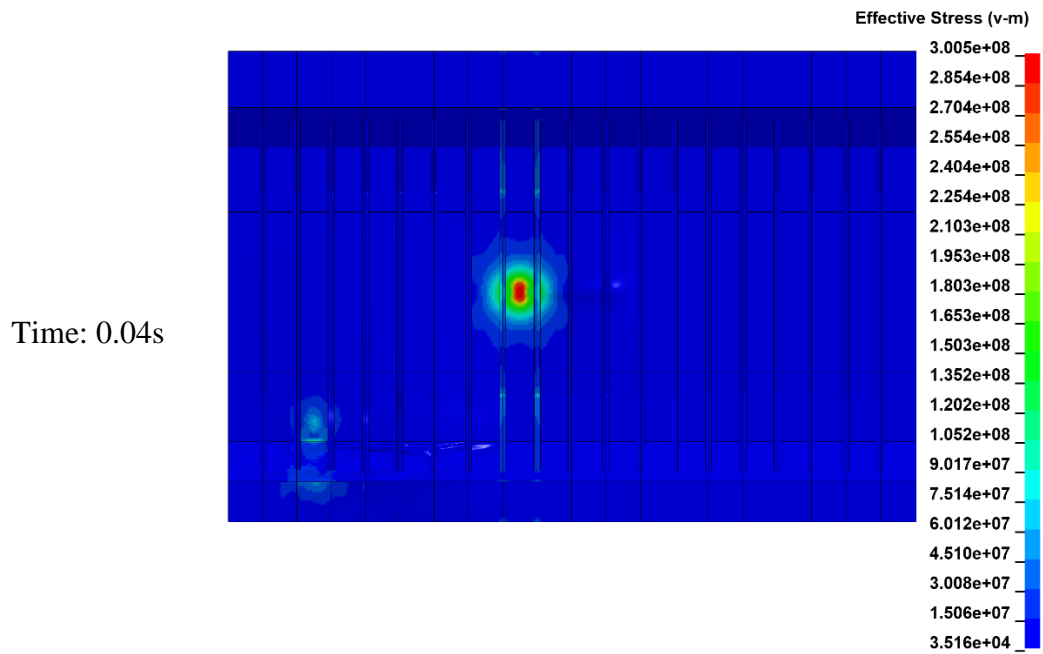


Figure 6-37 Von-Mises stress before and after ice fender contacted the structure (3000-tonne bergy bit)

Structural deformation is shown in Figure 6-38 at the end of simulation time (0.7s). The extensive structural deformation at the ice fender is similar to the large contact area simulation (see Figure 6-4). These two distinct deformation patterns are marked on the deformation contour in Figure 6-38. Simulations for 9000-tonne bergy bit leads to similar results, and no fracture was caused.

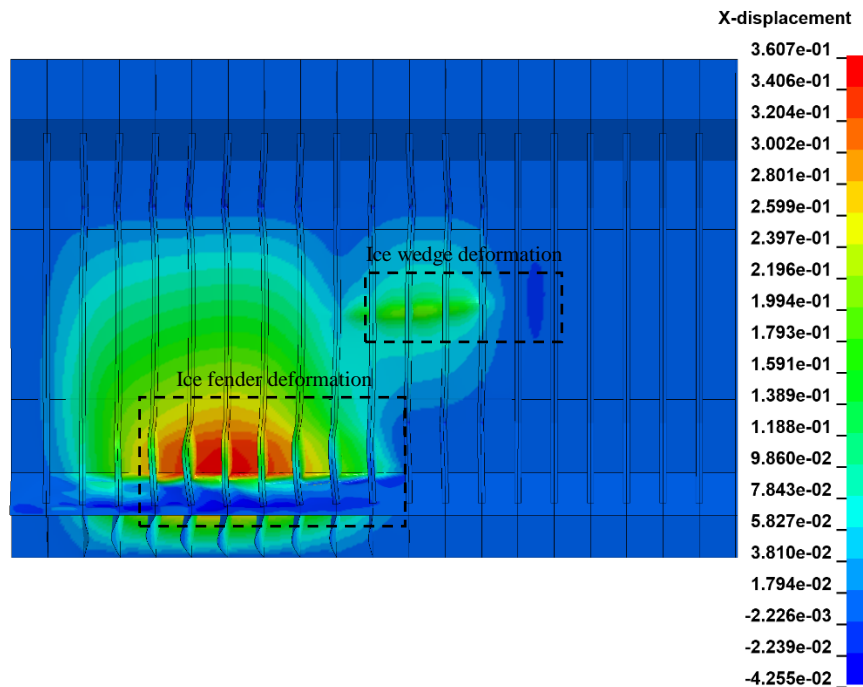


Figure 6-38 Structural deformation at the end of the simulation (3000-tonne bergy bit)

Besides the effect of the ice fender on the structural response, the new ice model caused a significant difference in ice movement due to the reaction forces. The rotation and movement of ice at the end of the simulation are shown in Figure 6-39. In this case, the additional moment due to the center of mass not being in the same plane of impact leads to large rotation. This significant rotation results in a comparatively shorter impact duration than the ring shape in the previous simulation.

The contact force diagram for this collision scenario showed (Figure 6-40) a steep increase in contact force because of the ice fender's additional load on the structure. Despite the sharp increase in contact force, it dipped quickly after the out-of-plane rotation started.

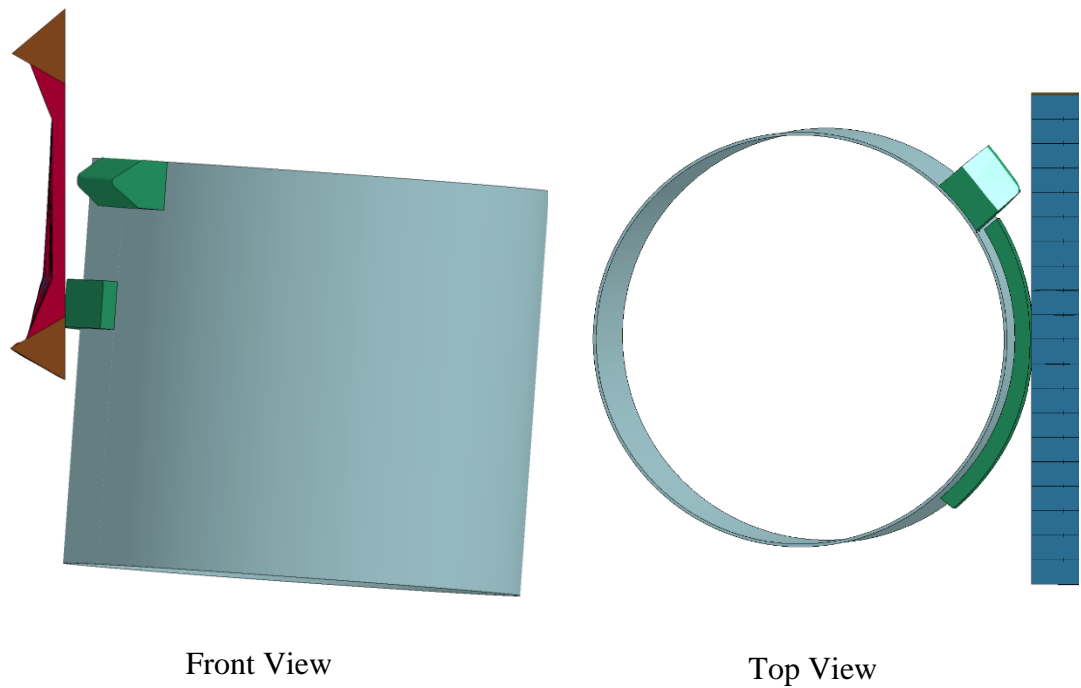


Figure 6-39 Ice rotation and separation from the structure at the end of the simulation (3000-tonne bergy bit)



Figure 6-40 Contact force for ice collision with long cylinder shape (3000-tonne bergy bit)

Results indicate that in an actual collision, ice's shape changes the impact time and rupture length. For slab-shaped ice that has a more considerable length to width ratio, the center of mass is far away from the collision point compared to a dome shape bergy bit, and as a result, the ice-structure interaction would be different. However, as discussed earlier in section 3, the ice model that is used in the simulations does not lead to accurate results for long simulations.

It could be concluded that for a conservative design approach, the ice indenter with the center of mass on the plane of impact is reasonable. For forensic analysis, however, the ice shape is to be modelled accurately.

It is also important to mention that the hydrodynamic effects such as drag force on the ice are shaped sensitive. It is formidable to include it implicitly in a structural analysis without modelling fluid-structure interaction. In this research, the hydrodynamic parameters were not included in the FE simulations.

6.9 Summary

Results of FE simulations were presented in this chapter. Various ice shapes and ice masses were studied to assess the structural capacity of single hull non-ice class ships in collision with ice. Highlights of research findings are presented in chapter 9.

Chapter 7 Results and Discussions- Part 2: Structural Response of Double Hull Structures

7.1 Introduction

Single hull structure is the main focus of this study; however, three double hull vessels with different framing systems were investigated. The following vessels were studied in this section:

- Double hull structure with transverse framing
- Double hull structure with longitudinal framing
- Offshore supply vessel with transverse framing

7.2 Double hull structure with transverse framing

Single hull structures are prone to extensive flooding compared to double hull ships. Therefore, the main focus of the research was to investigate single hull ships. However, it is necessary to study the double hull ships as well.

This section presents the results for a double hull structure with the transverse framing (as described in 5.2.2). Ice geometry with a small contact area was used in these simulations as discussed in the previous sections.

Figure 7-1 and Figure 7-2 compare the contact force and internal energy for various ice masses, respectively. Graphs show the same trend as for single hull simulations in the single-shell structure. The force to initiate rupture is independent of the mass of the bergy bit, and the contact area at collision is the crucial parameter. Based on the results of the

single hull simulations, the mass of the bergy bit is a dominant parameter in how long the ice can continue to damage the structure.

As opposed to the contact force graphs for the single hull structure, the existence of transverse web frames gives the graphs a distinct tooth shape appearance. Web frames in double side structures are designed with large openings to facilitate access to the confined spaces and reduce the lightweight. It is evident that the large openings are a weak point in collision accidents because they cause stress concentration that leads to rupture and fracture in the web frame.

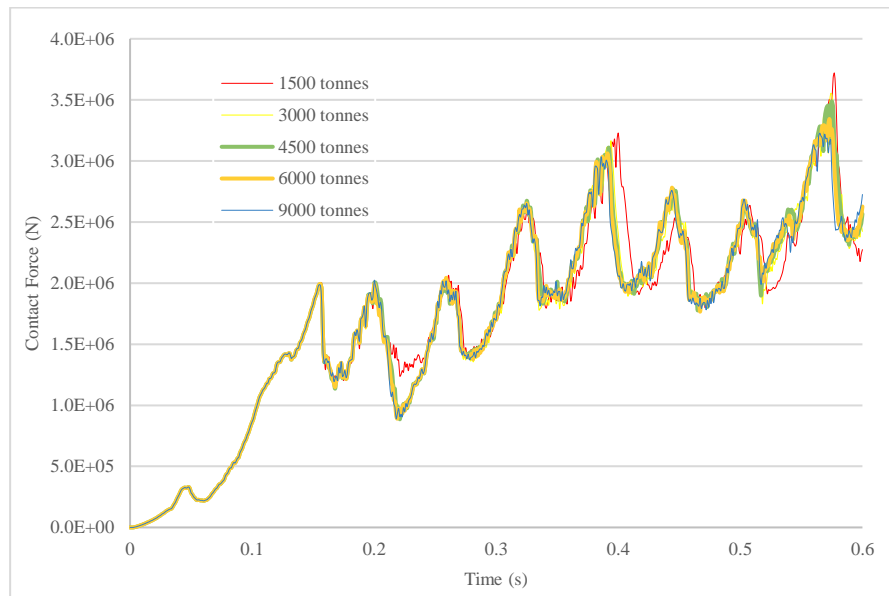


Figure 7-1 Contact force for various ice sizes impacts with double hull structure with transverse framing

Welding has a crucial effect on the structural crashworthiness analysis when considering the effect of web frame. The mentioned stress concentration on the weld lines often leads to large cracks in weld lines and separation of web frame from shell plate. As a result, in actual collisions, the web frame share in rupture energy could be lower than the predicted

values by FE simulation. Figure 7-3 shows a double side structure of a container ship after collision with a bulk carrier in the Persian Gulf. The separation of the web frame from the shell plate and failure in the weldment is evident in this photo.

One of the main questions regarding watertight integrity is whether the ice could breach the inner hull. The ice did not penetrate the inner shell for the simulated time frame, and deformations were observed in two frames on the inner shell (see Figure 7-4). As discussed previously, the current ice model could not predict the ice fracture; therefore, simulating the collision for a longer time will lead to ice penetrating the inner plate. Based on the results of prolonged simulations, no particular conclusion could be made. Any simulation long enough to capture the ice breach in the inner shell requires an ice material model that includes fracture and spalling of ice.

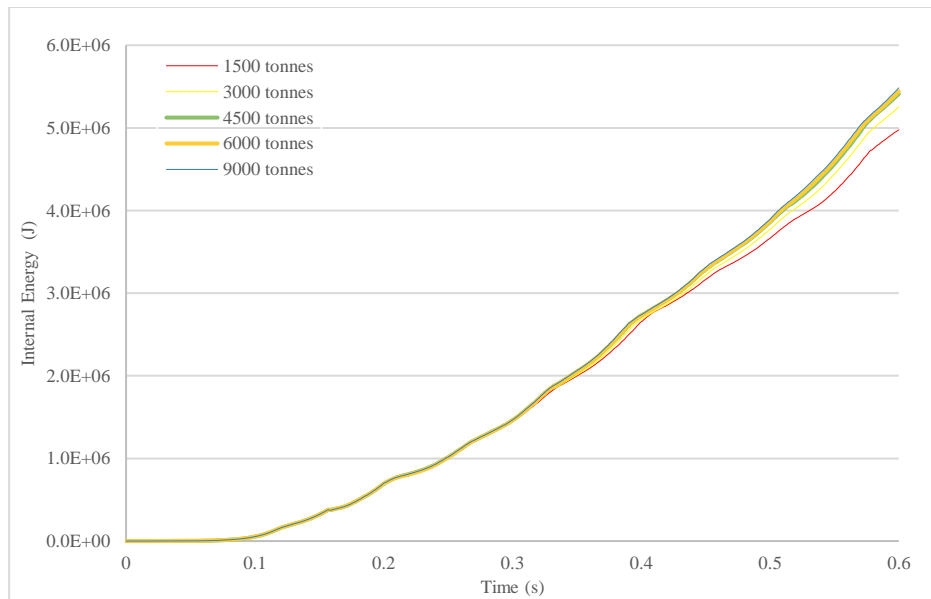


Figure 7-2 Internal energy for various ice sizes impacts with double hull structure with transverse framing



Figure 7-3 Double side structure of a container vessel after collision (taken by the author)

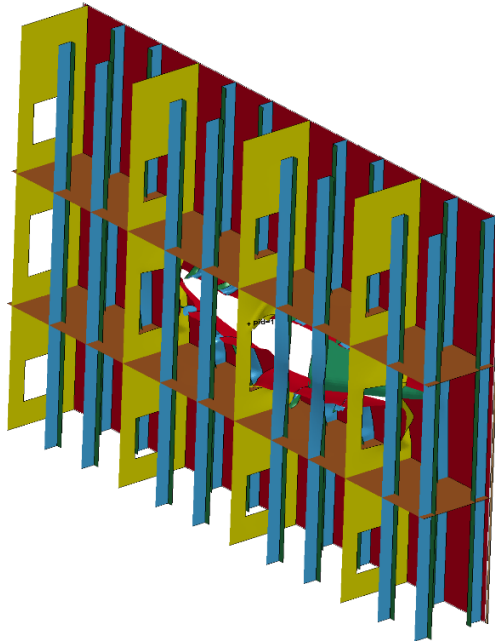


Figure 7-4 Rupture and deformation in the structure (9000-tonne bergy bit)

Vessel speed is a parameter that could have an influence on the results. As shown in Figure 7-1, the contact force is independent of ice mass for small contact area cases; therefore, any

ice mass in the investigated range can be used to study the effect of ship speed on the structural behaviour. A speed range from 11 knots to 17 knots was investigated, and the contact forces are shown in Figure 7-5 for three cases for clarity. The peaks are in the same range, and as the speed increased, the peaks occur earlier, but the force values are similar. The average force for all investigated cases is presented in Table 7-1. It is evident that in the case of a collision with bergy bits with sharp edges, the force level does depend on neither ice's mass nor ship speed. It is important to note that this result is applicable only for sliding impact, and for a head-on collision the ice load increases by increasing the ship's speed.

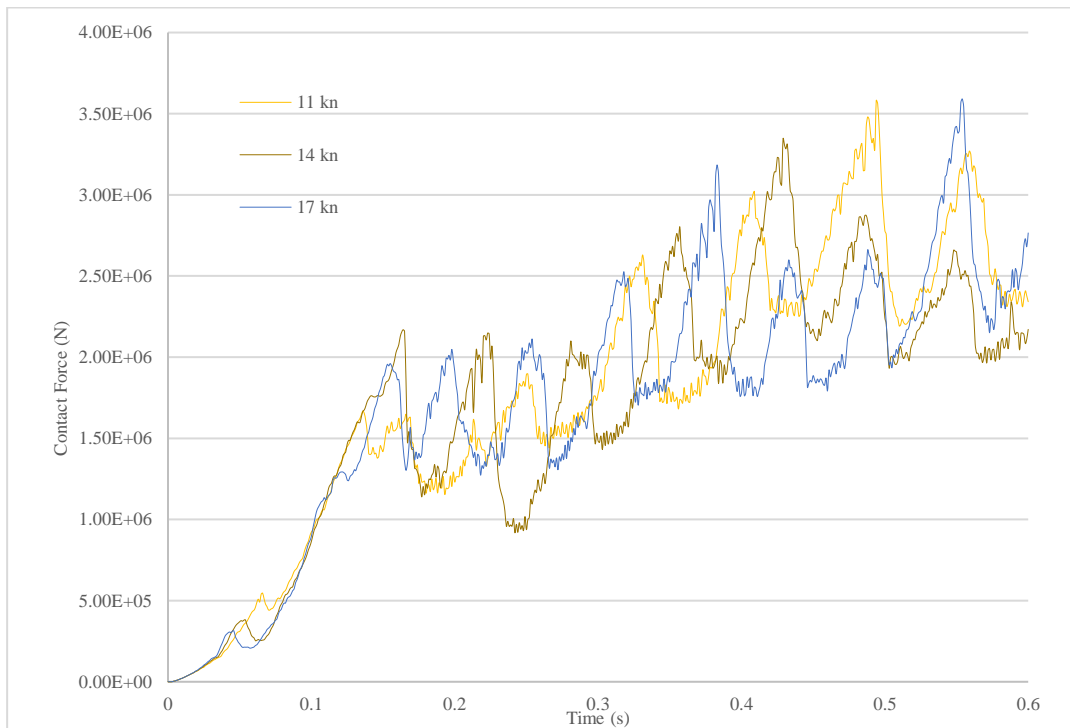


Figure 7-5 Contact force for 1500-tonne ice impact for various vessel's speed

Table 7-1 Average contact force for 1500-tonne ice impact for various vessel's speed

Ship's speed (kn)	11	12	13	14	15	16	17
Average contact force over entire duration (N)	1.79E6	1.78E6	1.74E6	1.70E6	1.69E6	1.72E6	1.72E6

7.3 Double hull structure with longitudinal framing

The double side structure with longitudinal framing is the most common ship structural arrangement for merchant ships. Therefore, the structural performance of a typical vessel that might navigate in polar water was studied in this section (refer to 5.2.3)

Three impact locations were simulated for a 1500-tonne bergy bit: plate, stiffener and stringer. Table 7-2 summarizes the damage extent length and the length between first contact and fracture initiation.

Table 7-2 Summary of rupture length for various impact locations

Impact Location	Damage length (m)	First contact to crack imitation (m)
Plate	6.106	1.223
Stiffener	5.971	1.376
Stringer	5.679	1.555

For both stiffener and stringer, the stiffness of the members pushed the ice to the plate, as schematically shown in Figure 7-6. As depicted in Figure 7-7, the graphs have similar patterns even though the force level is dramatically higher for impact on the stringer. For both collisions on stiffener and stringer, the initial rupture occurred later compared with the collision on the plate. Contact forces for plate and stiffeners are not very different, because

as mentioned, the ice moved over the plate panel. According to Figure 7-8, at the end of the simulation, the internal energy value for collision on the stiffener is 15.7% higher than the internal energy for impact on the plate.

As for each collision scenarios, the peaks are described in the following:

- Collision on stringer:
 - First peak: rupture initiation
 - Second peak: stringer start to buckle severely
 - Third peak: Upper and lower longitudinal frames buckled

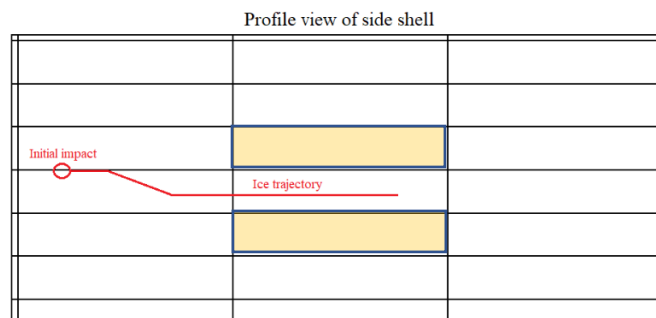


Figure 7-6 Ice trajectory for impact on stiffener (1500-tonne bergy bit)

- Collision on stiffener:
 - First peak: rupture initiation
 - Second peak: buckling of stiffener at the connection to the web frame was observed, and web frame rupture was initiated. After the second peak, the plate and adjacent stiffeners start to buckle (areas marked with orange colour in Figure 7-6).
 - Third peak: failure of the second web frame

Plate:

- First peak: rupture initiation
- Second peak: buckling of stiffeners and first web frame rupture
- Third: failure of the second web frame

As seen in Figure 7-9, in-plane loads due to ice penetration caused buckling in upper and lower stiffeners and attached plates. As the simulation continues, the far-away plates and stiffeners will be affected because the buckling reduces the load-bearing capacity of the structural members adjacent to the collision region.

The structure investigated in this section covers a typical oil tanker that might navigate in the polar water with a double skin structure and longitudinal framing system. The width of the double hull for tankers is governed by MARPOL [6] (see Table 7-3), and as the deadweight of the ship decreases, the width of the double skin reduces accordingly. Tankers with DWT 30000 tonnes and over should have double side width of 2 meters.

As discussed in previous sections, the ice center of mass influences the ice motion and limits the structural damage extent. In these simulations, the effect of ice shape was not considered, and in none of the cases, the inner shell was ruptured. Therefore, it can be concluded that it is unlikely that the collision with bergy bits with masses below 9000 tonnes can cause the rupture in the inner shell of oil tankers.

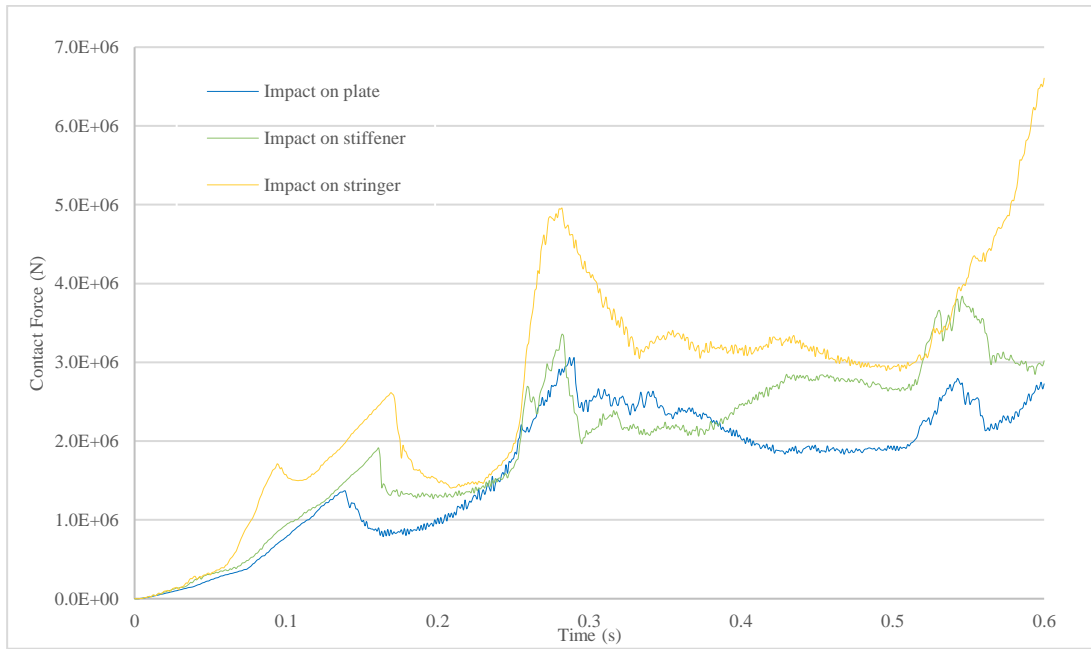


Figure 7-7 Contact force for various impact location (1500-tonne bergy bit)

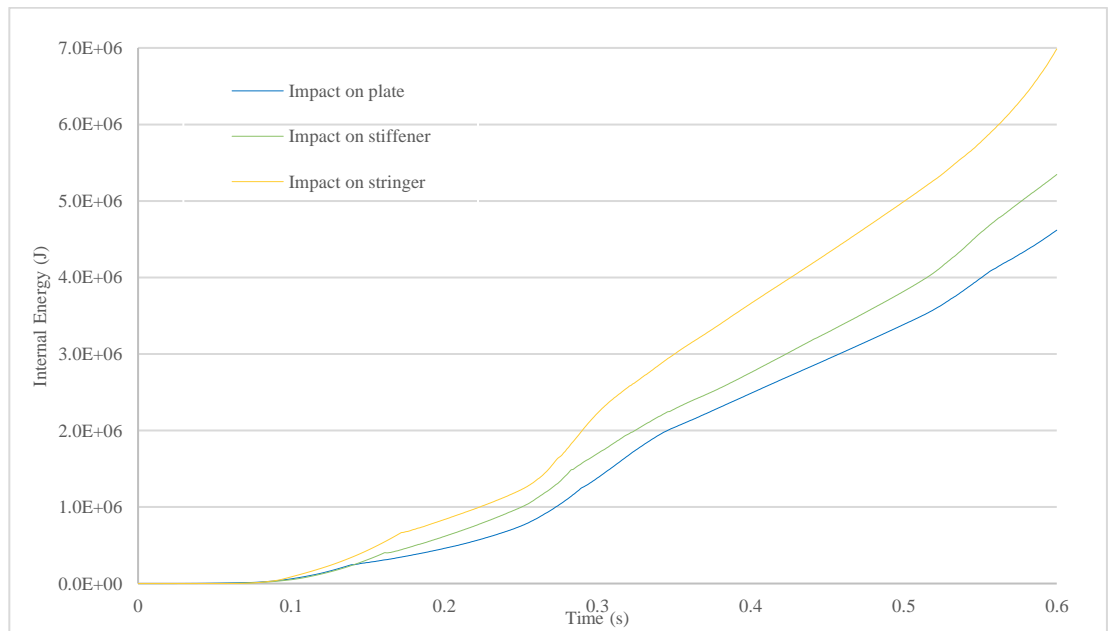


Figure 7-8 Internal energy for various impact location (1500-tonne bergy bit)

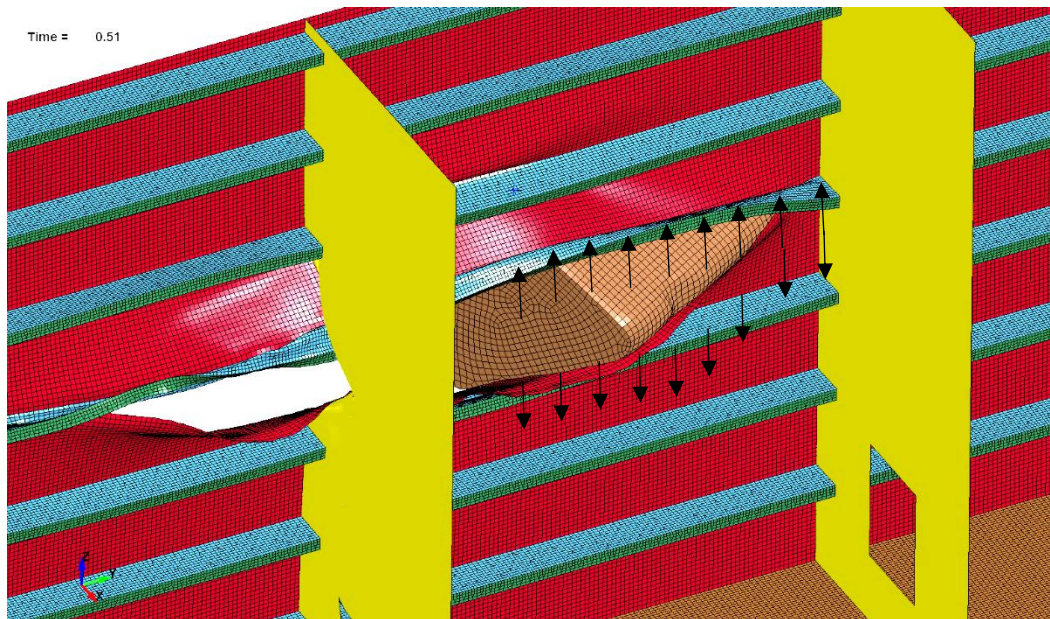


Figure 7-9 In-plane load caused by ice faces

Table 7-3 Double hull requirements for oil tankers delivered on or after 6 July 1996 [6]

	Wing tank width (m)
DWT > 5000 tonnes	$w = 0.5 + \text{DWT}/20,000$ (m), or $w = 2.0$ m, whichever is the lesser. The minimum value of $w = 1.0$ m.
DWT < 5000 tonnes	$w = 0.4 + 2.4 \text{ DW} / 20,000$ (m) Minimum value of $w = 0.76$ m.

7.4 Offshore supply vessel with transverse framing

According to the Code of Safe Practice for the Carriage of Cargoes and Persons by Offshore Supply Vessels (OSV Code), intact and damage stability of OSVs are to meet the

requirements specified in MSC Resolutions 235(82). Damage extent for damage stability purpose is summarized in Table 7-4.

Table 7-4 Damage extent for OSVs according to MSC Resolutions 235(82)

Longitudinal extent	$0.03 \times L + 3\text{m}$	Length of the vessel (L) >43m
	$0.1 \times L$	Length of the vessel (L) <43m
Transverse extent	760 mm	
Vertical extent	Full-depth of the vessel up to cargo deck or the continuation of the cargo deck	

The assumed longitudinal extent is between two transverse bulkheads, which means only one compartment is required to be flooded. The transverse damage extent is 760 mm; therefore, the double side width of these vessels designed to meet this requirement. The reason is that there would be no need to consider flooding of the large compartments adjacent to the inner shell.

Three bergy bit masses with the small contact area indenter are chosen according to the vessel's displacement: 500, 750, and 1000 tonnes. Internal energy and resultant contact force graphs are shown in Figure 7-10 and Figure 7-11, respectively. Similar to the previous simulation, by increasing the mass of the bergy bit, the internal energy increased. However, the value of contact forces is not different for small contact area indenter, as discussed in previous sections. The teeth-shaped graphs for contact forces indicate the effect of transverse frames on the structural response. In all cases, the contact force jumped at 0.44

s because the ice got in contact with the inner shell. The values for the 1000-tonne bergy bit declined sharply at 0.57s because the inner shell started to rupture.

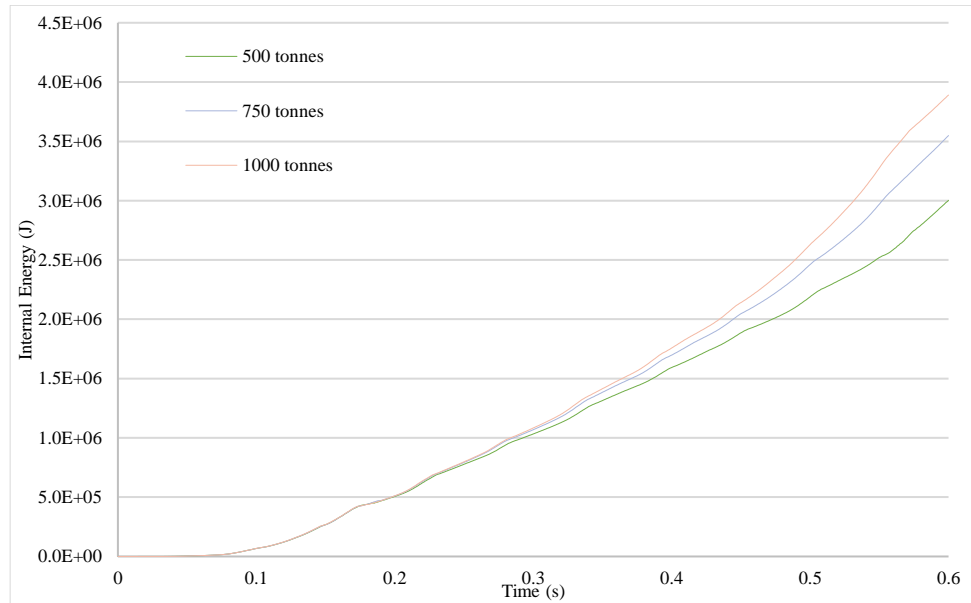


Figure 7-10 Internal energy for various bergy bit's masses collision with an OSV

Among the studied masses, only a 1000-tonne bergy bit penetrated the inner shell for the simulated period (see Figure 7-12). As it was mentioned, the width of the double side in OSVs is not large, and it is often chosen to be the minimum acceptable value, 760 mm, to meet the damage stability criteria and environmental protection requirements (for vessels that carry specific dangerous liquid). As a result, in a collision scenario with a bergy bit, it is probable that the ice penetrates the inner shell. Even for smaller bergy bits, the ice forces on the inner shell commenced early in the simulation because of the narrow double side. Therefore, it is possible that in collision with ice, the inner shell is penetrated by small bergy bits with sharp edges and enough velocity. It is important to note that this finding just highlight the need for more investigation for OSVs. The conservative approach of this

research leads to severe damage extents than actual collision. Therefore, in collision with sharp ice geometries, the ice failure would limit the damage extent.

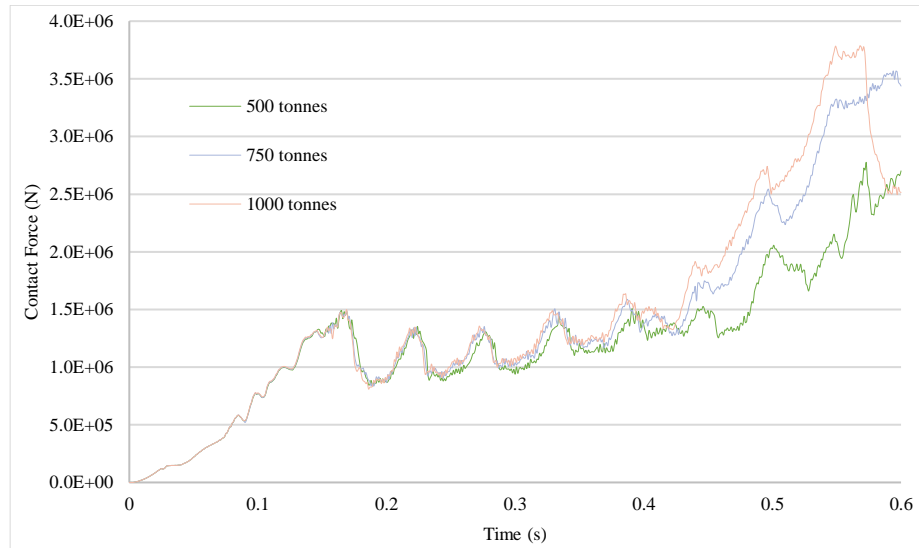


Figure 7-11 Contact force for various bergy bit's masses collision with an OSV

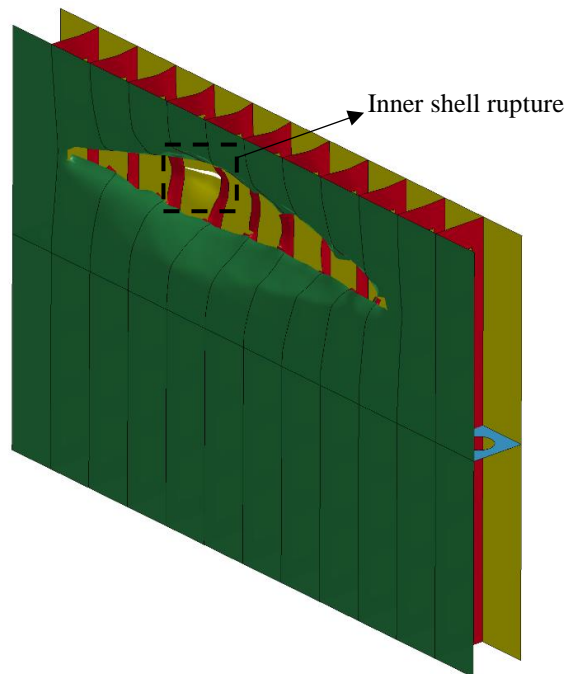


Figure 7-12 Inner shell rupture in 1000-tonne bergy bit impact

The current damage stability regulations for OSVs, assume the longitudinal extent of damage between two transverse bulkheads. It was shown in the previous cases that the transverse bulkheads do not stop the ice from penetrating adjacent compartments. Similar simulations were carried out for the OSV vessel, and a transverse bulkhead was added to the structure, as shown in Figure 7-13. The added structure is a stiffened plate with a plate thickness of 12 mm and the L200*10+90*12 stiffeners. The upper and lower boundaries of the bulkhead are assumed to be fixed because of the high rigidity of the deck and bottom structure.

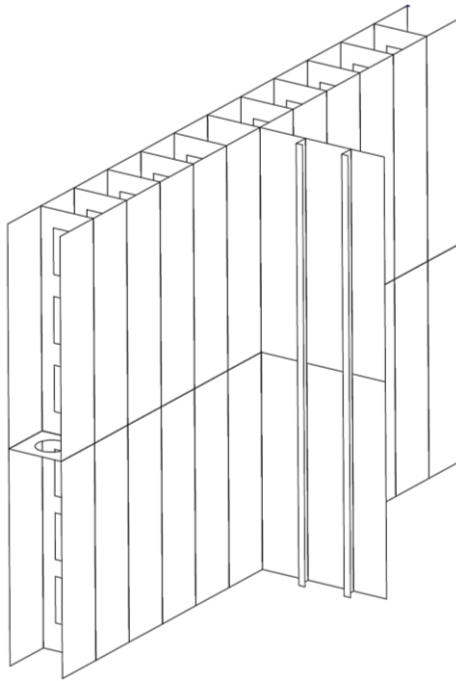


Figure 7-13 OSV model with transverse bulkhead

Figure 7-14 and Figure 7-15 compare the internal energy and contact force for various bergy bits in the case of a collision to structure with the transverse bulkhead. It is evident that the transverse bulkhead causes a sharp increase in the contact force and internal energy.

Despite the effect of BHD on the force levels, it does not stop the ice and the adjacent compartment was damaged.

As discussed in the previous section, the 1000-tonne bergy bit caused fracture in the inner shell. As for the structure with BHD, however, the ice did not cause fracture in the inner shell. The sharp increase in the force level caused a reduction in the kinetic energy of the ice. This leads to a lower energy level required for rupture initiation in the inner shell. Moreover, in actual collision when the ice failure happens, the dissipation of energy because of ice failure would be critical parameter in assessing the force levels and fracture extent in the structure.

Despite the effectiveness of the transverse bulkhead in preventing damage to the inner shell, it is observed that the assumption of OSV code to limit the damage length between two the transverse bulkhead would not be appropriate for vessels intend to navigate in polar water. Therefore, it is recommended to consider additional damage case scenarios for OSVs that might encounter bergy bits in open water.

Figure 7-16 compares the contact force for a 1000-tonne collision scenario for both with and without collision bulkhead. Graphs have two distinct differences over the simulated time frame. The first difference is the peak because of the transverse bulkhead in the model. The second difference is the decline in the force level at the end of simulation for the model without the transverse bulkhead due to the rupture initiation in the inner shell.

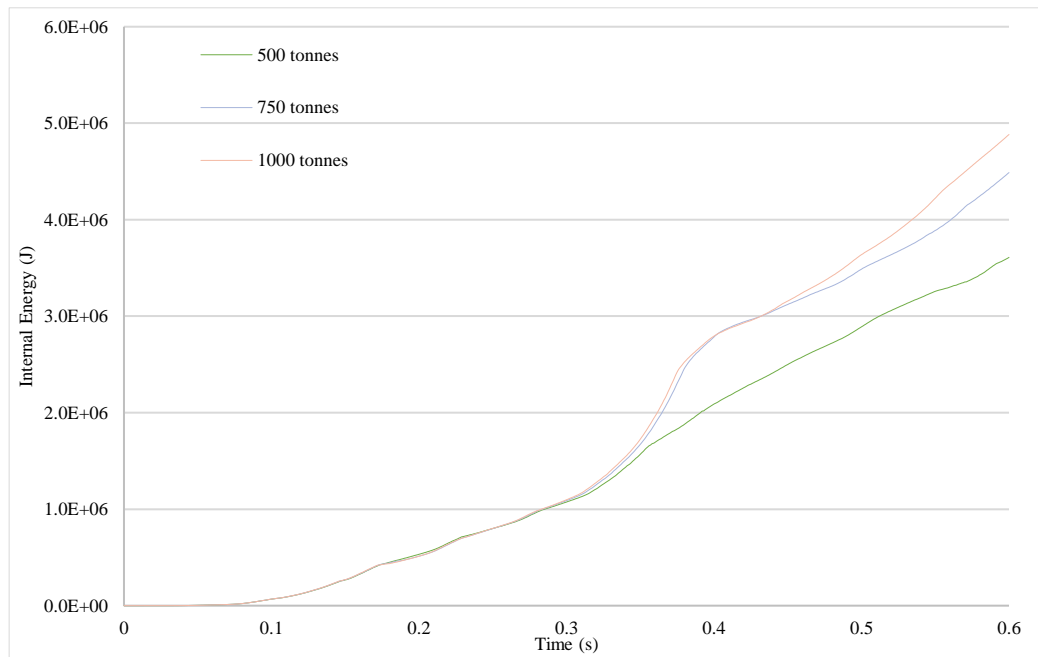


Figure 7-14 Internal energy for collisions with various ice masses (Structure with BHD)

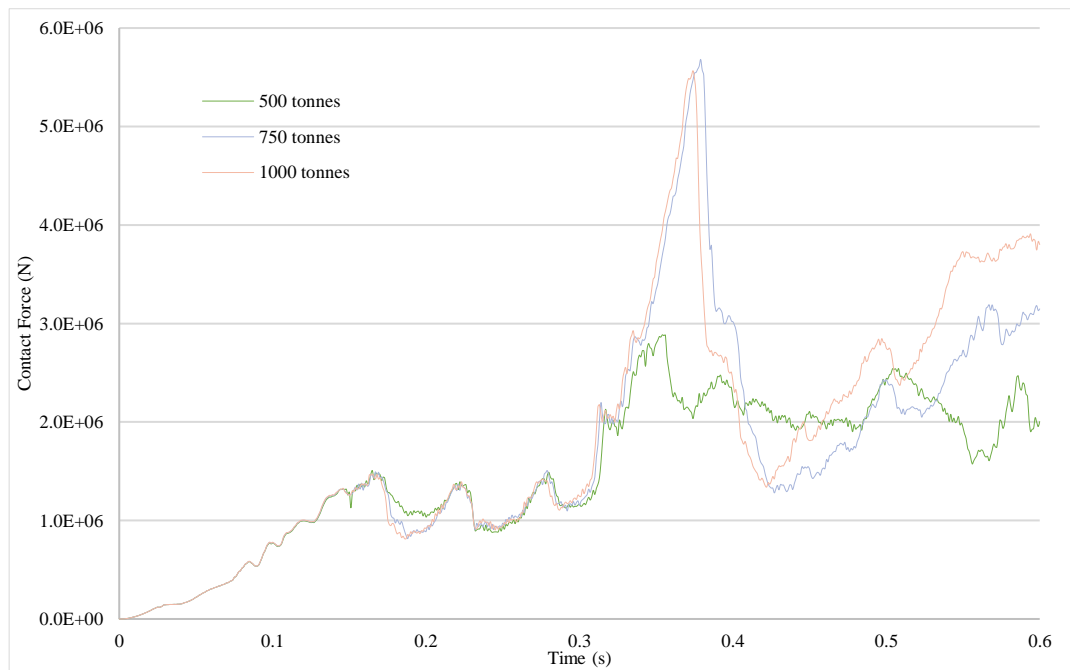


Figure 7-15 Contact force for collisions with various ice masses (Structure with BHD)

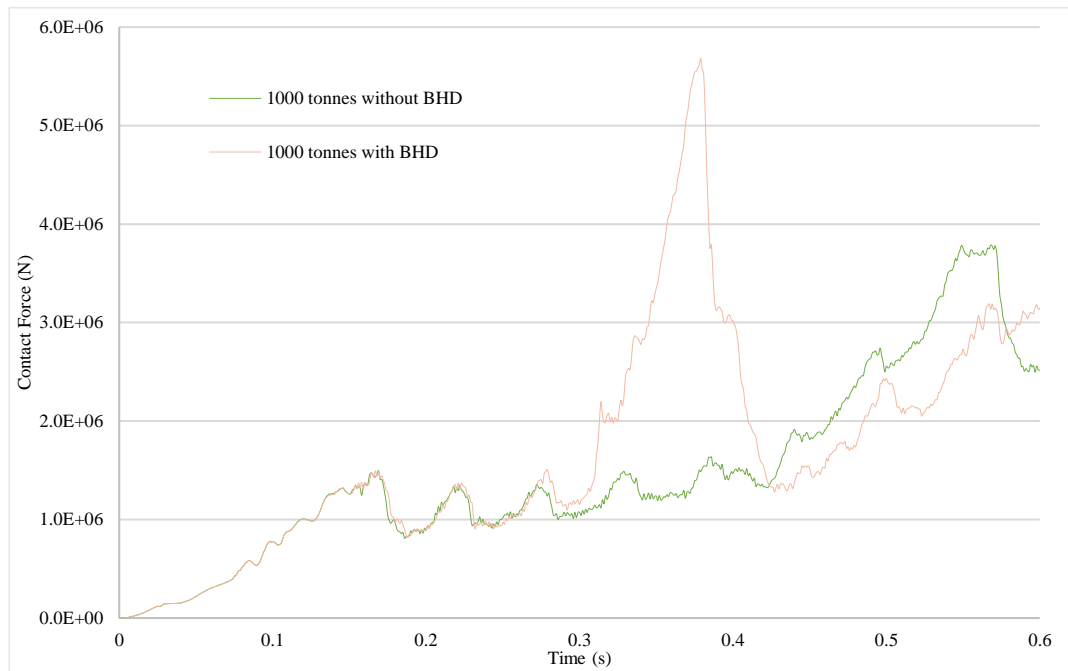


Figure 7-16 Internal energy for collisions for 1000-tonne bergy bit with and without BHD

7.5 Summary

Double hull structural response in collision with ice was the focus of this chapter. Results for small contact area simulations were similar to the results for the single hull model. Ice indenter could not penetrate the inner shell except for the OSV model. This was an indicator that for merchant ships, bergy bits with a mass lower than 9000 tonnes would not cause rupture in the inner shell. However, due to the conservative approach taken in this research, further investigation with considering fracture in ice should be conducted for OSVs.

Chapter 8 Application of Smearing Technique and Simplified Formulations in Ship-Ice Collision

8.1 Introduction

Simplified analytical and empirical methods are useful techniques that could be used to simplify an intricate problem. This simplification is advantageous when implementing sophisticated methods such as FE simulation is a challenge. In this chapter, the applicability of the smearing technique and empirical formulation proposed by Zhang [69] were studied.

8.2 Smeared structure with a small contact area

The small contact area ice shape was chosen for smeared structure simulations because it was established earlier that a large contact area would not cause the rupture in the structure. Equation 24 was used according to [69] to calculate the equivalent thickness for stiffened plate (see Figure 8-1). The equivalent plate thickness increased to 32 mm, and the side structure simplified as depicted in Figure 8-2.

$$t_{eq} = t_p + \frac{A_s}{s} \quad \text{[Equation 24]}$$

Where;

t_{eq} : the equivalent thickness of the stiffened plate

t_p : the thickness of the plate

A_s : sectional area of the stiffener

s : stiffener spacing

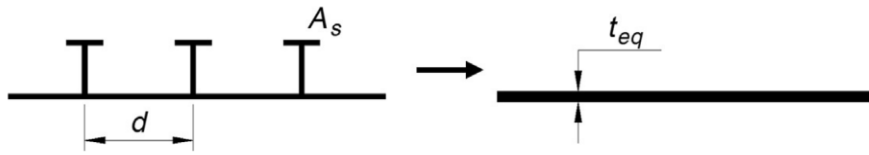


Figure 8-1 Equivalent plate thickness for stiffened plate [69]

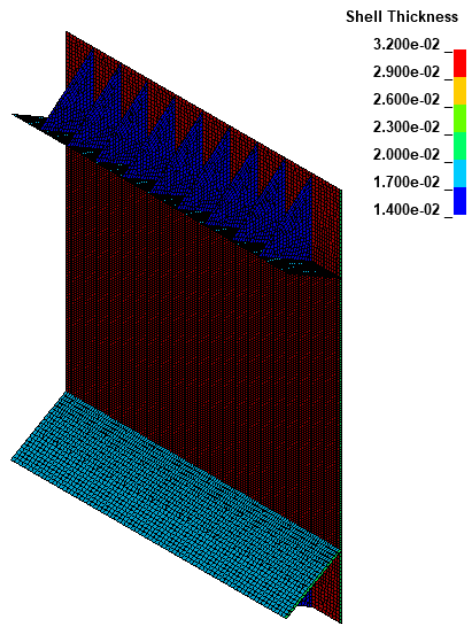


Figure 8-2 Smeared structure with equivalent plate thickness

Figure 8-3 and Figure 8-4 compare the internal energy and contact force for various ice sizes, respectively. For both graphs, the patterns are similar to what is illustrated for an actual structure without smearing.

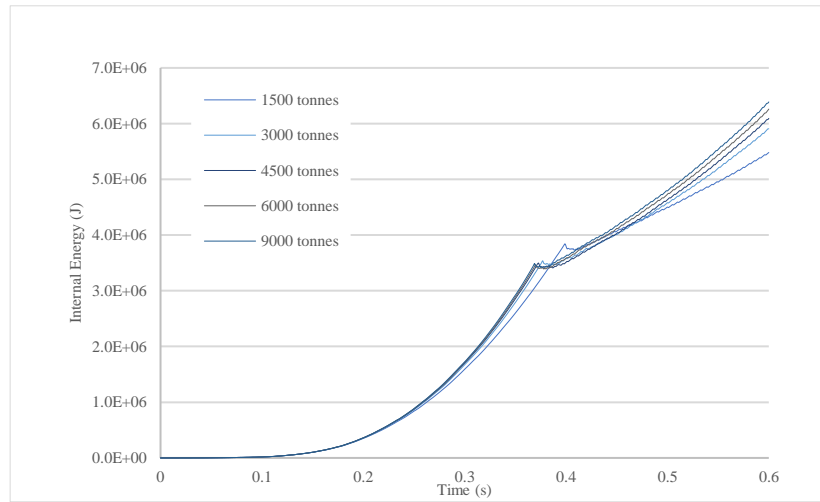


Figure 8-3 Internal energy for smeared structure (small contact area)

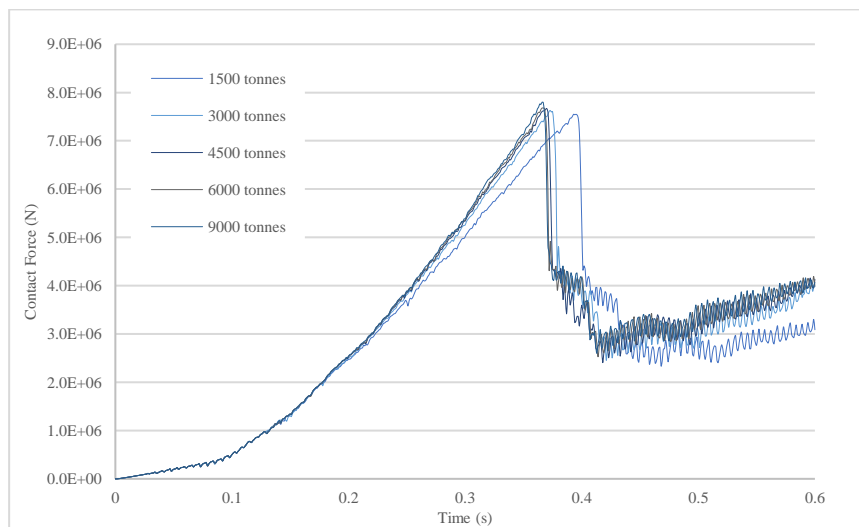


Figure 8-4 contact force for smeared structure (small contact area)

Equation 24 assumes the full effectiveness of the transverse frames in the equivalent plate thickness calculation. There is a significant difference between peak loads of original and smeared structures. This indicates that the shell plate thickness is the main controlling parameter in the structure's crashworthiness. In other words, frames are not as crucial as

plate thickness for the vessel's watertight integrity in collision with ice for short-duration impacts.

A structure with equivalent plate thickness, which is higher than the original plate thickness, has a higher peak force value than the original structure (refer to Figure 8-5). Equation 25 is the same as Equation 24 with a new parameter k_{eff} , that adjust the effectiveness of frames in the equivalent plate thickness. Various transverse frames' effectiveness could be considered, and in this study, two effectiveness ratios, 0.8 and 0.5, were assessed.

$$t_{eq} = t_p + k_{eff} \left(\frac{A_s}{s} \right) \quad \text{[Equation 25]}$$

Figure 8-5 illustrates the contact force for smeared cases and the original structure for 1500-tonne ice impact. It is evident that the equivalent plate thickness based on a fully effective transverse frame overestimates the structure's strength at the beginning of fracture. As for the effectiveness of 0.8, the response was similar to the fully effective case. The calculated equivalent plate thickness with the frame effectiveness of 0.5 predicted the peak force value accurately. After fracture initiation, all smeared cases converged into a steady fracture development.

The presented results highlighted the fact that smeared structures could not predict the structural response with a desirable level of accuracy. However, it is possible to estimate the initial rupture force by defining the effectiveness of frames, taking into account that the smear model simulation takes less time to finish (smear with 60 MPP processors took 00:13:28, and the original model took 01:14:21 with the same number of processors).

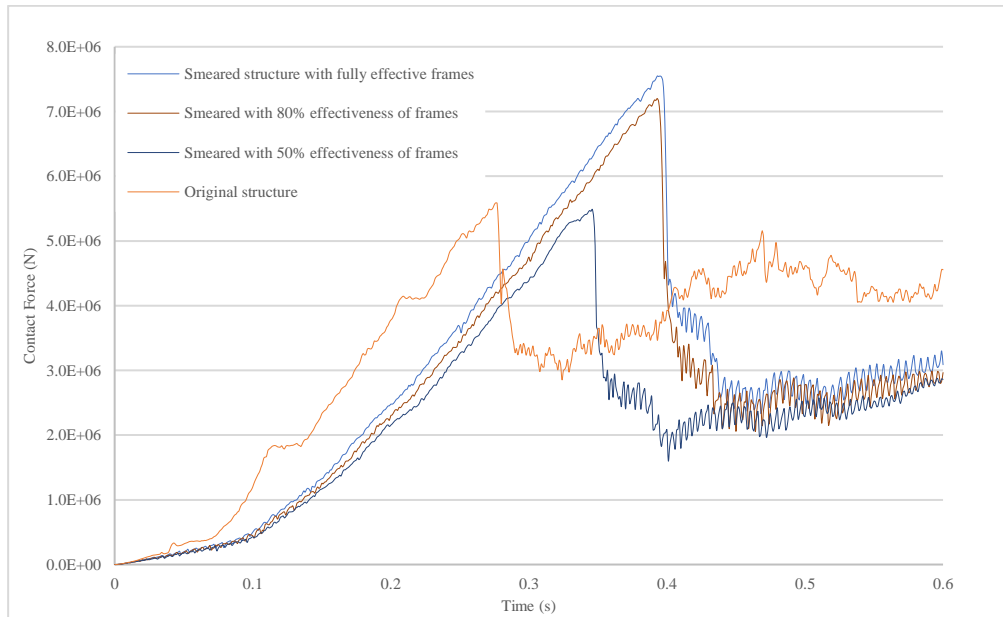


Figure 8-5 Comparisons among various frame effectiveness in contact force (1500-tonne scenario)

8.3 Wedge cutting simulations

The ship's hull is a complex structure, therefore modelling the crushing of the structural elements during a collision with a simplified analytical method is a challenging task. Ship structure members such as stiffened plates, web frames, and stringers absorb impact energy in mechanisms such as membrane deformation (shell stiffened plate), folding and crushing (web frames, stringers and transverse bulkheads) as noted in [69]. In [70], eight structural members (side shell, longitudinal bulkheads, decks, stringers, web frames, transverse bulkheads, longitudinal girders and transverse girders) have been listed that absorb 95% of the impact energy, and the authors concluded that the energy absorption by columns, struts and brackets is negligible.

There have been several attempts to formulate the grounding and collision accidents with a simplified wedge cutting scenario. Zhang [71] proposed Equation 26 to formulate wedge cutting force (refer to Figure 8-6):

$$F = 1.942\sigma_0 t^{1.5} l^{0.5} \varepsilon_f^{0.25} (\tan\theta)^{0.5} \left(1 + \frac{\mu}{\tan\theta}\right) \quad [\text{Equation 26}]$$

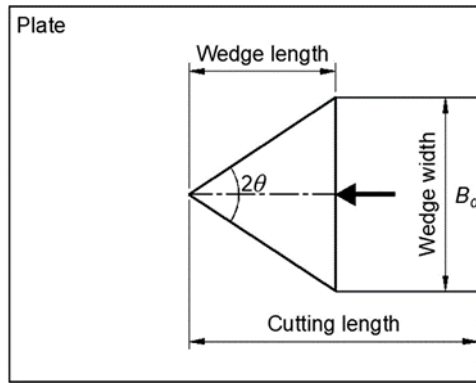


Figure 8-6 wedge cutting parameter definition for Equations 7 and 8

For the steady-state cutting phase, Equation 26 can be rewritten as follows [69]:

$$F = 1.942\sigma_0 t^{1.5} B_d^{0.5} \varepsilon_f^{0.25} \left(1 + \frac{\mu}{\tan\theta}\right) \quad [\text{Equation 27}]$$

Where:

σ_0 : flow stress equals to $\frac{\sigma_u + \sigma_y}{2}$

B_d : wedge width

t: plate thickness (smeared equivalent thickness)

ε_f : plate fracture strain

μ : friction coefficient

Constant cutting force was calculated for the plate and material used in the simulations for two wedge dimensions. The results are presented in Table 8-1 based on the plate's material characteristics and scantling discussed in chapter 5. As cited in [69], the friction coefficient was chosen based on Astrup's experiments [68].

Table 8-1 Parameters used to calculate steady-state cutting force with Equation 27

Case No.	σ_y (MPa)	σ_u (MPa)	σ_0 (MPa)	t (m)	B_d (m)	Wedge length (m)	ϵ_f	μ	θ (degree)	F (MN)
1	284	400	342	0.032	0.8	0.359	0.431	0.4	45	3.857
2	284	400	342	0.032	0.5	0.359	0.431	0.4	30	3.687

FE simulations were carried out with wedges with a round tip (radius=0.1m). The wedge tip was rounded to prevent contact problems in the simulations (see Figure 8-7).

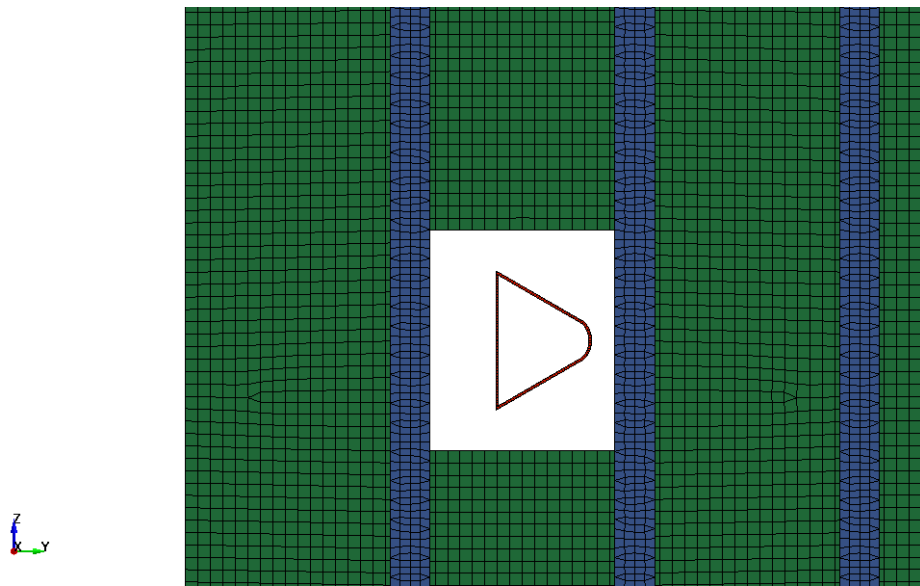


Figure 8-7 Hole and wedge schematic

An initial hole with dimensions of 840*840 mm was assumed in the side shell, as shown in Figure 8-7. Two different simulations with actual structure and smeared structure with

equivalent plate thickness were analyzed. As illustrated in Figure 8-8, the contact force value of wedge cutting with equivalent thickness is remarkably higher than the values for the original structure. The curves for the original structure with different wedge angles are similar, and it is evident that the force does not be varied significantly with changes in wedge angle. It is in good agreement with the calculated values based on Zhang's formulation. It is assumed that after the wedge cuts through the plate more than twice the wedge length, the cutting reaches the steady condition. Therefore, the steady cutting condition assumed as noted for all three cases, and the average values were calculated accordingly.

The average value for smeared model is noticeably higher than the other two cases and overestimated the cutting force. The original structure's average value rose 13% percent when the wedge angle increased from 30° to 45° .

The average contact forces predicted by Equation 27 were in good agreement with FE simulations. The differences were 9 and 4 percent for wedge angles 45 and 30, respectively. This finding shows that Zhang's formulation can estimate the average cutting force in the steady cutting condition.



Figure 8-8 Contact force for various simulated wedge cutting

It was shown that for ice impacts with small contact areas or sharp edges, the contact force in the range of 1500 tonnes to 9000 tonnes would not be significantly different. Therefore, a 1500-tonne impact case was compared with wedge cutting simulations' results in Figure 8-9. The average value for steady-state crack development has been chosen from the point that the force dropped after the first peak.

Figure 8-8 highlighted the fact that the average contact force in actual ice impact could be predicted with rigid wedge cutting. It also found that Zhang's empirical formula for steady-state cutting predicted the average force with high accuracy. The average contact force for

the ice impact with a small contact area was selected as a reference point, and other average values were compared. As shown in

Table 8-2, Equation 27 predicts the rupture force with 4.5% error, which is very accurate when considering the simplicity of the approach. This finding revealed that Equation 27 could be used in risk and reliability assessments of the damage extent.



Figure 8-9 comparisons of contact force in wedge cutting and ice impact with the small contact area

Table 8-2 Average contact force comparison among various approaches

	Force (N)	Error percentage based on ice impact average results (%)
Zhang's formula (Equation 27) with wedge angle 45°	3857382	4.5
Zhang's formula (Equation 27) with wedge angle 30°	3687360	8.7
Average force (FE results): original structure with wedge angle 45°	4203134	4.1
Average force (FE results): original structure with wedge angle 30°	3532144	12.5
Average force (FE results): ice impact for 1500-tonne case (small contact area)	4037987	---

8.4 Effect of the hole on the structure behaviour

Contact force graphs presented in the previous sections show that the damage extends fast and with lower required energy after the crack initiation. Various initial opening geometries could be considered for such simulation; however, for the ice indenter that has been used in these simulations, a narrow long rectangular shape has been selected. This geometry was chosen based on the results of the simulations carried out in the previous section (see Table 6-3). Contact between ice and the structure should be smooth, and plate edges cause severe element distortion in the ice indenter. Consequently, as shown in Figure 8-10 (hatched area in upper-left of the figure), the side plate was folded in to create a smooth surface-to-surface impact in the first contact between ice and structure.

It should be noted that the initial hole would have sharp edges with many irregularities, but the fracture strain is sensitive to mesh size, and it is not feasible to define strain fracture for many different shaped elements. Therefore, a regular shape is practical to implement in FE fracture simulations.

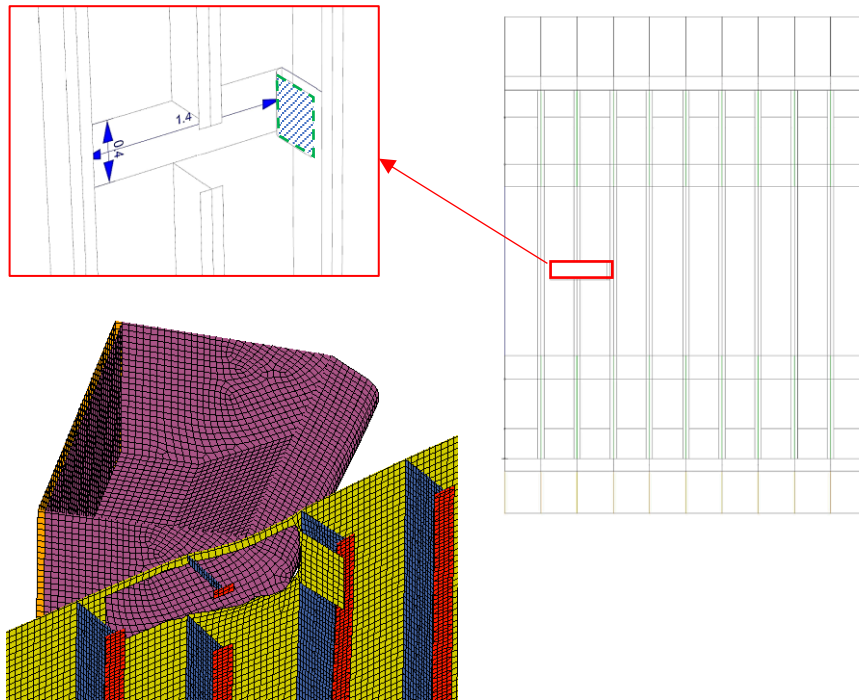


Figure 8-10 Geometry of the simulation with the initial opening

Figure 8-11 compares the contact force's results for 1500-tonne bergy bit impact for three cases: original structure, smeared structure with equivalent plate thickness (50% frame effectiveness), and original structure with the initial hole.

After the first peak, the plate rupture initiates and transverse frames contact the ice, and the contact force commences to rise.

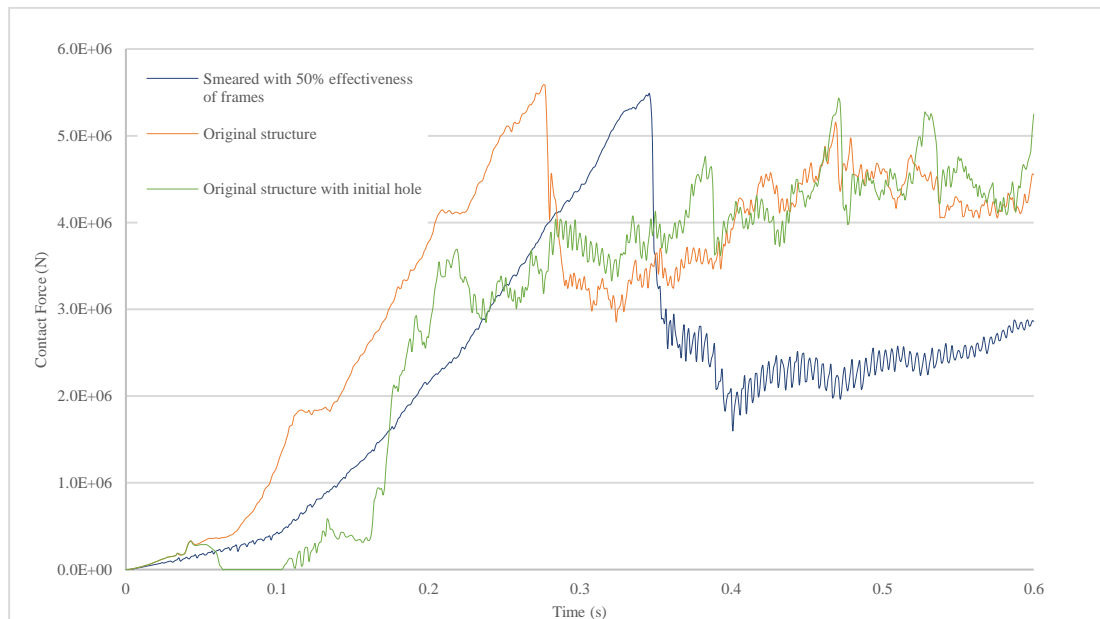


Figure 8-11 Contact force for various structural arrangement (1500-tonne bergy bit)

8.5 Summary

In this chapter, it was shown that Zhang's empirical formula [71] can be used to estimate the average rupture force in the steady-state condition. As a result, Zhang's formula [71] has the potential to be used in probabilistic models to calculate the rupture force. The smearing techniques could be utilized to estimate the plate rupture initiation if the effectiveness of the frames is selected accurately.

Chapter 9 Conclusions and Recommendations for Future Work

This chapter summarizes the highlights of the research findings and outcomes. In addition, the limitations of the research and possible future works based on developing this research are presented.

9.1 Highlights of findings

Different ice indenters were used in the simulations. For constant velocity and mechanical properties, ice mass and contact area are the controlling parameters. Results indicated that as the contact area decreases, the contact force and internal energy become less dependent on the mass of ice. Conversely, in collision with ice with a large contact area, the contact force and internal energy are controlled by ice mass. Ice mass is the dominant parameter when ice velocity is of concern. Heavier ice maintains its velocity for a longer time than the lighter ice pieces, which results in a more extensive damage area for heavier ices. The large contact area was gradually decreased, and it was observed that there is a critical contact area for each plate thickness and ice mass, after which the collision caused the rupture in the structure.

Results of impacts with small contact areas showed that the localized stress and strain lead to a rupture in the plate. For sharp ice wedges with a small contact area, the results were shown to be independent of the mass of ice. Sharp edges cause large holes in the plate with the force level lower than the large indenter cases. It showed the significance of ice geometry on the structural response.

Ice is a complex material, and modelling the ice in FE simulation is a challenging task. Therefore, the possibility of using rigid indenter instead of crushable foam material was investigated. The results indicate that the rigid indenter gives unrealistic results for sliding impact, and consequently, the crushable foam material model is necessary for ice impact simulations.

In grounding analysis, the smearing technique has been used to simplify the structure. The same technique was applied to the single hull model with different effectiveness ratios of frames. Based on the results presented in chapter 6, it could be concluded that the collision consists of two phases:

- 1- Large plastic deformation and fracture initiation
- 2- Crack growth

The smearing technique with the correct effectiveness ratio of frames can predict the peak force at fracture initiation. After the crack initiation, all smeared models with different effectiveness ratios converged on the steady-state fracture. It is also important to mention that the smear models need a lower computational capacity that is a significant advantage.

As it was noted, after the crack initiation, the simulations are converged to steady-state crack growth. This finding was examined by including an initial hole in the structure. It was shown that the idea of dividing a collision into two separate steps is an accurate technique for probabilistic models.

The effectiveness of the watertight bulkhead to limit the flooding to one compartment was one of the main questions of this research. Simulations showed that the bulkhead couldn't

stop the ice from tearing the plate. This is a critical finding for the damage stability requirement perspective.

Wedge cutting FE simulations for both original and smeared structures were compared with the empirical formula for rigid wedge cutting. It was shown that Zhang's empirical formula [71] could estimate the wedge cutting force with an acceptable level of accuracy. When the average force level for small contact area simulation was compared with Zhang's empirical formula [71], it was concluded that it is possible to use the formula to estimate the rupture force in actual ice collision.

Impact angle showed to be a critical parameter in fracture initiation. Impact angles that are too small or too large would not result in fracture. The impact angle between 40° and 60° showed to be dangerous. This idea could be developed as a guideline for navigators in open water that might encounter bergy bits.

Simulations with ice showed that the cone angles a dominant factor in fracture initiation. Cone angle 45° caused no fracture for ices of mass equal to 1500 and 4500 tonnes. Cone shape is a particular case, and in order to have ruptures in the plate, a sharp tip is necessary to localize the high-pressure zone. On the other hand, the ice should remain in contact with the structure long enough.

The effect of the center of mass was another parameter that was investigated in this thesis. The results indicated that the center of mass could dramatically change the high-pressure zones in contact between ice and ship. It also changes the dynamic response of the ice to the impact by increasing the rotation and movements. Not considering the actual ice

geometry results in a conservative force level in the collision that should be contemplated by the designers.

Simulations for double hull models showed that the inner shell of large merchant ships probably won't be breached by the ice with a range of mass that was investigated in this research. However, for OSV vessels in which the double side width is small, it is possible that ice penetrates the inner shell.

According to MARPOL damage stability calculations, for tankers whose length is less than 150m, the damage length is considered between two transverse bulkheads. Based on the FE results in this thesis, two adjacent compartments can be flooded. Therefore, it is necessary to investigate the damage stability of non-ice class ships in Canadian waters for this unique collision scenario that is not included in MARPOL. The same scenario was observed for OSV vessels.

9.2 Conclusion

Based on the extensive FE simulations, it could be concluded that the ice contact area is the key parameter in fracture initiation in the sliding collision. From the structural point of view, the side shell plate thickness is the main barrier against fracture and flooding. It also found that any collision that results in rupture is divided into two stages: initial rupture and crack growth. Initial rupture force can be calculated with FE simulation of smeared structure (with adequate effectiveness ratio of frame) without the need for detailed structural modelling. The steady-state crack growth can be estimated with Zhang's empirical formula [71]. This new perspective can be implemented in probabilistic models.

The effect of the ice contact area on the fracture extent was shown to be critical. Several other parameters such as the mass of ice, speed of the ship were shown to be not crucial in some collision scenarios. This indicated that sliding collision is fundamentally different than glancing collision, and more detailed investigations are required to understand all controlling parameters in sliding collision.

From a regulatory perspective, the damage stability requirements for tankers (less than 150m) and OSVs might not be as conservative as they thought to be. It was shown that the adjacent compartments could be flooded simultaneously.

Rupture length for damage stability calculations are specified for category A and B in Polar Code [7] as follows:

- Forward the maximum breadth of a ship (on the upper ice waterline): 4.5% upper ice waterline length
- Elsewhere: 1.5% upper ice waterline length

For the mid-body section of the ship, 1.5% of the vessel's length is to be used. The defined damage length should be considered anywhere along the ship's length, which means the transverse bulkheads are not contemplated effective in limiting the damage into one compartment. The fact that the transverse bulkheads are not effective in flooding control after collision with ice was proven in this research. The damage length is comparatively lower than the damage lengths specified in other IMO rules. IMO damage stability requirements are specified based on the statistical analysis of ship collisions, which are more severe than the collision with ice. MARPOL [6] considers damage length as $\frac{1}{3}(L)^{\frac{2}{3}}$

with maximum value of 14.5 meters that is higher than the polar code. The OSV code also contemplates more severe collision scenario compared to the polar code. The FE simulations showed that bergy bits lighter than 9000 tonnes could not lead to a damage scenario more severe than current IMO conventions except for two cases discussed earlier in this section.

9.3 Research limitations and future works

The following recommendations for future works are suggested based on the limitations of this research:

- 1- It was observed that plate thickness is a dominant parameter in fracture initiation. Therefore, it is possible to design an experiment to apply ice force over different ice contact areas and find a critical contact area for various plate thicknesses. The experiment has the potential to be a part of rule development for classification societies.
- 2- The crushable foam material does not capture ice fracture and cracking. Therefore, the results for long-duration impacts would not be accurate. Brittle material models have the potential to capture ice fracture, and the simulations can be carried out with a brittle material model to compare the results with the crushable foam material model.
- 3- It is suggested to implement the results into a probabilistic model. Series of simulations can be conducted to calculate the fracture initiation force for various plate thicknesses and derive an empirical formulation to be used in a simplified

model. For the steady-state phase, the available formulations showed to be sufficient to estimate the average rupture force.

- 4- Hydrodynamic effects and the energy that dissipates in motion of ice and ship is critical in collision assessment. It is suggested that in future research, the effect of hydrodynamic parameters be included in the analysis.
- 5- It was shown that the stiff structural members like web frames in double hull structures absorb a noticeable portion of impact energy. It means that the weld connections of boundaries of these members undergo significant forces. Therefore, the strength of weldment is another possible research area in the ice-ship collision.
- 6- Damage extent requirements for small tankers and OSVs need to be revisited for the ice collision with probabilistic models and more representative ice failure modes to study whether it is necessary to include additional damage cases for vessels that operate in the Canadian polar waters.

Bibliography

- [1] C. Daley, “Sea ice engineering for ships and offshore structures,” 2019.
- [2] O. M. Johannessen *et al.*, “Arctic climate change: Observed and modelled temperature and sea-ice variability,” *Tellus, Ser. A Dyn. Meteorol. Oceanogr.*, vol. 56, no. 4, pp. 328–341, Aug. 2004.
- [3] M. M. Holland, C. M. Bitz, and B. Tremblay, “Future abrupt reductions in the summer Arctic sea ice,” *Geophys. Res. Lett.*, vol. 33, no. 23, p. 23503, Dec. 2006.
- [4] W. Maslowski, J. C. Kinney, M. Higgins, and A. Roberts, “The Future of Arctic Sea Ice,” 2012.
- [5] “International Convention for the Safety of Life at Sea (SOLAS), 1974 (as amended), Chapter II-1.”
- [6] “International Convention for the Prevention of Pollution from Ships (MARPOL), Annex I, Chapter IV.”
- [7] “International Code for Ships Operating in Polar Waters (Polar Code), Part I-A, Chapter 4.”
- [8] J. W. Stettler and B. S. Thomas, “Flooding and structural forensic analysis of the sinking of the RMS Titanic,” *Ships Offshore Struct.*, vol. 8, no. 3–4, pp. 346–366, Jun. 2013.
- [9] S. Zhang, P. T. Pedersen, and R. Villavicencio, *External dynamics of ship collisions and grounding*. 2019.

- [10] A. A. Popov, Yu N; Faddeev, O V; Kheisin, D E; Yakovlev, *Strength of ships sailing in ice*. Leningrad: Sudostroyeniye Publishing House, 1969.
- [11] D. Y. Kheysin, V. A. Likhomanov, and V. . Kurdyumov, “Determination of Specific Breakup Energy and Contact Pressures Produced by the Impact of a Solid Against Ice,” in *Symp. on Physical Methods in Studying Snow and Ice, Leningrad, CRREL Translation TL539*, 1973.
- [12] C. Daley, “Energy Based Ice Collision Forces,” in *Proceedings of the 15th International Conference on Port and Ocean Engineering under Arctic Conditions*, 1999.
- [13] S. Zhang, R. Villavicencio, L. Zhu, and P. T. Pedersen, “Ship collision damage assessment and validation with experiments and numerical simulations,” *Mar. Struct.*, vol. 63, pp. 239–256, Jan. 2019.
- [14] D. G. Matskevitch, “Eccentric impact of an ice feature: Non-linear model,” *Cold Reg. Sci. Technol.*, vol. 26, no. 1, pp. 55–66, 1997.
- [15] D. G. Matskevitch, “Eccentric impact of an ice feature: linearized model,” *Cold Reg. Sci. Technol.*, vol. 25, no. 1, pp. 159–171, 1997.
- [16] Z. Liu and J. ;Amdahl, “A new formulation of the impact mechanics of ship collisions and its application to a ship-iceberg collision,” *Mar. Struct.*, vol. 23, no. 3, pp. 360–384, 2010.
- [17] P. T. Pedersen and S. Zhang, “On impact mechanics in ship collisions,” *Mar. Struct.*, vol. 11, no. 10, pp. 429–449, 1998.

- [18] W. J. Stronge, *Impact Mechanics*, 1st ed. University of Cambridge, 2000.
- [19] K. Tabri, P. Varsta, and J. Matusiak, “Numerical and experimental motion simulations of nonsymmetric ship collisions,” *J. Mar. Sci. Technol.*, vol. 15, no. 1, pp. 87–101, 2010.
- [20] M. Fuglem and K. Muggeridge, “Design Load Calculations For Iceberg Impacts,” in *International Society of Offshore and Polar Engineers*, 1999.
- [21] Z. Liu, J. Amdahl, and S. Løset, “Integrated numerical analysis of an iceberg collision with a foreship structure,” *Mar. Struct.*, vol. 24, no. 4, pp. 377–395, 2011.
- [22] M. Suominen *et al.*, “Full-scale measurements on board PSRV S.A. Agulhas II in the Baltic Sea,” *Proc. Int. Conf. Port Ocean Eng. under Arct. Cond. POAC*, no. February 2017, 2013.
- [23] M. Johnston, G. W. Timco, R. Frederking, and M. Miles, “Measuring global impact forces on the CCGS Terry Fox with an inertial measurement system called MOTAN,” *Cold Reg. Sci. Technol.*, vol. 52, no. 1, pp. 67–82, 2008.
- [24] H. Kim, C. Daley, and H. Kim, “Evaluation of large structural grillages subjected to ice loads in experimental and numerical analysis,” *Mar. Struct.*, vol. 61, no. July, pp. 467–502, 2018.
- [25] H. Kim, “Simulation of Compressive ‘Cone-Shaped’ Ice Specimen Experiments using LS-DYNA®,” *13th Int. LS-DYNA Users Conf.*, pp. 1–9, 2014.
- [26] R. E. Gagnon, “A numerical model of ice crushing using a foam analogue,” *Cold*

Reg. Sci. Technol., vol. 65, no. 3, pp. 335–350, 2011.

- [27] R. Gagnon, “Numerical rendition of ice crushing,” *NRC Publ. Arch.*, pp. 1–13, 2010.
- [28] D. M. Bae, A. R. Prabowo, B. Cao, J. M. Sohn, A. F. Zakki, and Q. Wang, “Numerical simulation for the collision between side structure and level ice in event of side impact scenario,” *Lat. Am. J. Solids Struct.*, vol. 13, no. 16, pp. 2691–2704, 2016.
- [29] B. W. T. Quinton, “Lateral (sliding) motion of design ice loads on IACS polar classed structures,” *Ships Offshore Struct.*, vol. 14, no. sup1, pp. 281–291, 2019.
- [30] B. W. T. Quinton, C. G. Daley, and R. E. Gagnon, “Realistic moving ice loads and ship structural response,” *Proc. Int. Offshore Polar Eng. Conf.*, no. June 2012, pp. 1208–1214, 2012.
- [31] B. W. T. Quinton, C. G. Daley, R. E. Gagnon, and D. B. Colbourne, “Guidelines for the nonlinear finite element analysis of hull response to moving loads on ships and offshore structures,” *Ships Offshore Struct.*, vol. 12, pp. S109–S114, 2017.
- [32] H. Kim and B. Quinton, “Evaluation of moving ice loads on an elastic plate,” *Mar. Struct.*, vol. 50, pp. 127–142, 2016.
- [33] Y. Gao, Z. Hu, and J. Wang, “Sensitivity analysis for iceberg geometry shape in ship-iceberg collision in view of different material models,” *Math. Probl. Eng.*, vol. 2014, 2014.
- [34] D. K. Park, D. K. Kim, J. K. Seo, B. J. Kim, Y. C. Ha, and J. K. Paik, “Operability

- of non-ice class aged ships in the Arctic Ocean—Part I: Ultimate limit state approach,” *Ocean Eng.*, vol. 102, pp. 197–205, 2015.
- [35] D. K. Park, D. K. Kim, J. K. Seo, B. J. Kim, Y. C. Ha, and J. K. Paik, “Operability of non-ice class aged ships in the Arctic Ocean-part II: Accidental limit state approach,” *Ocean Eng.*, vol. 102, pp. 206–215, 2015.
- [36] A. R. Prabowo, J. M. Sohn, J. H. Byeon, D. M. Bae, A. F. Zakki, and B. Cao, “Structural analysis for estimating damage behavior of double hull under ice-grounding scenario models,” *Key Eng. Mater.*, vol. 754 KEM, pp. 303–306, 2017.
- [37] S. T. Ince, A. Kumar, D. K. Park, and J. K. Paik, “An advanced technology for structural crashworthiness analysis of a ship colliding with an ice-ridge: Numerical modelling and experiments,” *Int. J. Impact Eng.*, vol. 110, pp. 112–122, 2017.
- [38] S. T. Ince, A. Kumar, and J. K. Paik, “A new constitutive equation on ice materials,” *Ships Offshore Struct.*, vol. 12, no. 5, pp. 610–623, 2017.
- [39] B. T. Hill, “Database of ship collisions with icebergs,” Canada National Research Council (NRC), Institute for Marine Dynamics, St. John’s. Newfoundland, Version 1.13.
- [40] E. Kim and J. Amdahl, “Discussion of assumptions behind rule-based ice loads due to crushing,” *Ocean Eng.*, vol. 119, pp. 249–261, 2016.
- [41] “Chapter 4 Navigation in Ice Covered Waters - Ice Navigation in Canadian Waters.” [Online]. Available: <http://www.cgc.gc.ca/Icebreaking/Ice-Navigation-Canadian-Waters/Navigation-in-ice-covered-waters?pedisable=true>. [Accessed: 10-Nov-

2019].

- [42] “What Are The Sizes And Shapes Of Icebergs.” [Online]. Available: <https://www.navcen.uscg.gov/?pageName=iipWhatAreTheSizesAndShapesOfIcebergs>. [Accessed: 04-Nov-2019].
- [43] B. J. O’Connell, “Marine radar for improved ice detection,” *Proc. Int. Conf. Port Ocean Eng. under Arct. Cond. POAC*, vol. 1, pp. 446–454, 2009.
- [44] S. Dunlop, *Oxford Dictionary of Weather*, 2nd ed. Oxford University Press, 2008.
- [45] I. J. Jordaan, M. A. Maes, P. W. Brown, and I. P. Hermans, “Probabilistic analysis of local ice pressures,” vol. 1, no. February 1993, 1992.
- [46] M. Fuglem, I. Jordaan, and G. Crocker, “Iceberg-structure interaction probabilities for design,” *Can. J. Civ. Eng.*, vol. 23, no. 1, pp. 231–241, 1996.
- [47] R. S. Taylor, I. J. Jordaan, C. Li, and D. Sudom, “Local design pressures for structures in ice: Analysis of full-scale data,” *J. Offshore Mech. Arct. Eng.*, vol. 132, no. 3, pp. 1–7, 2010.
- [48] F. Ralph, R. McKenna, and R. Gagnon, “Iceberg characterization for the bergy bit impact study,” *Cold Reg. Sci. Technol.*, vol. 52, no. 1, pp. 7–28, 2008.
- [49] J. Amdahl, “Impact from ice floes and icebergs on ships and offshore structures in Polar Regions,” *IOP Conf. Ser. Mater. Sci. Eng.*, vol. 700, no. 1, 2019.
- [50] W. Lu, J. Amdahl, R. Lubbad, Z. Yu, and S. Løset, “Glacial ice impacts: Part I: Wave-driven motion and small glacial ice feature impacts,” *Mar. Struct.*, vol. 75, no.

September 2020, 2021.

- [51] V. P. Astakhov, “Mechanical Properties of Engineering Materials: Relevance in Design and Manufacturing,” in *Introduction to Mechanical Engineering*, J. P. Davim, Ed. Cham: Springer International Publishing, 2018, pp. 3–41.
- [52] “American Bureau of Shipping (ABS), Rule Requirements for Materials and Welding,” 2021.
- [53] S. Murakami, *Continuum damage mechanics: A continuum mechanics approach to the analysis of damage and fracture*, vol. 1, no. 2012.
- [54] W. Zhang and Y. Cai, *Continuum Damage Mechanics and Numerical Applications*. 2010.
- [55] Y. Bao and T. Wierzbicki, “On fracture locus in the equivalent strain and stress triaxiality space,” *Int. J. Mech. Sci.*, vol. 46, no. 1, pp. 81–98, 2004.
- [56] Y. Bai, X. Teng, and T. Wierzbicki, “On the application of stress triaxiality formula for plane strain fracture testing,” *J. Eng. Mater. Technol. Trans. ASME*, vol. 131, no. 2, pp. 0210021–02100210, 2009.
- [57] Y. Bai and T. Wierzbicki, “A new model of metal plasticity and fracture with pressure and Lode dependence,” *Int. J. Plast.*, vol. 24, no. 6, pp. 1071–1096, 2008.
- [58] S. Ehlers, J. Broekhuijsen, H. S. Alsos, F. Biehl, and K. Tabri, “Simulating the collision response of ship side structures: A failure criteria benchmark study,” *Int. Shipbuild. Prog.*, vol. 55, no. 1–2, pp. 127–144, 2008.

- [59] B. C. Cerik and J. Choung, “Ductile fracture behavior of mild and high-tensile strength shipbuilding steels,” *Appl. Sci.*, vol. 10, no. 20, pp. 1–21, 2020.
- [60] C. L. Walters, “Framework for adjusting for both stress triaxiality and mesh size effect for failure of metals in shell structures,” *Int. J. Crashworthiness*, vol. 19, no. 1, pp. 1–12, 2014.
- [61] M. Körgesaar and J. Romanoff, “Influence of mesh size, stress triaxiality and damage induced softening on ductile fracture of large-scale shell structures,” *Mar. Struct.*, vol. 38, pp. 1–17, 2014.
- [62] Livermore Software Technology Corporation, *LS-DYNA Keyword User’s Manual Volume II R12*, vol. II, no. 5442. 2020.
- [63] Z. Liu, J. Amdahl, and S. Løset, “Plasticity based material modelling of ice and its application to ship-iceberg impacts,” *Cold Reg. Sci. Technol.*, vol. 65, no. 3, pp. 326–334, 2011.
- [64] H. A. Nisja, “Numerical Modelling of Brittle Failure in Ice Structures,” NTNU, 2014.
- [65] Japan P&I Club, “Loss Prevention Bulletin :Marine Weather Ship Handling in Rough Sea Head and countering / Following Seas,” 2019.
- [66] R. E. Gagnon and A. Derradji-Aouat, “First Results of Numerical Simulations of Bergy Bit Collisions with the CCGS Terry Fox Icebreaker,” in *Proceedings of the 18th IAHR International Symposium on Ice*, 2006.

- [67] R. Zong, “Finite element analysis of ship-ice collision using ls-dyna,” Memorial University of Newfoundland, 2012.
- [68] O. Astrup, “Cutting of thick plates by a wedge- an experimental study. MIT-Industry Joint Program on Tanker Safety, Report No. 27, Department of Ocean Engineering, MIT, USA.,” 1994.
- [69] S. Zhang, P. T. Pedersen, and R. Villavicencio, “Internal mechanics of ship collision and grounding,” in *Probability and Mechanics of Ship Collision and Grounding*, 2019, pp. 147–270.
- [70] J. A. W. Sajdak and A. J. Brown, “Modeling longitudinal damage in ship collision (SSC 437),” 2005.
- [71] S. Zhang, “Plate tearing and bottom damage in ship grounding,” *Mar. Struct.*, vol. 15, no. 2, pp. 101–117, Mar. 2002.